RESEARCH

2009-01

Development of a Real-Time Arterial Performance Monitoring System Using Traffic Data Available from Existing Signal Systems

LRRB
LOCAL ROAD RESEARCH BOARD

Take the steps... Research...Knowledge...Innovative Solutions!

Transportation Research

Technical Report Documentation Page

1. Report No.	2.	3. Recipients Accession No.	
MN/RC 2009-01			
4. Title and Subtitle Development of a Real-Time Arterial Performance Monitoring System Using Traffic Data Available from Existing Signal Systems		5. Report Date December 2008 6.	
7. Author(s) Henry X. Liu, Wenteng Ma, Xinkai Wu, and Heng Hu		8. Performing Organization Report No.	
9. Performing Organization Name and Address Department of Civil Engineering University of Minnesota 500 Pillsbury Dr. SE Minneapolis, Minnesota 55455-0220		10. Project/Task/Work Unit No. 11. Contract (C) or Grant (G) No. (c) 89261 (wo) 19	
12. Sponsoring Organization Name and Address Minnesota Department of Transportation 395 John Ireland Boulevard Mail Stop 330 St. Paul, Minnesota 55155		13. Type of Report and Period Covered Final Report 14. Sponsoring Agency Code	
15. Supplementary Notes http://www.lrrb.org/PDF/200901.pdf			

16. Abstract (Limit: 200 words)

Data collection and performance measurement for signalized arterial roads is an area of emerging focus in the United States. As indicated by the results of the 2005 Traffic Signal Operation Self-Assessment Survey, a majority of agencies involved in the operation and maintenance of traffic signal systems do not monitor or archive traffic system performance and thus have limited means to improve their operation. With support from the Transportation Department of Hennepin County, Minneapolis, MN, a system for high resolution traffic signal data collection and arterial performance measurement has been successfully built. The system, named SMART-SIGNAL (Systematic Monitoring of Arterial Road Traffic Signals), is able to collect and archive event-based traffic signal data simultaneously at multiple intersections. Using the event-based traffic data, SMART-SIGNAL can generate time-dependent performance measures for both individual intersections and arterials including intersection queue length and arterial travel time. The SMART-SIGNAL system has been deployed at an 11-intersection corridor along France Avenue in south Minneapolis and the estimated performance measures for both intersection queue length and arterial travel times are highly consistent with the observed data.

17. Document Analysis/Descriptors	18. Availability Statement		
Traffic Signal, Performance Measures, Arterial Travel Time, Queue Length	No restrictions. Document available from: National Technical Information Services, Springfield, Virginia 22161		
19. Security Class (this report) Unclassified	20. Security Class (this page) Unclassified	21. No. of Pages 117	22. Price

Development of a Real-Time Arterial Performance Monitoring System Using Traffic Data Available from Existing Signal Systems

Final Report

Prepared by

Henry X. Liu
Wenteng Ma
Xinkai Wu
Heng Hu

Department of Civil Engineering
University of Minnesota

December 2008

Published by

Office of Research Services
Minnesota Department of Transportation
Transportation Bldg
395 John Ireland Blvd
St Paul MN 55155-1899

Acknowledgements

This project was supported by Minnesota Local Road Research Board and USDOT's Research and Innovative Technology Administration through the Intelligent Transportation Systems Institute of the University of Minnesota. The authors would like to thank James Grube, Eric Drager, Roy Doron, Darryl Dobesh, and Tom Switzen of the Hennepin County Transportation Department, and Steve Misgen of the Minnesota Department of Transportation (Mn/DOT) for their support on the field implementation of the SMART-SIGNAL system. Kevin Balke, Hassan Charara, and Ricky Parker of Texas Transportation Institute (TTI) also gave suggestions to the authors in the building of data collection units of the SMART-SIGNAL system. The authors appreciate their help.

Eric Drager of the Hennepin County Transportation Department served as the Technical Liaison to this project. Shirlee Sherkow of Mn/DOT was the Administrative Liaison of this project.

Table of Contents

Chapter 1. Introduction 1
1.1 Project Motivation 1
1.2 Project Objectives 3
1.3 Project Contributions 3
1.4 Project Overview 5
Chapter 2. Literature Review 7
2.1 Data Collection 7
2.2 Performance Measurement 9
2.2.1 Background 9
2.2.2 Queue Length Estimation 11
2.2.3 Estimation of Turning Movement Proportion 13
2.2.4 Travel Time Estimation 14
2.3 Summary 16
Chapter 3. SMART-SIGNAL Data Collection System 17
3.1 SMART-SIGNAL System Architecture 17
3.2 Data Collection System 17
3.3 Serial Port Communication 21
3.4 Hardware-in-the-loop Simulation 25
3.5 Sample Data 28
3.6 Data Preprocessing 31
3.7 SMART-SIGNAL Data Processing Flow Chart 33
3.8 Internet Access 34
3.9 Detector Configuration Discussion 36
Chapter 4. Intersection Performance Measurement 39
4.1 Queue Estimation 39
4.2.1 Definition of Queue 39
4.2.2 Queue Discharge Process 40
4.2.3 Short Queue Estimation Model 42
4.2.4 Long Queue Estimation Model 46
4.2.5 Case Study 53
4.2 Turning Movement Proportion Estimation 61
4.2.1 Problem Description 61
4.2.2 Proposed Model 62

4.2.3 Results Analysis 65
4.3 Summary 66
Chapter 5. Arterial Performance Measurement 68
5.1 Background 68
5.2 Virtual Probe Vehicle Approach 69
5.2.1 Problem Statement 69
5.2.2 States of the Virtual Probe 69
5.2.3 Virtual Probe Maneuver Decision Tree 71
5.2.4 Virtual Probe Position and Speed Calculation 72
5.2.5 Self-correction Property 75
5.3 Model Implementation and Testing 77
5.3.1 Study Site 77
5.3.2 Results Analysis 78
5.4 Summary 85
Chapter 6. Field Implementation 86
6.1 Case Study Description 86
6.2 Comparisons of Intersection Performance Measures 86
6.3 Comparisons of Arterial Performance Measures 90
6.4 Summary 94
Chapter 7. Conclusion 95
References 97
Appendix A
Appendix B

List of Tables

Table 2.1: Major Arterial Performance Measures Studied in This Project..... 10
Table 4.1: Comparisons of Observed vs. Identified Traffic State Change Points. 56
Table 4.2: Comparisons of Observed vs. Estimated Maximum Queue. 58
Table 5.1: Observed vs. Estimated Travel Time on France Avenue. 82
Table 5.2: Results of Parameters Sensitivity Analysis. 83

List of Figures

Figure 1.1: National Traffic Signal System Performance. 2
Figure 1.2: Project Contributions. 3
Figure 2.1: Traffic Data Available at Twin Cities, MN. 8
Figure 3.1: SMART-SIGNAL System Architecture. 18
Figure 3.2: Flow Chart of the Traffic Data Collection Component. 19
Figure 3.3: Demonstration of the Traffic Data Collection Components. 19
Figure 3.4: Signal Flow of Traffic Controller Interface Device. 20
Figure 3.5: Flow Chart of Data Collection Program. 21
Figure 3.6: Waveform Example of RS-485 Protocol. 22
Figure 3.7: B&B RS485 Converter (Model No. 485SD9TB). 22
Figure 3.8: RS485 Converter Connection. 23
Figure 3.9: Surge Protection for RS485 Circuit. 23
Figure 3.10: Communication Process of RS485 Network in Field. 24
Figure 3.11: Qwest M1000 DSL Modem. 25
Figure 3.12: Schematic Diagram of Hardware-in-the-loop Simulation. 26
Figure 3.13: Hardware-in-the-loop Simulation Status Window. 27
Figure 3.14: Hardware-in-the-loop Implementation with VISSIM. 28
Figure 3.15: Bird's-eye View of the Study Intersection at 76th Street and France Avenue at Minneapolis, MN. 29
Figure 3.16: Detector Layout and Signal Timing Plan at the Study Intersection. 30
Figure 3.17: Sample Data Collected at the Study Intersection. 31
Figure 3.18: Sample Preprocessed Volume Data at the Study Intersection. 31
Figure 3.19: Sample Preprocessed Occupancy Data at the Study Intersection. 32
Figure 3.20: Sample Preprocessed Signal State Data at the Study Intersection. 32
Figure 3.21: Sample Preprocessed Signal Timing Plan at the Study Intersection. 33
Figure 3.22: SMART-SIGNAL Data Process Flow Chart. 34
Figure 3.23: Internet Access to Intersection Performance Measures. 35
Figure 3.24: Internet Access to Arterial Performance Measures. 35
Figure 3.25: Configurations of Lane-based and Link-based Detectors. 36
Figure 3.26: Missing Count Problem at Advance Loop Detectors. 37
Figure 3.27: Missing Count Problem at Left-turn Loop Detectors. 37
Figure 4.1: Queue at a Signalized Intersection. 40
Figure 4.2: Demonstration of Queue Development at a Signalized Intersection. 41
Figure 4.3: Demonstration of Queue Discharge at a Signalized Intersection. 42
Figure 4.4: Queue Discharge Time Headway at a Signalized Intersection. 43
Figure 4.5: Demonstration of Short Queue at a Signalized Intersection. 44

Figure 4.6: Demonstration of Long Queue at a Signalized Intersection..... 46
Figure 4.7: Relationship of Queue Development and Occupancy Profile at a Signalized Intersection..... 48
Figure 4.8: Maximum Queue Length Estimation for Long Queues. 50
Figure 4.9: Queue Length Formulation Hypothesis — Triangle Curve. 51
Figure 4.10: Queue Length Formulation Hypothesis — Trapezoid Curve. 52
Figure 4.11: Bird's-eye View of the Study Approach. 54
Figure 4.12: Sample Video Snapshots at the Study Approach. 54
Figure 4.13: Cyclic Occupancy Profiles at the Advance Loop Detector. 55
Figure 4.14: Comparisons of Observed vs. Estimated Maximum Queue Length. 60
Figure 4.15: Comparisons of Observed vs. Estimated Maximum Queue Size. 60
Figure 4.16: Comparison of Observed vs. Estimated Cyclic Queue Length Curve. 61
Figure 4.17: Typical Movements at a Dual-ring Actuated Signalized Intersection. 63
Figure 4.18: Comparisons of Observed vs. Estimated Northbound Cyclic Right-turning Movement Proportion at the Study Intersection. 66
Figure 5.1: Geometric Layout of a Signalized Arterial Street. 69
Figure 5.2: State Variables of the Virtual Probe. 70
Figure 5.3: Maneuver Decision Tree of a Virtual Probe. 71
Figure 5.4: Acceleration Maneuver Selection. 73
Figure 5.5: Deceleration Maneuver Selection. 74
Figure 5.6: No-speed-change Maneuver Selection. 75
Figure 5.7: Demonstration of Self-correction Property. 76
Figure 5.8: An Illustrative Example of the Self-correction Property 77
Figure 5.9: Study Site in Minneapolis, MN: France Avenue (69th Street ~ 84th Street). 78
Figure 5.10: Example Virtual Probe Trajectory on May 14th, 2007. 79
Figure 5.11: Observed vs. Estimated Corridor Travel Time on France Avenue. 80
Figure 5.12: Travel Time Estimation Model Performance without Long Queue Consideration. 84
Figure 5.13: Travel Time Estimation Model Performance with Long Queue Consideration. 85
Figure 6.1: Comparison of Vehicle Arrivals within One Cycle at the Study Intersection. 87
Figure 6.2: Comparisons of Cyclic Volume and Occupancy Profiles at the Study Intersection. . 88
Figure 6.3: Comparisons of Delay at the Study Intersection. 88
Figure 6.4: Comparisons of LOS at the Study Intersection. 89
Figure 6.5: Comparisons of Queue Length at the Study Intersection. 89
Figure 6.6: Comparisons of Queue Size at the Study Intersection. 90
Figure 6.7: Comparisons of Travel Time at the Study Corridor. 90
Figure 6.8: Comparisons of Delay at the Study Corridor. 91
Figure 6.9: Comparisons of Number of Stops at the Study Corridor. 91
Figure 6.10: Comparisons of Number of Stop Time at the Study Corridor. 92
Figure 6.11: Comparisons of Virtual Probe Trajectories at the Study Corridor. 93
Figure 6.12: Comparisons of Averaged Northbound Virtual Probe Trajectories at the Study Corridor. 93

Executive Summary

Performance monitoring for arterial traffic control and management system is an area of emerging focus in the United States. To properly study traffic flow at signalized intersections, both arrival & departure traffic flow data and associated signal status data are required. Although many existing signal control systems are capable of generating data to support performance assessment, most do not make it "easy" for the managing agencies to prioritize improvements and plan for future needs. Indeed, the 2005 Traffic Signal Operation Self Assessment Survey indicated that the majority of agencies involved in the operation and maintenance of traffic signal systems do not monitor or archive traffic system performance data in an effort to improve their operation. Therefore, despite studies having shown that the benefits of investments in improved signal timing outweigh the costs by 40:1 or more, signal retiming is often not repeated frequently enough to account for rapidly changing traffic patterns, largely due to the expense of manual data collection and performance measurements.

The need to address the above problems inspired this project. The goal is to develop a real-time arterial performance measurement system, which can automatically collect and archive high-resolution traffic signal data, and build a rich list of performance measures. The objectives of this project are two-fold: 1) to develop a system for high-resolution traffic signal data collection, archival, and preprocessing; and 2) to develop a set of methodologies that can measure traffic signal performance, including queue length, delay and level of service (LOS) for individual intersections and travel time and number of stops for an arterial corridor.

In this project, a system for high-resolution traffic signal data collection is successfully built. The system, named as SMART-SIGNAL (Systematic Monitoring of Arterial Road Traffic and Signals), is an arterial data collection and performance measurement system, which simultaneously collects "event-based" high-resolution traffic data from multiple intersections and generates arterial performance measures in real time. In the SMART-SIGNAL system, a complete history of traffic signal control, including all signal events such as vehicle actuations on detectors and signal phase changes, is archived and stored.

Using the collected "event" data, mathematical models are built to calculate intersection and arterial performance measures. A time-dependent queue length estimation model is proposed that can handle long queues under both under-saturated and over-saturated conditions. The model examines the changes in signal detector's occupancy profile within a cycle, and derives queue length by identifying traffic flow pattern changes during the queue discharging process. A turning movement proportion estimation model is also offered in this report. Detector counts from surrounding intersections are used to calculate right turning traffic for the subject intersection.

An innovative algorithm is proposed in this project for arterial performance measurement by tracing virtual probe vehicles from origin to destination. One of three maneuvers, acceleration, deceleration or no-speed-change, is selected based on the current traffic states of the virtual probe. The step-by-step maneuver calculation stops until the virtual probe "arrives" at the destination, and various arterial performance measures, including travel time, can thus be estimated. An interesting property of the proposed model is that travel time estimation errors can be self-corrected with the signal status data, because the differences between a virtual probe

vehicle and a real probe can be reduced when both of them meet the red signal phase. The virtual probe mimics regular travel behaviors of arterial drivers and thus can be treated as a representative vehicle traversing the arterial.

The SMART-SIGNAL data collection system has been installed on an 11-intersections arterial corridor along France Avenue in Hennepin County, Minnesota since February 2007. Event-based signal data are being collected in a 24/7 mode and then immediately archived in the SMART-SIGNAL system, thus yielding a tremendous amount of field data available for research. The field study shows that the proposed mathematical models can generate accurate time-dependent queue lengths, travel times, numbers of stops, and other performance measures under various traffic conditions.

Chapter 1. Introduction

1.1 Project Motivation

With increasing traffic on major roads controlled by traffic signals, many problems have become common, specifically during periods of peak demand. In most urbanized settings worldwide, drivers have become accustomed to undesirable congestion and excessive delay. The traffic congestion makes them trifle time away on roads and lose the opportunity to do other things. Energy is unnecessarily wasted and the environment is contaminated by emission discharged from idling engines. In 2005, in 85 major urban areas of America, congestion robbed an average of 44 hours in delay and 31 gallons of gasoline from the road users, which caused a total loss of 67.7 billion (Schrank & Lomax, 2007). This is the equivalent of nearly one workweek that people could spend with families or on work that was wasted in their cars.

Efficiently operated traffic signals can reduce congestion and bring about significant payoffs in time and energy benefits. As indicated in the new released 2007 National Traffic Signal Report Card, an optimally operated traffic signal can reduce traffic delay by 15~40 percent, fuel consumption up to 10 percent, and harmful emission up to 22 percent (National Transportation Operations Coalition, 2007). Today, there are more than 272,000 traffic signals in the nation (National Transportation Operations Coalition, 2007). They control two-thirds of all miles driven on roadways (Federal Highway Administration, 1995). In a typical urban area, a traffic signal might carry as many as 100,000 Average Daily Traffic (ADT). In fact more than ten percent of the signalized intersections in California direct over 60,000 vehicles per day (Highway Safety Research Center, 1999). Nowadays, it is difficult to widen existing roads or build new roads in urban areas to improve the service of traffic networks. Better utilizing the existing traffic facilities is the only reasonable answer to most of the traffic congestion problems. The need for efficient traffic signal operation has never been more important.

Despite traffic signals playing critical roles in urban traffic networks, they are often not well operated and proactively managed. More than half of the signals across the United States need to be repaired or upgraded (Federal Highway Administration, 2008). Meanwhile, traffic signals are not regularly monitored; management activities are frequently delayed or canceled due to limited resources. As shown in Figure 1.1, it comes as no surprise that the National Traffic Signal Report Card assigned a grade of "*D*" for traffic signals in the United States, which means the traffic signals are not operating efficiently and causing unnecessary delay to road users (National Transportation Operations Coalition, 2007).

Addressing congestion problems at signalized intersections is not a simple issue; this is due to the complexities that come with the interruption of traffic flow at signalized intersections. Whereas traffic flow is typically characterized by speed, flow, and density, interrupted traffic flow has an additional element – traffic signal control. To properly study traffic flow at signalized intersections, both arrival / departure traffic flow data and associated signal status data are required. Although many existing signal control systems are capable of generating data to support performance assessment, most do not make it "easy" for the managing agencies to prioritize improvements and plan for future needs. Indeed, the 2005 Traffic Signal Operation Self Assessment Survey also indicated that the majority of agencies involved in the operation

and maintenance of traffic signal systems do not monitor or archive traffic system performance data in an effort to improve their operation.

Figure 1.1: National Traffic Signal System Performance.
[Source: National Transportation Operations Coalition, 2007]

As indicated in Figure 1.1, traffic monitoring and data collection is the worst performance component of the management of traffic signal systems. A grade of "*F*" indicates a failing state-of-the-practice in this area. Traffic data are the basis for evaluating system performance, diagnosing potential operational problems and fine-tuning signal control to improve the service of the system. Without regular data collection and system monitoring efforts, it is difficult for transportation agencies to estimate performance measures and identify accurate traffic conditions in the system. It would be impossible to efficiently improve traffic control and service level.

Therefore, despite studies showing that the benefits of investments in improved signal timing outweigh the costs by 40:1 or more (Sunkari, 2004), signal retiming is often not repeated frequently enough to account for rapidly changing traffic patterns, largely due to the expense of manual data collection and performance measurement. Given the need for field data collection, data analysis, signal timing optimization, testing and implementation, the overall signal retiming process can be expensive and time consuming. On average approximately 25 to 30 hours of engineer labor is needed to generate four timing plans (AM peak, noon, PM peak, and off-peak), the cost of retiming traffic signals is roughly $2,500 ~ $5,500 per intersection, and over 50% of the cost is on data collection (Sunkari, 2004). Considering that there are more than 400 signals in Hennepin County, Minnesota, a complete signal retiming will cost over $1M.

1.2 Project Objectives

The need for addressing the deficiency of traffic signal data collection and performance monitoring inspires this project. The goal of this project is to develop a real-time arterial performance measurement system, which can automatically collect and archive high-resolution traffic signal data, and build a rich list of performance measures. The system is designed for the closed-loop signal control system, which represents 90% of the traffic signal systems in the nation. The objectives of this project are then two-fold:

- To develop a data collection system where high-resolution traffic signal data can be collected, archived, and preprocessed;
- To develop a set of methodologies that can use the collected data to calculate traffic signal performance measures, including queue length, delay, level of service (LOS) and turning movement proportion (TMP) for individual intersections and travel time and number of stops for an arterial corridor.

1.3 Project Contributions

The contributions of this project are depicted as Figure 1.2, which can be divided into two categories: the practical contributions and the methodological contributions.

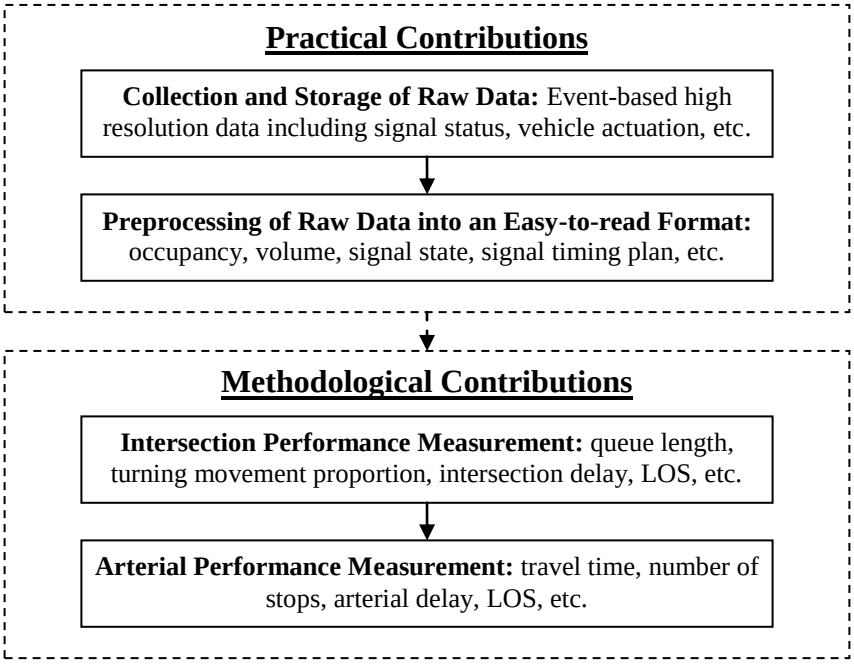

Figure 1.2: Project Contributions.

- **Practical Contributions**

The practical contributions have two major system parts that are separated from one another depending on the level of processing that the data undergoes. The first system part consists of

collection and storage of raw data; at this level no data processing takes place. The raw data correspond to the events that take place in the intersection / network, such as detector actuations, green signal gap outs, or green signal max outs. The second system part massages the raw data; at this level the raw data are converted to an easy-to-read format and are preprocessed and archived. The preprocessed data include occupancy, volume, signal state, signal timing plan, time headway and other necessary data. The raw data can be processed at a second-by-second resolution, cycle-by-cycle, or other suitable resolutions.

With the support of the Transportation Department of Hennepin County, Minnesota, the SMART-SIGNAL arterial data collection system is successfully developed in this project. The system simultaneously collects "event-based" high-resolution traffic data from multiple intersections and generates arterial performance measures in real time. In the SMART-SIGNAL system, a complete history of traffic signal control, including all signal events such as vehicle actuations on detectors and signal phase changes, is archived and preprocessed. The SMART-SIGNAL system has been installed on 11 intersections along France Avenue in Hennepin County, Minnesota since February 2007. The data collection effort with the SMART-SIGNAL system serves as a solid foundation for the proposed theoretic work in this project. Event-based signal data are being collected on a 24/7 basis and then immediately archived in the SMART-SIGNAL system, thus, yielding a tremendous amount of field data available for the performance measurement research.

- **Methodological Contributions**

The methodological contributions are a set of mathematical models proposed to estimate signal performance measures. Depending on the scope of the measures, the contributions can be divided into two parts: intersection performance measurement and arterial performance measurement. In this project, reliable analytical models are proposed to estimate queue lengths and turning movement proportions at signalized intersections and travel time at arterial corridors under various traffic conditions. Other important performance measures, including delays, LOS, and numbers of stops, can be derived accordingly.

At the intersection level, a time-dependent queue length estimation model is proposed that can handle long queues under both under-saturated and over-saturated conditions. When the queue does not exceed the advance detector location in size, the queue length can be estimated using the cumulative input-output difference. However, when a queue spills over the advance detector or even back to the upstream intersections under congestion conditions, the arrival flow cannot be measured using the advance detector. In this project, we propose a method to account for the long queue situations, which utilizes the detector occupancy profile to identify traffic flow pattern changes during the queue discharging process. A turning movement proportion estimation model is proposed that is based on the relationships of the entering traffic volumes and exiting traffic volumes during different signal phases. The model only relies on short-term traffic counts from the detectors deployed in the field.

At the arterial level, a virtual probe approach is proposed in this project to calculate the time-dependent arterial travel time based on the data from existing signal controllers and vehicle detection systems. All available traffic information, including not only the detector data but also the corresponding signal status data, is fully utilized to conduct the estimation. Unlike most of

the previous work that simply aggregates the travel time as the sum of free flow travel time and delays, the proposed model considers the correlations of the states of the vehicle and thus to make the maneuver decision at each time step. Moreover, the impact of yellow time, which is usually omitted, is also included. An interesting property of the proposed model is that travel time estimation errors can be self-corrected, because the differences between a virtual probe vehicle and a real one can be reduced when both of them meet at a red signal phase and/or a vehicle queue. Therefore, the model can be implemented under various traffic conditions, and can generate accurate results even on congested arterials.

The field study at an 11-intersection corridor along France Avenue in Minneapolis, MN shows promising results. The proposed mathematical models generate good estimations of intersection queue lengths and arterial travel times. The methods are used to evaluate a signal retiming effort on France Avenue.

1.4 Project Overview

Performance monitoring for arterial traffic control and management systems is an area of emerging focus in the United States. As indicated by the results of the 2005 Traffic Signal Operation Self-Assessment Survey, the majority of agencies involved in the operation and maintenance of traffic signal systems do not monitor or archive traffic system performance data and thus have limited means to improve their operation. This is changing as advances in computer and telecommunication technologies enable traffic management system operators to improve the tools and methods used to collect traffic signal data.

In this project, the proposed work aims to develop a systematic approach for performance monitoring of vehicle-actuated signal control systems. We successfully build a system for high resolution traffic signal data collection and performance measurement. The system, named SMART-SIGNAL, is able to simultaneously collect and archive event-based traffic signal data at multiple intersections. A set of methodologies are then proposed to calculate traffic signal performance measures based on the collected data. Various real-time performance measures, including queue length, delay, LOS and TMP for individual intersections and travel time and number of stops for an arterial corridor, are generated with accurate estimation.

The body of this report begins with a literature review of arterial performance monitoring in Chapter 2, in which previous arterial data collection practices and performance measurement research work are discussed. Chapter 3 provides the description of the system architecture and functionality of the SMART-SIGNAL system. The techniques for collecting, archiving, transmitting and preprocessing event-based traffic data are explained in this chapter. Chapter 4 illustrates the mathematical models proposed for intersection performance measurement. Here, we describe a time-dependent queue length estimation model that can handle long queues by examining signal detector occupancy profiles. A turning movement proportion model that utilizes traffic data from upstream intersections is also offered in this chapter. Chapter 5 presents a virtual vehicle probe model that can accurately estimate arterial travel time. Number of stops and some other arterial performance measures are generated as byproducts. A field case study is presented in Chapter 6, which examines the effectiveness of a signal retiming effort on a major arterial corridor in Minneapolis, MN, based upon the data collected by the SMART-SIGNAL

system and the mathematical models proposed in this report. Finally, concluding remarks and future research directions are offered in Chapter 7.

Chapter 2. Literature Review

2.1 Data Collection

Traffic data are the basis of monitoring traffic operations in urban networks. Accurate and reliable arterial traffic data collection becomes increasingly important for traffic engineers with the growing implementation of both traffic management and traveler information systems (Nee & Hallenbeck, 2001). Moreover, archiving traffic data, reporting real-time travel conditions, and predicting traffic flow can help travelers to make reasonable travel plans and save travel costs.

Although the importance of traffic data collection has long been recognized (Illinois Department of Transportation, 2005), most data collection and traffic monitoring research has been concentrated on freeway networks, where several systems have been developed and are being used for freeway performance monitoring such as in Chicago, Detroit, the Twin Cities, San Antonio, and Seattle (Smith, 2003). Most notable of these systems is the freeway Performance Measurement Systems (PeMS) developed by the PATH program at UC Berkeley, which collects and analyzes real-time freeway traffic data, and generates comprehensive performance measures for traffic engineers and commuters (Chen, 2003).

On the other hand, research on data collection and performance monitoring for arterials is quite limited (Lin *et al.*, 2003). Figure 2.1 shows the available traffic data in the metropolitan area of Twin Cities, MN. As can be seen, comparing with the data available on freeway systems (Figure 2.1(a)), there is little data available on arterial networks (Figure 2.1(b)). This does not mean the data do not exist. Tremendous arterial traffic data are there, just not collected and utilized.

Although arterial traffic data collection is rare in practice, there have been several relevant research studies reported. A few cities currently use closed-circuit television (CCTV) surveillance cameras on arterials and provide snapshots of arterial roadway traffic conditions to the public via the Internet, such as Seattle, Honolulu, and Oakland County. Similarly, some transportation agencies collect traffic counts and vehicle speeds from loop detectors or video detectors deployed on arterial intersections for operating signals, such as San Jose, Montgomery County, Athens, and Toronto (Smith, 2003).

It is noteworthy that the creators of PeMS are working on a counterpart for arterials, arterial PeMS, or APeMS, which is an on-going project conducted by the University of California, Berkeley in cooperation with the Los Angeles Department of Transportation (LADOT) (Petty *et al.*, 2005). Similar to PeMS, APeMS depends on volume and occupancy data aggregated in 30 second intervals. In contrast to SMART-SIGNAL, APeMS does not record traffic events, which limits its operational and performance applications. In a 2004 paper by Tsekeris & Skabardonis, several models were evaluated for arterial link travel time estimation, and concluded that the generalized delay model demonstrated the most promising estimation. Their experience with the development of arterial data collection and performance measurement provides us with a good reference point.

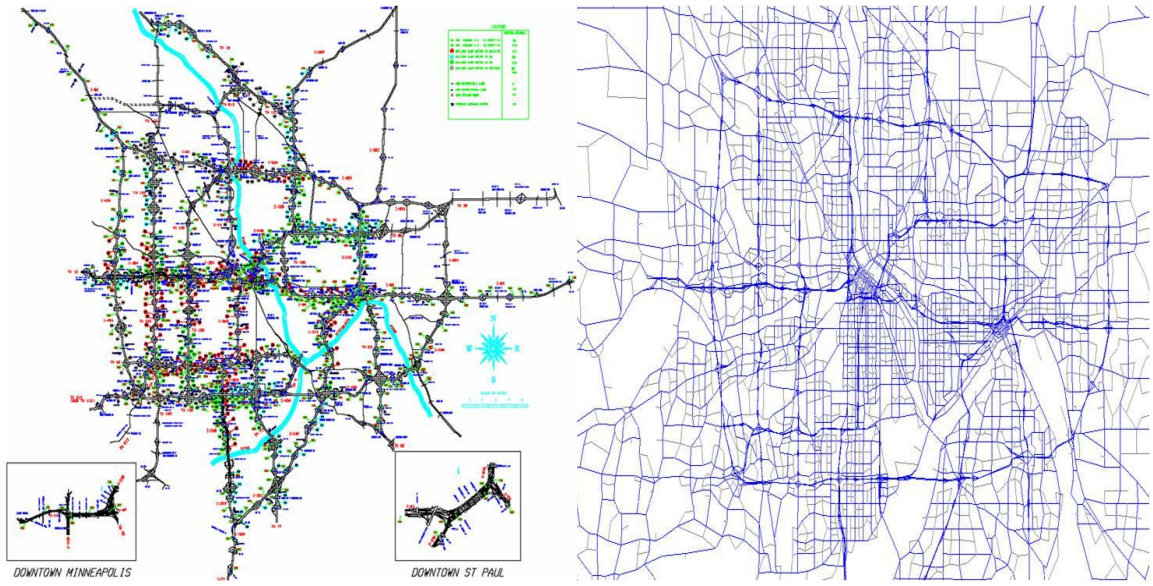

a) Data-Rich Freeway System **b) Data-Poor Arterial System**

Figure 2.1: Traffic Data Available at Twin Cities, MN.
[Source: Minnesota Department of Transportation]

Another important ongoing research project is the ACS Lite led by the Federal Highway Administration (FHWA). ACS Lite is a scaled down version of the FHWA's Adaptive Control Software (ACS). It is a cooperative work between FHWA, Siemens, University of Arizona, Purdue University, and some traffic controller manufactures including Eagle, Econolite, McCain and Peek (Federal Highway Administration, 2007). Traffic controllers from various vendors are enhanced by preloaded software to log time stamped phase and detector state changes. The software is licensed by Siemens and needs to be integrated by the controller venders to operate with their hardware.

The major limitations of the current implementations on arterial traffic data collection can be summarized as follows. First, arterial traffic data are not periodically and continuously collected and archived. In practice, collection of traffic data at signalized intersections is typically a sporadic effort in response to citizen complaints, high crash rates, and legislative mandates (Balke & Herrick, 2004; Balke *et al.*, 2005). Day-to-day operational data is not stored or analyzed, which prevents proactive management of signal control systems. Secondly, data collected from the arterials are limited; archived loop detector data or snapshots can only generate few traffic measures, such as volumes and speeds. Signal status data are omitted by most of the implemented data collection systems. Simultaneously collecting and analyzing both detector data and signal status data can generate much more useful performance measures. Third, the collected arterial traffic data are not properly stored; data are usually aggregated into static time intervals (30 seconds; 5, 15, and 60 minute) as with freeway monitoring systems. Arterial networks are different in many ways, specifically due to the effect of signal timing on flow characteristics. It is, therefore, necessary to develop different methods to archive arterial data. Second-by-second resolution data can be better utilized for representing arterial conditions.

Advances in the deployment of Intelligent Transportation Systems (ITS) technologies make real-time and historical traffic data more readily available. The Texas Transportation Institute (TTI) recently completed research on developing the Traffic Signal Performance Measurement System (TSPMS) that automatically collects both detector and signal status data from existing traffic detection systems. A list of performance measures, including cycle time, time to service, and queue service time, are determined for isolated intersections (Balke *et al.*, 2005). Its elements can essentially be divided into two categories: the existing traffic signal elements and the additional data collection elements. Existing elements include the vehicle detection units, the traffic signal controller and the back panel of the traffic cabinet. The additional components include a Traffic Controller Interface Device (CID), a Traffic Signal Event Recorder (TSER), and a Performance Measure Report Generator (PMRG). The CID is a piece of hardware which physically connects the existing traffic signal components with an industrial computer installed in the cabinet on site. The industrial computer is operated by the TSER software program to monitor and store raw data. The PMRG software runs on a computer to generate the performance measures. The proposed SMART-SIGNAL data collection component uses a similar architecture to that of TSPMS.

2.2 Performance Measurement

2.2.1 Background

It is said that "If you cannot tell how your system performed yesterday, you cannot expect to manage it today" (Varaiya, 1997). Transportation system performance measures constitute an invaluable source of information for decisions related to infrastructure resource allocation, investment plan monitoring and project evaluation. The advent of Intelligent Transportation Systems has further increased the significance of obtaining timely and accurate transportation performance measures, which can be used for either optimizing traffic management strategies or informing travelers with respect to their optimal travel paths. The challenge for transportation system has been diverted from developing basic infrastructure to managing and operating the existing transportation resources and delivering better services to road travelers under various conditions. Performance measurement becomes the critical tool to meet such challenges (National Cooperative Highway Research Program, 2003). In the last few years, measuring and monitoring performance of traffic management systems has become one of the priorities of the Federal Highway Administration as indicated in the transportation bill SAFETEA-LU (Federal Highway Administration, 2006).

Performance measurement is useful for both road travelers and traffic engineers. For road travelers, performance measures can help them make smart travel decisions, select the best travel time and travel path, avoid unnecessary delays and thus save on travel costs. For traffic engineers, performance measurement is an effective tool for monitoring network traffic operations from single movements at an intersection to the entire traffic network. Performance measures can help traffic engineers evaluate the effectiveness of current operational strategies; they provide agencies with indicators that help evaluate the system performance. Performance measures can also be used to identify problems in the traffic network, and help decision makers improve and fine-tune transportation services.

Turner *et al.* (1996a) indicated that an effective performance measure should be applicable to the users, easy to calculate, accurate, and can be clearly and consistently interpreted. The National Cooperative Highway Research Program (NCHRP) issued a synthesis in 2003 and enumerated more than 70 possible performance measures for highway monitoring, in which the average travel time, speed, average delay and LOS were considered as key measures. The synthesis also indicates that the current state of the practice needs to be enhanced and expanded and intelligent transportation systems provide great opportunities for improvement of data collection techniques to support performance measurement.

In this project, we categorize the performance measures of urban networks into two groups in terms of scope, i.e. intersection performance measures and arterial performance measures. Intersection performance measures are used to determine or evaluate the service quality provided by the existing road facilities and the control plans at an intersection. Intersection measures usually can be calculated or estimated based on traffic data collected from the subject intersection and its surrounding intersections. Correspondingly, arterial performance measures reflect the service quality supplied by the studied arterial network and the control strategies of the network. Arterial measures can be derived from intersection measures and traffic data collected in the network.

Table 2.1 lists some common intersection and arterial performance measures that studied in this project. At the intersection level, some measures can be directly collected or computed from the existing systems. For example, vehicular measures, including occupancy and volume, can be calculated based on collected detector actuations; the signal measures, including green time, red time, yellow time and cycle length, can be obtained from traffic controllers. On the other hand, some measures, including queue length, turning movement proportion (TMP), queue size, intersection delay and level of service need to be estimated with mathematical models. Amongst these measures, queue length and TMP are particularly critical for transportation researchers. Other intersection measures can be derived accordingly based on queue length and TMP information. This project proposes analytical models for queue length and TMP estimation, which are described in Chapter 4.

Table 2.1: Major Arterial Performance Measures Studied in This Project.

Scope	Performance Measures
Intersection	occupancy, volume, green time, red time, yellow time, cycle length; queue length, turning movement proportion (TMP), queue size, intersection delay, level of service (LOS);
Arterial	travel time, number of stops, average speed, delay, level of service (LOS);

At the arterial level, most of the performance measures cannot be directly obtained. Mathematical models are needed to estimate travel time, number of stops, delay and the like. Amongst these, travel time is a crucial measure which is important for both travelers and traffic engineers. It is not only widely used to help road users make travel decisions, but also used to evaluate network operations. Travel time also helps generate some other arterial measures, such as average speed, delay, and level of service. Number of stops is another important measure which provides useful arterial operation information. In this project, a virtual vehicle probe model is proposed which can easily generate numbers of stops as well as arterial travel time. The details of the model are discussed in Chapter 5.

Previous research on arterial performance measurement generally provide offline assessment procedures based on established methods such as the Highway Capacity Manual (HCM) (Transportation Research Board, 2000); they typically calculate traffic performance measures, such as queue length or travel time, according to historical data. Brief reviews of previous studies on queue length, turning movement proportions and travel time are offered in the following in this chapter.

2.2.2 Queue Length Estimation

Queue length has long been recognized as a valuable measure for traffic engineers to evaluate performance of a controlled intersection. It provides important information for estimating other arterial performance measures, such as intersection delay, travel time and level of service. At signalized intersections, queue length is a necessary input data for many signal optimization strategies (Bang & Nilsson, 1976; Lin & Vijayakumar, 1988).

Earlier queue estimation models are designed for stable traffic conditions, where traffic flows are assumed to be constant (Webster, 1958; Miller, 1968). Corresponding to the traffic control strategies presently employed, they usually focus on fixed-time signal plans (Newell, 1989). Compared to these so-called "*steady-state*" models, Akçelik (2001) classified the back of queue models presented in the Highway Capacity Manual 2000 as a "*time-dependent*" expression. He claimed that the steady-state models are only valid when the traffic flows are under-saturated; when the degrees of saturation exceed 0.95, time-dependent models need to be applied to predict queue length.

Robertson (1969) first proposed to model the vehicle arrival and departure profiles according to small time steps. The method was extended by Strong *et al.* (2006a, 2006b) and named the incremental queue accumulation (IQA) method. The extensions relax the constant saturation flow rate and uniform arrival rate assumptions made in the HCM, resulting in a more accurate and flexible treatment. The method is validated by Kyte *et al.* (2008) with data sets generated by the FHWA's Next Generation Simulation Model (NGSIM).

Viti and Zuylen (2006) assessed the consistency of different dynamic queuing models by dividing them into three classes based on the level of assumed flow and cost details: macroscopic, mesoscopic, and microscopic. Macroscopic models represent aggregated traffic flows and costs in time and space; mesoscopic models study the probabilities of characteristics of individual vehicles to estimate the probabilities of traffic flows and costs; and microscopic

models investigate traffic flows and costs at the individual vehicle level by making assumptions on individual driver behavior and vehicle characteristics. The authors compared the three types of models under homogeneous traffic conditions with stochastic vehicle arrivals, and found that the results generated from the three models are quite close, which implies the difference in the level-of-detail does not influence queue estimation.

In general, a queuing model can be simplified as Equation 2.1:

$$q(t) = q(t-1) + N_A(t) - N_D(t) \quad (2.1)$$

where $q(t)$ is the number of queued vehicles at time *t*, $q(t-1)$ is the residual queue from previous periods, and $N_A(t)$ and $N_D(t)$ are vehicle arrivals and departures within time interval $[t-1, t]$. For the deterministic case and within a certain time period (such as a cycle), the expression can be reformatted as Equation 2.2 (Catling, 1977):

$$q(t) = q(t-1) + [x(t) - 1] \cdot c \cdot t \quad (2.2)$$

where $x(t)$ is the average degree of saturation, *c* is the number of departures and *t* is the length of the time interval (such as cycle length). The equation is straightforward and has been widely used to estimate intersection delay (Canadian Institute of Transportation Engineers, 1996; Transportation Research Board, 2000). However, the deterministic models do not consider vehicle arrival times or vehicle arrival distributions and the vehicles are assumed to be vertically queued, which severely restricts their accuracy and scope. The model cannot reflect true traffic conditions especially when travel time between queue front and queue rear are significant and unpredictable.

Various models have been proposed by researchers to overcome the deficiencies of deterministic queuing models since the 1960's. For example, shock-wave theory based models have been developed to describe horizontal queues (Rorbech, 1968; Cronjr, 1983; Stephanopoulos and Michalopoulos, 1979). The randomness of flow arrivals and departures has been investigated with stochastic queuing analysis (Miller, 1968; Akçelik, 1980). Time-dependent models are also derived to include the variability of traffic flows with time, which are necessary for real-time performance measurement systems (Kimber and Hollis, 1979; Akçelik, 1988).

Markov Chain processes are also proposed to accommodate the stochastic and dynamic nature of traffic queues (Viti and Zuylen, 2005). The system is assumed as a Markov Chain renewal process, and queue length is estimated based on observation or estimation from previous time steps. Vehicle arrivals and departures are all assumed with certain distribution. Therefore, the accuracy of the model highly depends on the assumptions of initial queue and traffic arrival / departure patterns.

With the improvement of computer computation ability, individual vehicle behavior can be investigated in queue length estimation. Car following, lane changing, vehicle acceleration / deceleration, driver reaction time, and the like can be addressed to generate more accurate results. Time-dependent queue lengths and variability are also well presented by the microscopic models (Viti and Zuylen, 2006). Although high computation costs and consistency issues

limited the models from being widely used for online traffic signal operations, they have a bright future as computer technologies continue to improve. Additionally, there are some microscopic models which estimate the trajectories of vehicles between the advance detector and stop-lines proposed for online traffic control (Chang, *et al.*, 2000; Xu, *et al.*, 2006).

The advancements in the field of real time data collection can also result in efficient measurement of signal performance measures, including queue length. Sharma *et al.* (2007) proposed two real-time performance measurement algorithms for estimating approach delay and maximum queue length using detector actuations, phase change data, and parametric data (saturation headway, storage capacity, etc.) as model inputs. However, both techniques are essentially based on cumulative input-output techniques, which can only be used for the estimation of queue length when the rear of the queue does not exceed the advance detector. Such input-output techniques cannot handle long queues exceeding beyond the advance detector, therefore applications of these techniques are limited.

Most of the previous models do not consider long queues, when queues spill over the advance loop detector or even back to the upstream intersections under congestion. Vehicle arrivals are not available, and thus queue estimation models become more complicated and difficult. Additional information, beyond vehicle counts provided by the advance loop detector, is apparently needed. Long queues are very common during peak hours under congested traffic conditions, little research has been reported on long queue estimation. One possible approach to deal with long queues is to investigate the relationship between queue length and occupancy values of advance loop detectors. When queues extend over the detector, high values of detector occupancy can be observed. Mueck (2002) proposed a linear relationship between the queue length and the occupancy value of advance loop detector. Geroliminis and Skabardonis (2007) also utilized occupancy information as a key factor to study long queue estimation.

2.2.3 Estimation of Turning Movement Proportion

Turning movement proportion is an important intersection measure for advanced traffic management systems. It is the input data that can improve functionality of many adaptive control systems, such as SCATS (Sydney Coordinated Adaptive Traffic System) and SCOOT (Split Cycle Offset Optimization Technique) (Lan and Davis, 1999). For most of the existing detection facilities, right-lane detectors are normally not deployed. Some approaches, especially the minor approaches, right-turn movement traffic shares lanes with through or left-turn movement traffic. Therefore, turning counts cannot be directly measured from the road, and mathematical estimation models are needed.

The study of turning movement proportion estimation at arterial intersection has been broadly explored. To some extent, the estimation of turning movement proportions at junctions are equivalent to the estimation of dynamic origin-destination flows in a “small” network; therefore, OD estimation techniques are extensively applied to turning movement proportion estimation. Measured counts from the traffic surveillance systems on the roads are utilized as input data. Many mathematical models, especially statistical models, were proposed accordingly.

The least-squares (LS) based methods are studied since 1980's by various researchers (Cremer and Keller, 1981, 1987; Kessaci *et al.*, 1989; Bell, 1991). They assume that full-set detectors are available for all approaches, and thus the in-flow and out-flow counts can be obtained for the estimation. Although the LS-based methods can produce unbiased estimates of turning movement proportions, there are usually limited for field applications. Most of the traffic signals in the field do not have full set of detectors. The methods, however, become unreliable when only partial set of detectors are available or some of the detectors fail (Nihan and Davis, 1987, 1989).

Maher (1984) compared three models, the Information Minimizing approach, the Bayesian approach, and the Maximum Likelihood method, pointing out that the three models are very similar. Although the models require counts for only one cycle, they need prior turning movement proportions as input. The accuracy of the models highly depends on how well the prior estimate results match the true turning movement proportions. On the other hand, time-series methods do not need prior estimates but require a long time frame which impedes their responsiveness. These estimates become highly inaccurate during times of sudden and highly irregular turning movement changes caused by unforeseen events such as traffic accidents, in which they are needed mostly by the traffic signal system.

Another method which estimates intersection turning movement proportions from less-than-complete sets of traffic counts was proposed by Lan and Davis (1999). In their method both entering and exiting traffic counts at each of an intersection's approaches are used, on some occasions it even works under conditions where the number or placement of detectors does not support complete counting. However, the method is greatly restricted to specific geographic scenarios, if the detector configuration does not satisfy an identifiable condition, it fails to work. Chang and Tao (1998) give a time-dependent turning estimation for signalized intersections, which, by including the approximate intersection delay, the model can account for the impacts of signal setting on the dynamic distribution of intersection flows. To improve the estimation accuracy, some pre-estimated turning fractions from a relatively long time interval serve as additional constraints for the estimation.

Nobe (2002) developed four closed-form estimation methods in his dissertation, maximum entropy (ME), generalized least-squared (GLS), least-squared (LS) error and least-squared error / generalized least-squared error (LS /GLS), which either need prior turning proportion estimates or require counts for three cycles. Despite several layouts being considered, all of the four models have a fixed two-phase cycle, and the right turning movements in each phase are always set as "protected". In fact, most right turning maneuvers at signalized intersections are permitted, and constitute minor movements throughout whole cycle.

2.2.4 Travel Time Estimation

Travel time is one of the most important measures for evaluating the performance of traffic networks and accurate and reliable travel time information becomes increasingly important for traffic engineers. Travel time is also one of the most understood measures for road users, helping them make informed decisions on travel choice, and avoidance of unnecessary delay.

The interrupted nature of traffic flows in most urban networks makes travel time estimation much more challenging for arterials than for freeways. During the past decade, research studies on freeway travel time estimation were rich and successful, as exemplified by the California's freeway Performance Measurement System (PeMS) developed at the University of California, Berkeley. PeMS collects and analyzes real-time freeway traffic data, and generates comprehensive performance measures including freeway travel time (Chen, 2003). To the contrary, research on arterial travel time estimation is limited. Though travel time has long been recognized as a valuable measure of effectiveness for arterial network, no comparable system like PeMS has been developed and implemented for surface streets with signalized intersections. The difficulty is that travel time on arterial networks is usually not only a function of traffic flow, link capacity and speed limit, but also involves numerous other factors such as signal timing and conflicting traffic from cross streets.

To the best of our knowledge, there is no reliable methodology readily available that utilizes high-resolution traffic data to derive on-line travel time for arterials, mainly due to the limited data collection capabilities. A number of regression (Turner *et al.*, 1996b; Frechette and Khan, 1998; Zhang, 1999) and heuristic methods (Takaba *et al.*, 1991; Cheu *et al.*, 2001) are proposed by researchers to provide offline and steady state assessment using historical traffic volume and signal timing data. Probe vehicles are also widely used in practice to estimate arterial travel times (Turner *et al.*, 1998; Dailey and Cathey, 2002), but only limited sample points at fragmented times can be collected due to costs. The wider-scale implementation of intelligent transportation systems provides another trend of performance measurement techniques. Video detection, cellular-phone location technology or acoustic methods are developed to identify or track vehicles (Coifman *et al.*, 1998; Courage *et al.*, 1998; Shuldiner and Upchurch, 2001). However, these vehicle identification techniques are expensive, immature and mostly involve privacy concerns.

Though varying degrees of success have been achieved by such research work, few of the models developed to date have been applied to real world situations. There is still no reliable methodology readily available that utilizes traffic surveillance data to derive accurate travel time for arterial streets, partially due to limited data collection efforts. The existing methods do not appropriately account for the needs of a real-time performance measurement system. These needs are related to reducing complexity, simplifying data requirements and increasing computational efficiency. There are two reasons for this deficiency: 1) some of the models require traffic data that are not or cannot be routinely collected from loop detectors, and 2) some of the models are site-specific and cannot be applied to other locations without recalibration. However, the major limitation of previous models is that they do not fully utilize the available data from existing infrastructure to estimate travel time. Most of these models only take into account low-resolution data from the detection system, while the status of the signal data is omitted or not fully considered.

Recent research on arterial travel time estimation started to consider the impact of signal settings. Skabardonis and Geroliminis (2005) derive an analytical model based on data collected from both loop detectors and signal controllers. The authors utilize kinematic wave theory to model the queuing traffic at signalized intersections while also considering signal coordination. Liu and Ma (2007) propose an arterial travel time estimation model which leverages the dynamic property of the signal settings and high-resolution detector data. However, as with most previous

work, the above two models calculate travel time by decomposing it into free flow travel time and delay. The free flow travel time and delays are estimated separately and then aggregated linearly, while the correlations of the decomposed components are less considered. Moreover, the impact of yellow time is omitted by the models. Driver behavior during yellow intervals is complicated, and cannot be simply assumed to be the same as behavior during green or red interval.

2.3 Summary

Over the past decades, the lack of resources has prevented agencies from collecting high resolution traffic signal data. This is all changing as advances in computer and telecommunication technologies have enabled us to improve the tools and methods used to manage transportation infrastructure. Nonetheless, despite the growing needs to improve signalized intersection management, we still see that current data collection efforts for signalized arterial networks are dispersed, both spatially and temporally. Additionally, the aggregate nature of collected data fails to capture the true dynamics at play, and hence properly evaluate system operations. Complexities that come with interrupted traffic flow can be mitigated by collecting the control dimension of the data, which involves collecting data on an event-by-event basis. An event here refers to anything that can be recorded by current closed loop systems such as an actuation, a green extension, or an indication change. While several systems have been built for freeway traffic management, very little, if any, work has been done to produce a systematic framework for high resolution (event-based) data collection and management of arterial networks.

The proposed work aims to develop a systematic approach for data collection and performance monitoring of closed loop signal control systems named SMART-SIGNAL (Systematic Monitoring of Arterial Road Traffic and Signals). The tasks under this project involve 1) the development of a data collection system for collecting and archiving high-resolution traffic data; and 2) the development of procedures and methodologies for extracting a rich set of performance measures from high resolution data.

With support from the Minnesota Department of Transportation and Hennepin County, Minnesota, the research team has successfully built a system for high resolution data collection and direct performance measurement. The SMART-SIGNAL data collection system has been successfully installed in the field, yielding a tremendous amount of field data available for research. The implementation of the SMART-SIGNAL system and detailed discussion of the proposed performance measurement models are presented in the following chapters.

Chapter 3. SMART-SIGNAL Data Collection System

3.1 SMART-SIGNAL System Architecture

The proposed SMART-SIGNAL (Systematic Monitoring of Arterial Road Traffic Signals) system is a cohesive event based data collection, storage, and analysis system. The system can be scaled to an isolated intersection, an arterial, or a network of signalized intersections. The SMART-SIGNAL System has three major components; including event-based data collection system, performance measure calculation system and user interface (Internet Access).

As shown in Figure 3.1, the first box indicates the Data Collection System of SMART-SIGNAL which is implemented in the field. Two types of data, the signal event and detector event are collected by the system and stored in a log file every day. Data in different intersections is transmitted to the master cabinet by using serial ports of computers and then sent back to the database which locates at the Traffic Lab in University of Minnesota by DSL (Digital Subscriber Line). In the second box, a rich set of performance measures are generated in the database, including both intersection level and arterial level, such as volume, queue, delay, travel time and etc. One website is being constructed and different users can log onto the website to search the information they need, for example the volume in one approach of one intersection in a certain time as shown in the third box of Figure 3.1.

3.2 Data Collection System

Two kinds of event signals would be captured by the Data Collection System, which are vehicle actuation events and signal phase change events. A detector call, or actuation, simply indicates a vehicle arriving "event", and that the vehicle demands service for a particular movement. In addition, signal phase changes can also be regarded as an "event". The signal event and detector event are acquired separately from the data collection units located in the traffic signal cabinets. Vehicle actuation events are captured by inductive loop detectors, whose inductance can be changed when a vehicle passing by. Detection units in the cabinet convert the change of inductance to the change of voltage and a typical digital signal is sent out to the back panel after modulation which will be used by the traffic controller in the cabinet. Signal status is determined by the controller and a high/low digital control signal is sent out to switch the traffic lights.

SMART-SIGNAL adopts TSPMS developed by TTI (Balke *et al.*, 2005) as the data collection component at single intersections, but expands the scope to a group of consecutive intersections on arterials by multiple installations of TSPMS. At each intersection, an industrial PC with a data acquisition card is installed, and event data (including both vehicle actuation events and signal phase change events) collected at each intersection are transmitted to the data server in the master controller cabinet through the existing communication line (in this case, spare twisted pair) between signalized intersections.

Data collection at each intersection is described in Figure 3.2. Its elements can essentially be divided into two categories: the existing traffic signal elements (the light blue boxes in the figure) and the additional data collection elements (the light green boxes in the figure). Existing elements include the vehicle detection units, the traffic signal controller, and the back panel of

the traffic cabinet. The additional components include a Traffic Controller Interface Device (CID), a Traffic Event Recorder software program, and a Traffic Log Database. The CID is a piece of hardware which physically connects the existing traffic signal components with an industrial computer installed in the cabinet on site. As the vehicle actuation events and signal status change events will be finally represented by the high-low voltage changes on the back panel, digital data acquisition card can be used to capture these events.

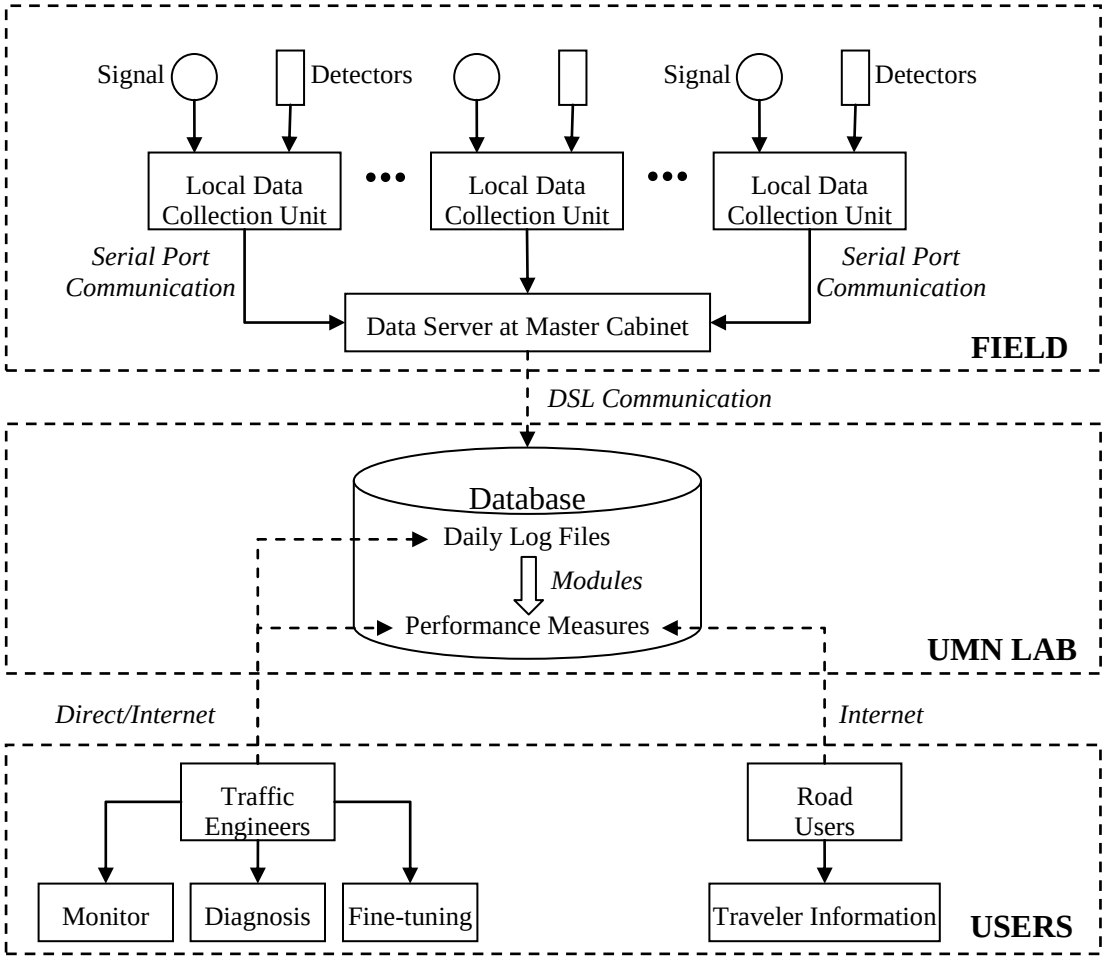

Figure 3.1: SMART-SIGNAL System Architecture.

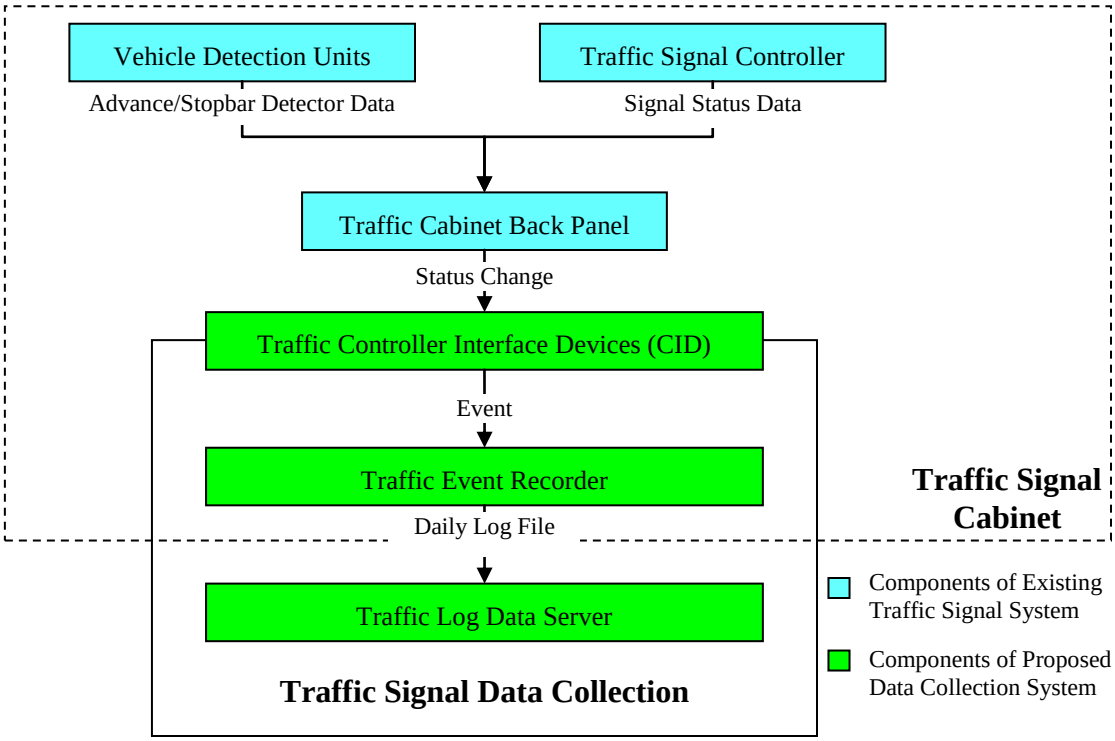

Figure 3.2: Flow Chart of the Traffic Data Collection Component.
[Source: Balke et al., 2005]

In the France Avenue case, a PCI-6528 digital input / output (I/O) data acquisition card produced by the National Instruments (2006) was implemented, which has 24 input channels, as shown in Figure 3.3(a). In order to limit the input direct current (DC) to a safe range, a terminal strip was designed, as shown in Figure 3.3(b). Basically, the terminal strip is made up with 24 resistors (16.2 k), 1 fuse (200mA) and couple of connectors. The in-site view of the data collection components is shown in Figure 3.3(c), with all the wire collections.

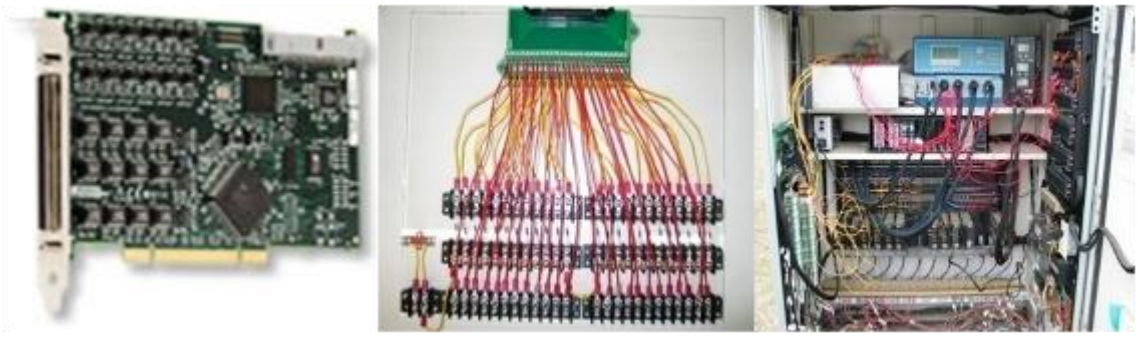

a) Data Acquisition Card **b) Terminal Strip** **c) Traffic Cabinet**

Figure 3.3: Demonstration of the Traffic Data Collection Components.

The signal flow of the Data Collection System is illustrated in Figure 3.4. Digital voltage changes on the back panel indicate different traffic events in the field, in terms of traffic light status switch and vehicle actuation. Through the terminal strip, the digital signals are captured by the Data Acquisition Card which is installed into the industrial computer.

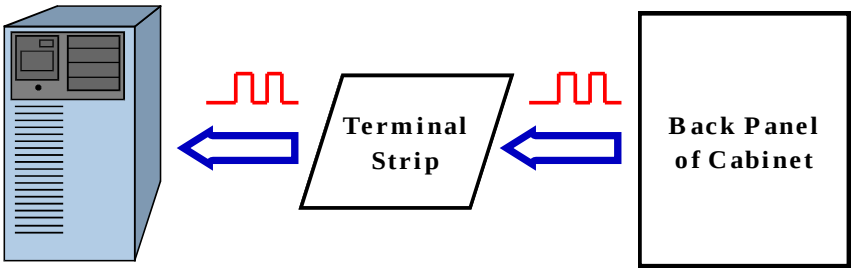

Figure 3.4: Signal Flow of Traffic Controller Interface Device.

The Traffic Event Recorder software program is developed using the Microsoft Visual C# programming that runs on the industrial computer in the field to record the events (for example, phase 1 green changed from "ON" state to an "OFF" state) into a log file. Figure 3.5 shows the flow chart of the data collection program in the field, which will watch the status of all channels of data acquisition card all the time and make a record once a status change happens. The resolution of the record is very high, where the accuracy of the time would be in millisecond level.

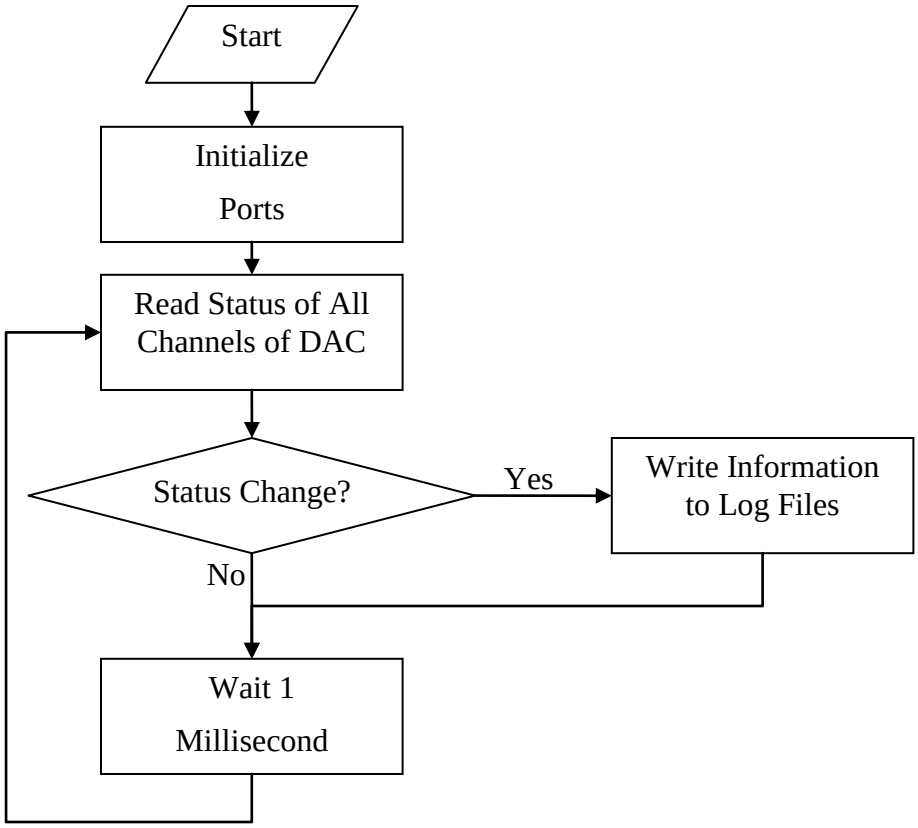

Figure 3.5: Flow Chart of Data Collection Program.

3.3 Serial Port Communication

Due to the limitation of the field, the existing twisted pair communication lines which are buried underground are chosen as the communication media and a protocol of RS-485 is used to transmit data between cabinets. Figure 3.6 shows a waveform example of the RS-485 protocol, which uses the difference between the wires' voltages to represent logic 0 and logic 1 (Ovesen, 2008). The difference of potential must be at least 0.2 volts for valid operation, and any applied voltages should be between +12 V and -7 volts. RS-485 can be used to communicate with remote devices at distances up to 4000 ft (1200 m) and a network up to 32 nodes.

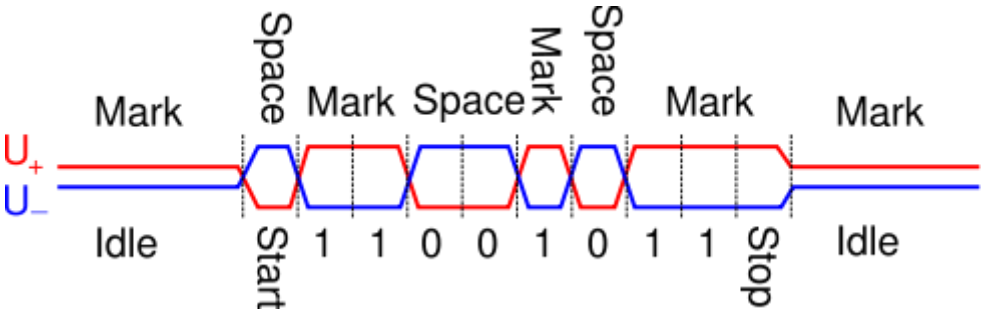

Figure 3.6: Waveform Example of RS-485 Protocol.
[Source: Ovesen, 2008]

A RS-485 converters (Model No.485SD9TB) produced by the B&B Electronics (2003) are used in this project, as shown in Figure 3.7 and the whole RS-485 network is presented in Figure 3.8. In each cabinet, one RS-485 converter is plugged into the DB9F serial port of the industrial computer and three lines come out of the terminal block, in terms of TD(B)+, TD(A)- and GND. Actually, different nodes of the network share one common signal pair and one ground, therefore only 2 computers of the network can communicate with each other at the same time, which is one of the drawbacks of this protocol.

Figure 3.7: B&B RS485 Converter (Model No. 485SD9TB).
[Source: B&B Electronics, 2003]

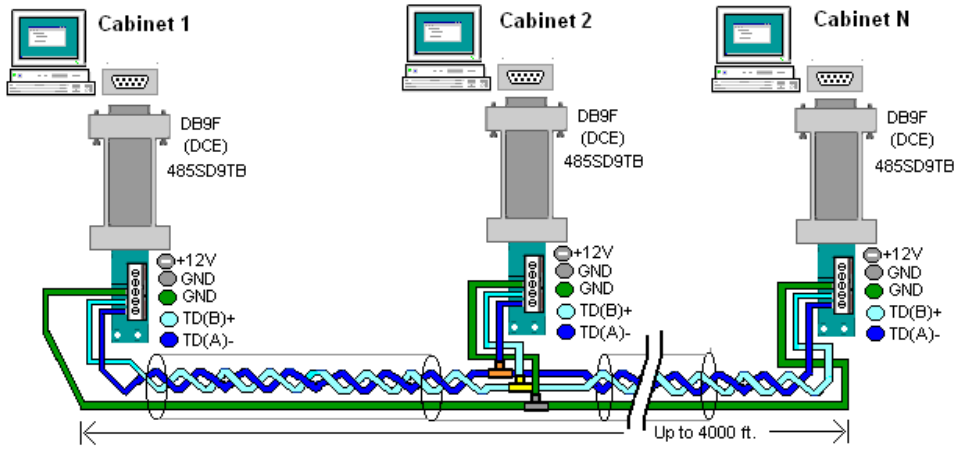

Figure 3.8: RS485 Converter Connection.
[Source: B&B Electronics, 2003]

Surge protection circuits are made for each RS-485 converter to prevent the whole system from damage. Basically, the circuit, as shown in Figure 3.9, makes use of two sets of back to back Zener Diodes (1n755 – 7.5V, 20mA, 400mW), which limit the voltages on the signal lines to approximately 7.5 Volts.

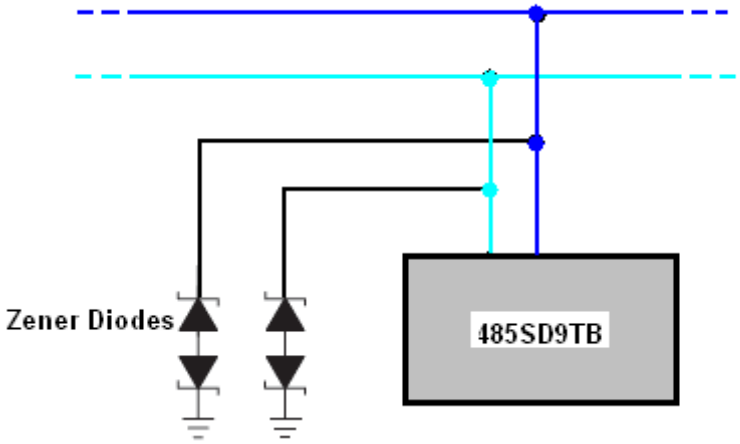

Figure 3.9: Surge Protection for RS485 Circuit.
[Source: B&B Electronics, 2003]

A serial port communication software program developed using the Microsoft Visual C# programming operates the data transfer and time synchronization in this stage and the process is shown in Figure 3.10. At 12:00 am every day, the Master computer, whose CPU clock is synchronized with internet time through DSL or wireless every day, would send out a message containing its current CPU time, as shown in the first picture of Figure 3.10. All the computers in the RS485 network would receive this message and synchronize their time with the Master computer. 10 seconds later, the Master computer would send out another message which request Slave 1 computer to send out data, as shown in the second picture of Figure 3.10. All the

computers in the network would receive the message, but only Slave 1 computer will respond and send its data to the master computer, as shown in the third picture of Figure 3.10.

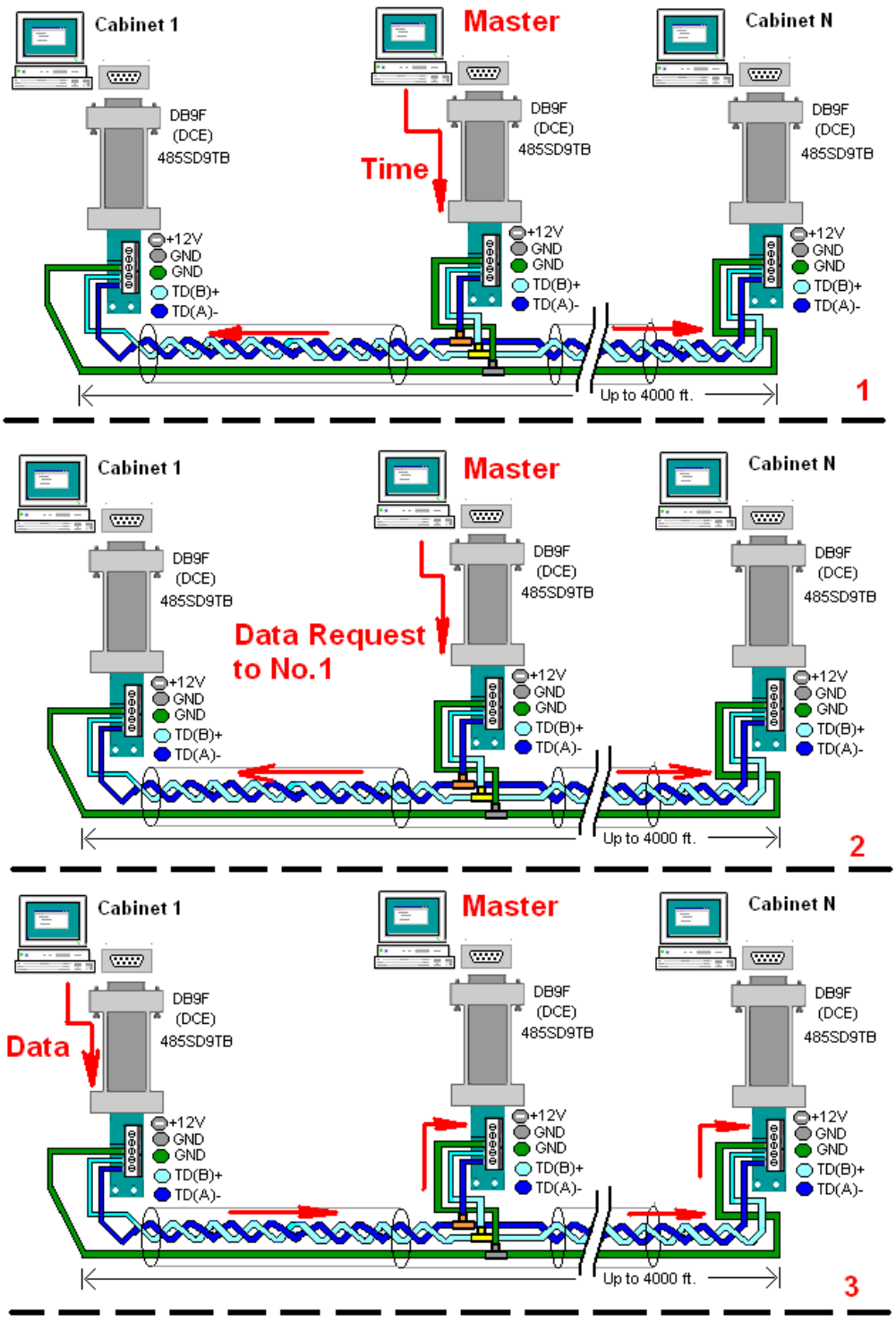

Figure 3.10: Communication Process of RS485 Network in Field.
[Revised On: B&B Electronics, 2003]

After Slave 1 computer finishes its data transfer work, Master computer would ask Slave 2 computer to transfer data and so on so forth. Actually, the RS-485 network works very well between the cabinets from 84th Street to Parklawn Avenue, where the distance in between is approximately 4000 ft. But, unfortunately, the communication from beyond Gallagher Avenue to the master cabinet still has some problem, which can be ascribed to the long distance. Two possible resolutions are proposed to solve this, in terms of the use of RS-485 repeaters and the implementation of cellular wireless communication.

The DSL service provides communication between the data server located in the master control and the database located in the University Traffic Lab. The service is supplied by Qwest, and the used modem is shown in Figure 3.11. The service fee is $40/month and the namely maximal speed is 5 Mbps for download and 2 Mbps for upload. An FTP server is set up on the master industrial computer for the access of the data server. With serial port communication and DSL communication through the data server, the daily log files can be automatically and timely transmitted from the field local industrial computers to the university database.

Figure 3.11: Qwest M1000 DSL Modem.

3.4 Hardware-in-the-loop Simulation

Hardware-in-the-loop Simulation (HILS) is used to test the SMART-SIGNAL data collection before field implementation. Hardware-in-the-loop Simulation is a technique used to evaluate complex real-time systems. It can substantially lower the cost and time for testing expensive, fragile, and unique systems (Gomez, 2001). In transportation engineering, field studies for examing traffic control strategies are not always preferable. They are usually difficult, unsafe and time consuming, which make field studies less attractive compared with microscopic traffic simulation. However, the internal signal control models of the current microscopic simulators lack versatility and some advanced features provided by the real traffic controllers. More importantly, the diversity and complexity of the real world can hardly be presented with a pure software simulator.

The Hardware-in-the-loop Simulation concept bridges the above gaps between the real world traffic operation and simulation. A HILS refers to a system in which parts of a pure simulation is replaced with an actual physical component. The concept of HILS was used in the aerospace industry for more than 40 years (Engelbrecht *et al.*, 1999). In 1995, Venglar and Urbanik introduced the concept of HILS to the field of transportation engineering for the "SMART" diamond project that included a real-time traffic simulation model based on HILS. In 1998, Bullock and Catarella described a real-time simulation environment for evaluating traffic

signal systems, which uses the HILS concept as a testing tool. HILS increases the realism of the simulation and it provides the accessibility to the advanced traffic controller features.

In the transportation engineering field microscopic simulations are becoming important tools to model real world traffic and transportation problems. The existing microscopic simulation engines or models (such as VISSIM) use the internal software controller to perform the signal control operation during simulations. These internal controllers are able to simulate basic fixed time control operations, basic signal coordination and in some cases could simulate actuated controller logic. Advanced signal control, advanced signal coordination, cyclic transition algorithms, signal preemption and transit priority strategies are difficult to emulate in the internal software controller. The internal software controllers are not required to conform to any specifications or standards as required for the external traffic controller. Therefore, introducing an external actual controller would achieve high fidelity and give good credibility to the use of microscopic traffic simulation.

Figure 3.12 represents a schematic diagram of the hardware-in-the-loop simulation. The Hardware-in-the-loop simulation consists of mainly three components; namely: the simulation engine, the controller interface device (CID), and the actual traffic controller. The external controller (hardware) is connected to the simulation engine through an interfacing device know as Controller Interface Device. The CID communicates with the hardware component (actual traffic controller) and software component (microscopic simulation engine) of the system. The CID transmits the signal control indications and synchronization information from the actual traffic controller to the simulation engine, and passes on the detector call / actuation from the simulation engine to the external traffic controller.

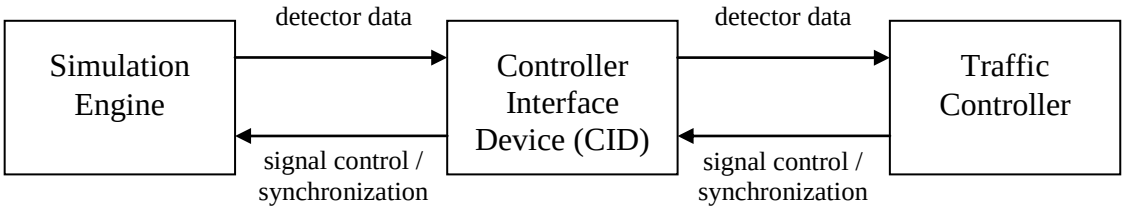

Figure 3.12: Schematic Diagram of Hardware-in-the-loop Simulation.

A software interface module linking a VISSIM simulation model with an Econolite ASC/2-2000 controller has been developed for the Hardware-in-the-loop Simulation. The controller is the same model that is used in the field study. Figure 3.13 shows a snapshot of the HILS running window. The left-side shows the event log window which depicts traffic events. Each logged event starts with a time stamp that includes date, hour, minute, second and millisecond (based on the industrial computer system time), followed by different types of event data including phase change and detector actuation. The right-side is a call-response window which shows the traffic state of the simulated intersection. The rectangles represent detectors and the arrows represent movements with noted phase numbers. A blue-solid rectangle means a vehicle is occupying / passing the detector. Different arrow colors represent different traffic right-of-way status: green arrows mean the movements have the right-of-way, and red arrows

mean the moments have to stop to wait. The current elapsed phasing times are also indicated beside the movement arrows. For example, the figure indicates that Phase 4 and Phase 8 have the right-of-way, and the greens for the phases have been elapsed for 25 seconds. The advance detector for Phase 6 is being occupied by a vehicle. The simulation can also indicate pedestrian calls with a small "human-like" symbol. As shown in the figure, pedestrian calls are received in the northbound and southbound directions (corresponding to Phase 2 and Phase 6, respectively).

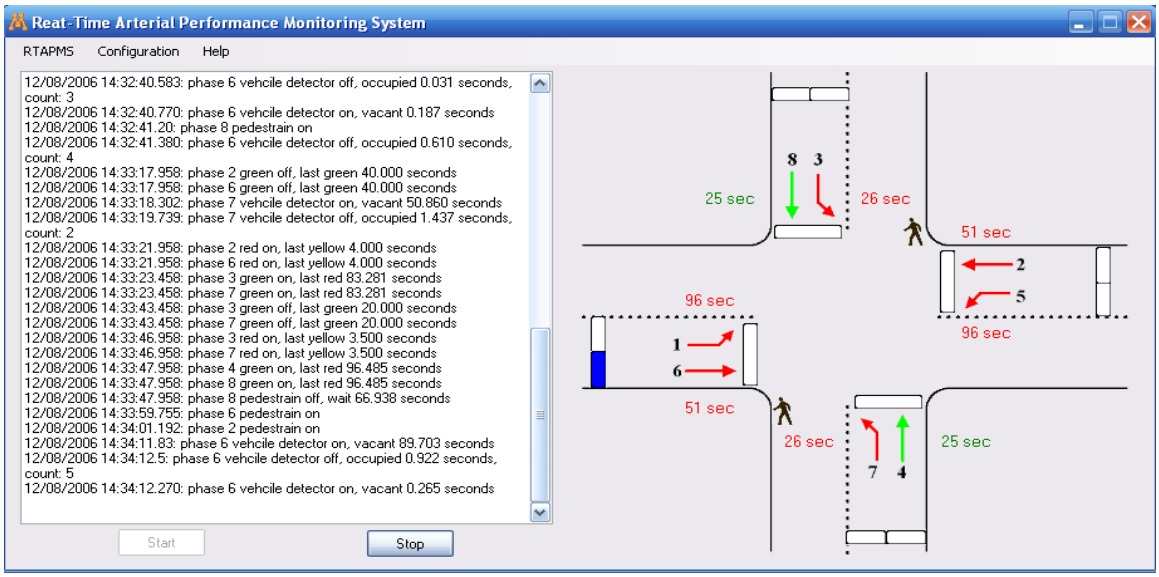

Figure 3.13: Hardware-in-the-loop Simulation Status Window.

Figure 3.14 demonstrates the hardware-in-the-loop of a hypothetical simple network simulated with VISSIM. The left-hand side shows the simulated intersection in VISSIM, and the right-hand side shows the call-response window for the intersection. The signal data are received from the traffic cabinet and the vehicle actuations are received from the VISSIM simulator. As can be seen in the figure, the hardware-in-the-loop simulation can well represent the simulation and traffic control. Both figures show that Phase 1 and Phase 5 are the current right-of-way movements. The states of all the detectors are identical as shown in the two figures. The Hardware-in-the-loop Simulation illustrates the good performance of the SMART-SIGNAL data collection system; field testing can thus be implemented accordingly.

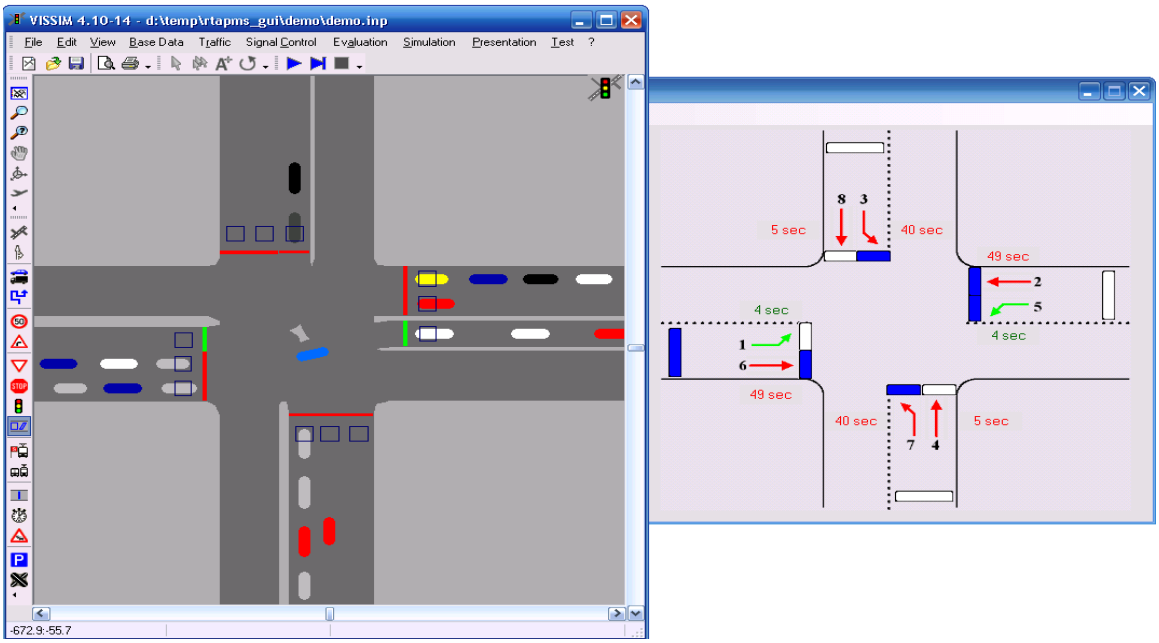

Figure 3.14: Hardware-in-the-loop Implementation with VISSIM.

3.5 Sample Data

SMART-SIGNAL has been installed on 11 intersections of France Avenue in Hennepin County, Minnesota since February 2007. France Avenue was selected for field deployment because it has a wide variety of traffic conditions and it is one of the most congested urban arterials in the Twin Cities Metropolitan Area.

One of the 11 intersections, 76th Street and France Avenue, is selected to demonstrate the data collection process. Figure 3.15 shows the bird's-eye view of the intersection. The intersection is a typical 4-leg actuated signal controlled intersection, so are all other 10 intersections along the study corridor. The 76th Street intersection is selected as the representative because a video camera is installed and operated at this intersection by the Hennepin County Transportation Department. Moreover, system detectors are installed for collecting vehicle counts. The existences of video camera and system detectors provide us ground truth data for validating our proposed arterial performance measurement models. It should be noted that vehicle actuations of the system detectors are recorded by the SMART-SIGNAL, but the data are not used to generate results. They are only used for validation purpose. Most of the signalized intersections do not have system detectors; therefore, we want to propose a more genetic model that has good portability.

Figure 3.15: Bird's-eye View of the Study Intersection at 76th Street and France Avenue at Minneapolis, MN.
[Source: Microsoft Virtual Earth]

The detector layout and signal timing plan of the intersection is shown in Figure 3.16, the rectangles in the figure represent detectors and the arrows in the figure represent phases. Advance detectors for through movements (Phase 2 and Phase 6) and stop-line detectors for left-turn movement (Phase 1 and Phase 5) are installed at the major approaches (approaches on France Avenue); stop-line detectors for both through movement (Phase 4 and Phase 8) and left-turn movements are installed at the minor approaches (approaches on 76th Street). There are system detectors installed at the major approaches as can be seen in the figure.

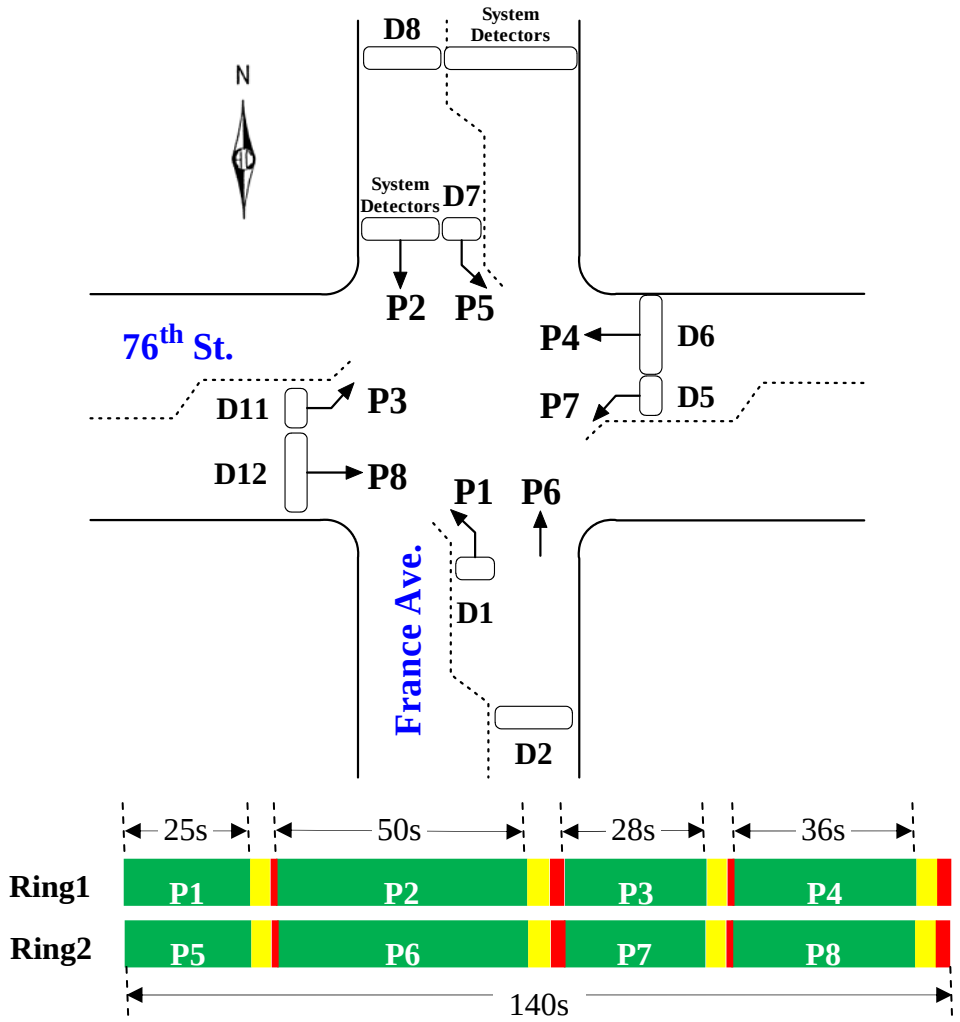

Figure 3.16: Detector Layout and Signal Timing Plan at the Study Intersection.

The timing plan shown in the figure is an eight-phase dual-ring timing plan at peak hours. The cycle length is 140 seconds, and Phase 2 and Phase 6 are the recall phases. To be noted that here the phase means individual movement as defined in NEMA TS-2 (National Electrical Manufacturers Association, 2003).

A sample of data collected at the intersection of 76th Street and France Avenue at Minneapolis, MN at Apr. 19th, 2007, is shown in Figure 3.17. Each logged event starts with the time stamp that includes date, hour, minute, second and millisecond (based on the industrial computer system time), followed by different types of event data including phase change, detector actuation. For example, an event record "16:17:51.687, D2 off, 0.312s" means Detector 2 was off at 16:17:51.687 of the day, and it was occupied for 0.312 seconds; an event record "16:17:54.750, P6 off, 84.594s" means the green time for Phase 6 movement traffic was off at 16:17:54.750, and the green duration was 84.594 seconds.

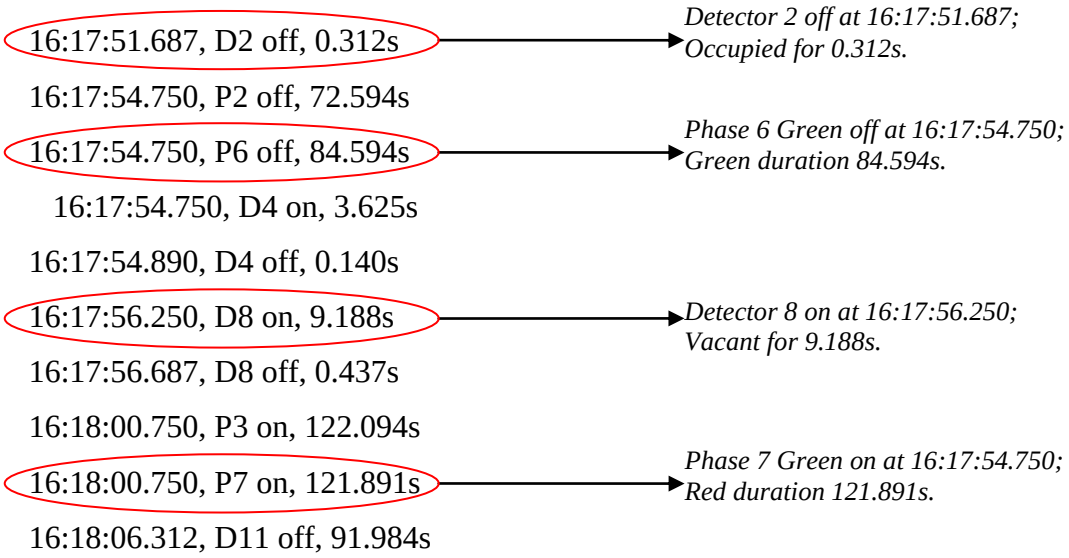

Figure 3.17: Sample Data Collected at the Study Intersection.

3.6 Data Preprocessing

The raw data need to be preprocessed and converted to an easy-to-read format before the performance measurement can be conducted. This section depicts a sample of preprocessed data files including volume, occupancy, signal state and signal timing plan. The four samples in the figure are obtained from the intersection of 76th Street and France Avenue in Minneapolis, MN on Apr. 19th, 2007.

Figure 3.18 shows second-by-second volume recorded at the intersection. Each line of the sample represents a record of one second. The record starts with the record time, which is followed by the vehicle counts within the second at every detectors of the intersection. The detectors are numbered in sequence as *D1*, *D2*, and so on.

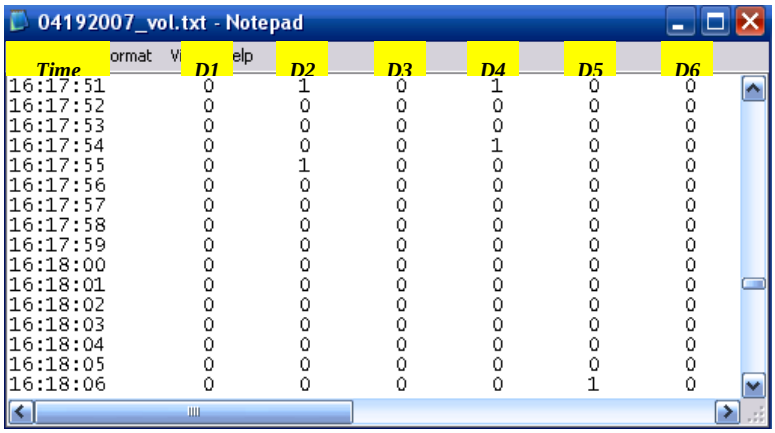

Figure 3.18: Sample Preprocessed Volume Data at the Study Intersection.

Similarly, Figure 3.19 is the second-by-second occupancies of every detectors of the intersection. Each line represents a record of one second that starts with the record time and is followed with the detector occupancies. Both vehicle count and detector occupancy can be directly calculated from the raw detector event data.

04192007_occ.txt - Notepad

Time	D1	D2	D3	D4	D5	D6
16:17:51	1.0	0.3	0.0	0.1	1.0	1.0
16:17:52	1.0	0.0	0.0	0.0	1.0	1.0
16:17:53	1.0	0.0	0.0	0.0	1.0	1.0
16:17:54	1.0	0.0	0.0	0.1	1.0	1.0
16:17:55	1.0	0.4	0.0	0.0	1.0	1.0
16:17:56	1.0	0.0	0.0	0.0	1.0	1.0
16:17:57	1.0	0.0	0.0	0.0	1.0	1.0
16:17:58	1.0	0.0	0.0	0.0	1.0	1.0
16:17:59	1.0	0.0	0.0	0.0	1.0	1.0
16:18:00	1.0	0.0	0.0	0.0	1.0	1.0
16:18:01	1.0	0.0	0.0	0.0	1.0	1.0
16:18:02	1.0	0.0	0.0	0.0	1.0	1.0
16:18:03	1.0	0.0	0.0	0.0	1.0	1.0
16:18:04	1.0	0.0	0.0	0.0	1.0	1.0
16:18:05	1.0	0.0	0.0	0.0	1.0	1.0
16:18:06	1.0	0.0	0.0	0.0	0.8	1.0

Figure 3.19: Sample Preprocessed Occupancy Data at the Study Intersection.

Figure 3.20 shows second-by-second signal states of the intersection. Each record starts with the record time and is followed by the states of every signal phases. The signal phase state includes three parts. The first part is a character which indicates the signal status of the phase at the record time: 'R' represents red signal, 'Y' represents yellow signal, and 'G' represents green signal. The second part is a number which is the elapsed seconds of the signal status indicated in the first part. The last part is a number which is the remaining seconds of the signal status indicated in the first part. For instance, the first line in Figure 3.20 means at time 16:17:51, the red time of Phase 1 was elapsed for 70 seconds and the remaining red time was 62 seconds; the green time of Phase 2 was elapsed for 69 seconds with 3 seconds left.

04192007_sig.txt - Notepad

Time	Phase1	On	Remain	Phase2	On	Remain
16:17:51	R	70	62	G	69	3
16:17:52	R	71	61	G	70	2
16:17:53	R	72	60	G	71	1
16:17:54	R	73	59	Y	0	4
16:17:55	R	74	58	Y	1	3
16:17:56	R	75	57	Y	2	2
16:17:57	R	76	56	Y	3	1
16:17:58	R	77	55	R	0	72
16:17:59	R	78	54	R	1	71
16:18:00	R	79	53	R	2	70
16:18:01	R	80	52	R	3	69
16:18:02	R	81	51	R	4	68
16:18:03	R	82	50	R	5	67
16:18:04	R	83	49	R	6	66
16:18:05	R	84	48	R	7	65
16:18:06	R	85	47	R	8	64

Figure 3.20: Sample Preprocessed Signal State Data at the Study Intersection.

Figure 3.21 shows cycle-by-cycle signal timing plans of the intersection. Each records starts with the cycle length and is followed by the cycle starting time and the timing plans of every signal phases. The signal phase timing plan includes four parts. The first part is the green starting time of the phase, and the other three are the green duration, yellow duration, and red duration of the phase. For instance, the first line in Figure 3.21 means a 140-seconds cycle started from time 16:03:54. The green time of Phase 1 started at time 16:04:47, and the green duration, yellow duration, and red duration of the Phase 1 were 18.4 seconds, 3.5 seconds and 402.4 seconds, respectively. This record implies that Phase 1 was skipped during former cycles since its red duration is longer than the cycle length. Note that Phase 6 is the recall phases of the intersection and the ending time of Phase 6 is counted as the starting time of next cycle of this intersection. Both signal state and signal timing plan can be also directly calculated from the raw signal event data.

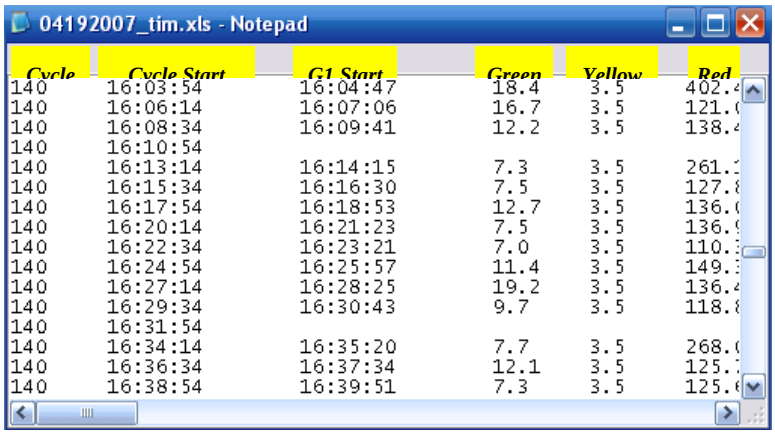

Figure 3.21: Sample Preprocessed Signal Timing Plan at the Study Intersection.

3.7 SMART-SIGNAL Data Processing Flow Chart

Figure 3.22 shows the SMART-SIGNAL data processing flow chart. The data process begins after the raw data is transmitted back to the University lab. The first module in this procedure is the Data Verification, which examine all the raw records to see whether there are some errors in the data set. For instance, if one detector is occupied 24 hours a day, it is obviously that the detector goes wrong. Also, if one phase or one detector never occurs in one file, it is most likely that the corresponding connection is loose, which need to be fixed in the field.

The second module is the Preprocessing module, which generates some basic measures from the raw data. The preprocessed data has 4 groups, in terms of volume, occupancy, signal state and timing plan, and all the future performance measures are based on these preprocessed data.

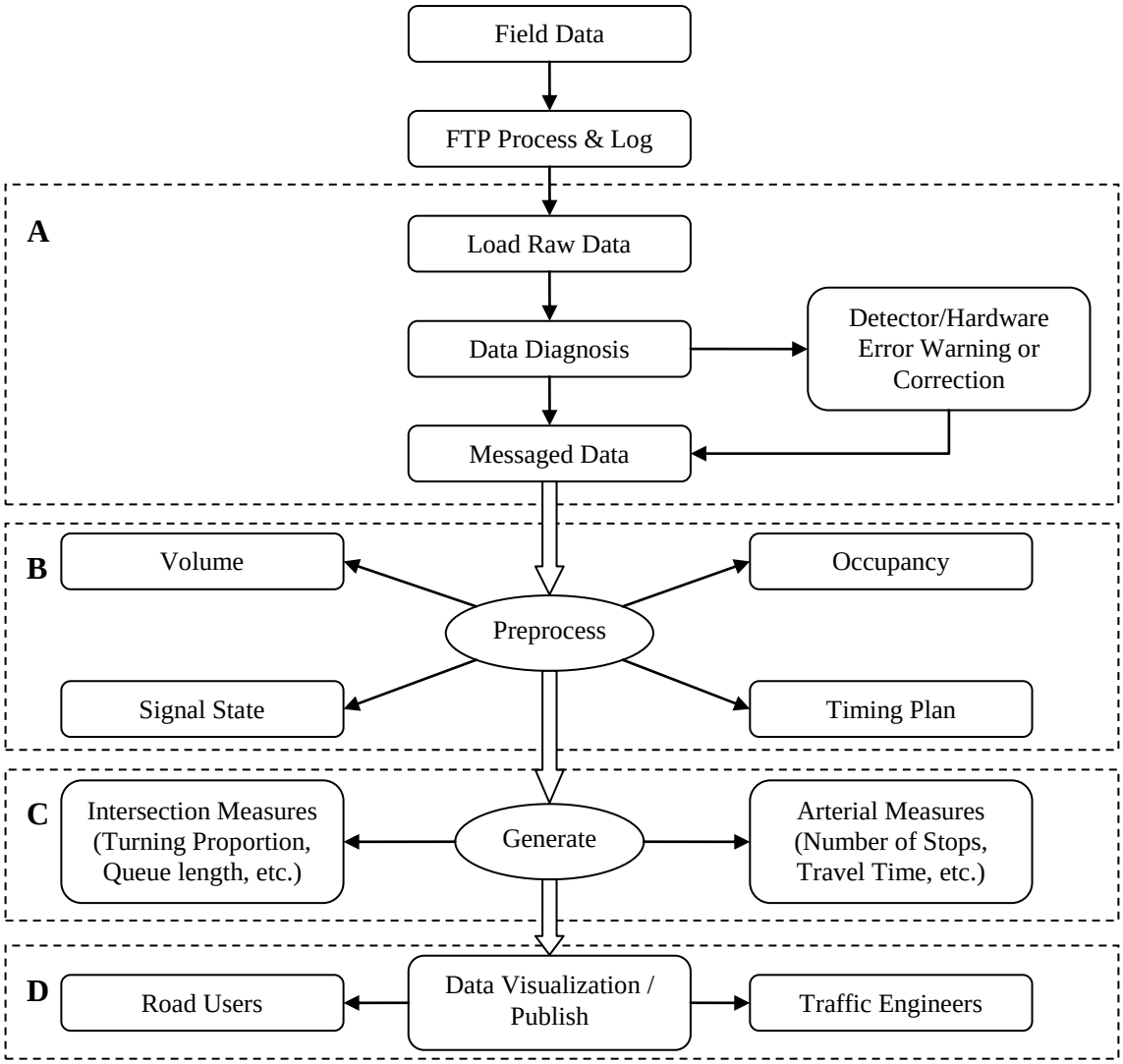

Figure 3.22: SMART-SIGNAL Data Process Flow Chart.

The third level of the data processing is the performance measure calculation. In this part, aggregated volume, delay, queue size, queue length, travel time and etc are derived from the preprocessed data using different algorithms. Finally, the generated measures can be visualized and published through various techniques for road users and traffic engineers. Based on the different types of performance measures, diagnosis and fine-tune of traffics signal system can be achieved.

3.8 Internet Access

Once the performance measures are generated by the proposed mathematical models, different users can use the interfaces on the internet to access these data and process specific calculations. As shown in Figure 3.23, users can choose a date and intersection they concern, performance measures in a certain period can be calculated and displayed on the website, in terms of Volume,

Queue Size, Queue Length and etc. Also as shown in Figure 3.24, on the arterial level, if the user specifies a starting intersection and ending intersection, travel time and average speed along this corridor can be generated as well.

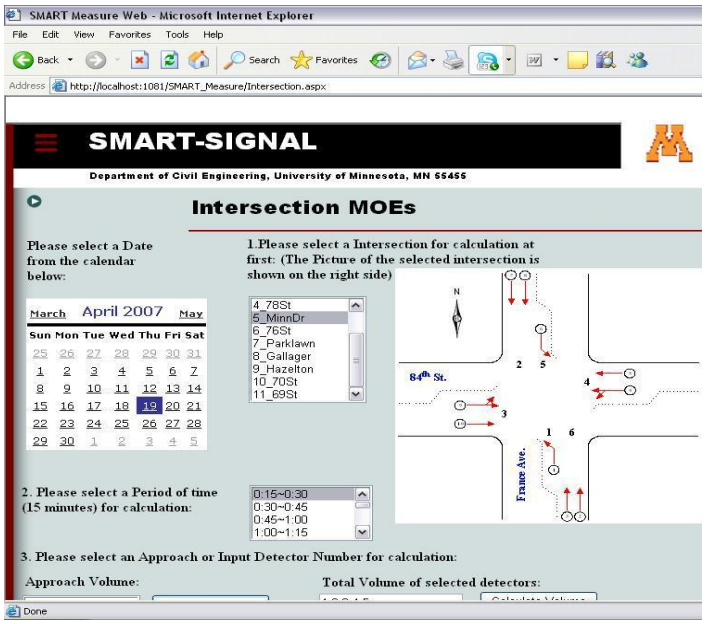

Figure 3.23: Internet Access to Intersection Performance Measures.

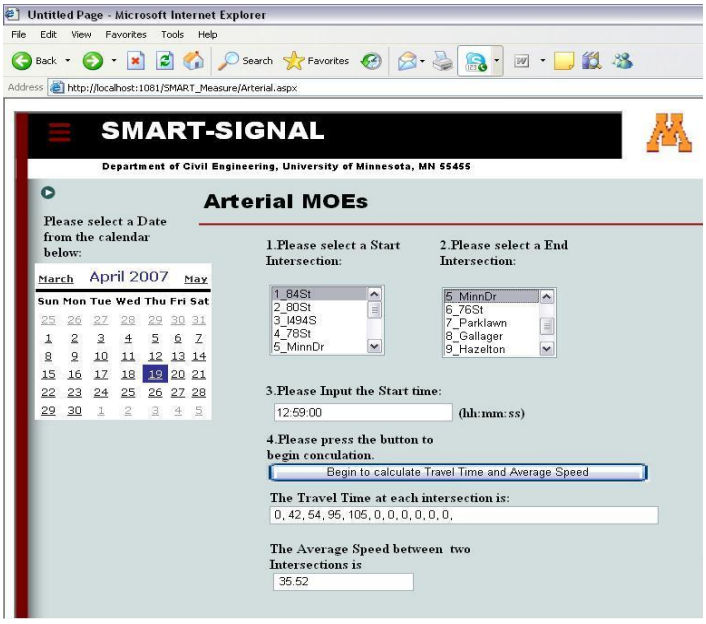

Figure 3.24: Internet Access to Arterial Performance Measures.

3.9 Detector Configuration Discussion

Detector plays an important role in field traffic collection. All of the vehicle actuation data are directly obtained from field detectors. Their functionality, configuration, and location determine not only the quantity and quality of traffic data, but also the applicability and validity of performance measurement models.

For many actuated signalized intersections, detectors are deployed as the intersection of 76th Street and France Avenue shown in Figure 3.16 (except the system detectors): advance detectors, not stop-line detectors, are installed at the major roads to extend green time for though traffic; stop-line detectors are installed at the minor roads and the left-lanes of the major roads; and there is no specific detectors installed for right-turn movement traffic.

The detector configuration will significantly impact the accuracy of the data collected from field. Essentially, there are two types of detectors on a multiple-lane link as shown in Figure 3.25: lane-based detectors and link-based detectors. Lane-based detectors are parallel installed at each lane. Every detector has specific wire to connect with the back panel of the traffic cabinet, and they respond vehicle actuation separately. Link-based detectors are also installed at individual lanes; however, they are wired together to connect the traffic cabinet. They can only generate one response and the traffic cabinet cannot distinguish the source of the actuation in terms of lanes. Link-based detectors can only indicate the presence of the vehicle, so they are also called as presence detectors. The detectors installed in the study site (i.e., France Avenue) are link-based detectors.

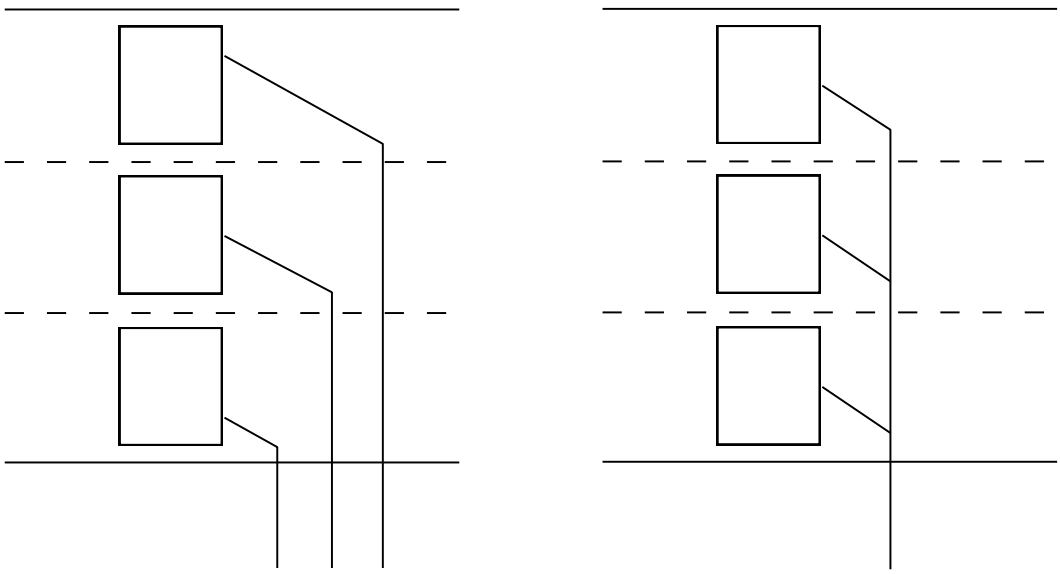

a) Lane-based Detector ***b) Link-based Detector***

Figure 3.25: Configurations of Lane-based and Link-based Detectors.

Comparing with link-based detectors, lane-based detectors provide more accurate vehicle counts; however, majority of transportation agencies do not archive traffic counts at most of their managed intersections. Detectors are only used for the actuated traffic signals. Link-based

detector configurations may reduce maintenance work to traffic engineers, but will have missing count problems when they are used for counting purpose.

Figure 3.26 shows missing count problem at advance detectors. When two vehicles parallel passing the detector at almost the same time, i.e., the latter vehicle is on the detector before the former vehicle is off the detector, the detector will only report one actuation instead of two actuations to traffic cabinet. Traffic flow count is thus under-measured.

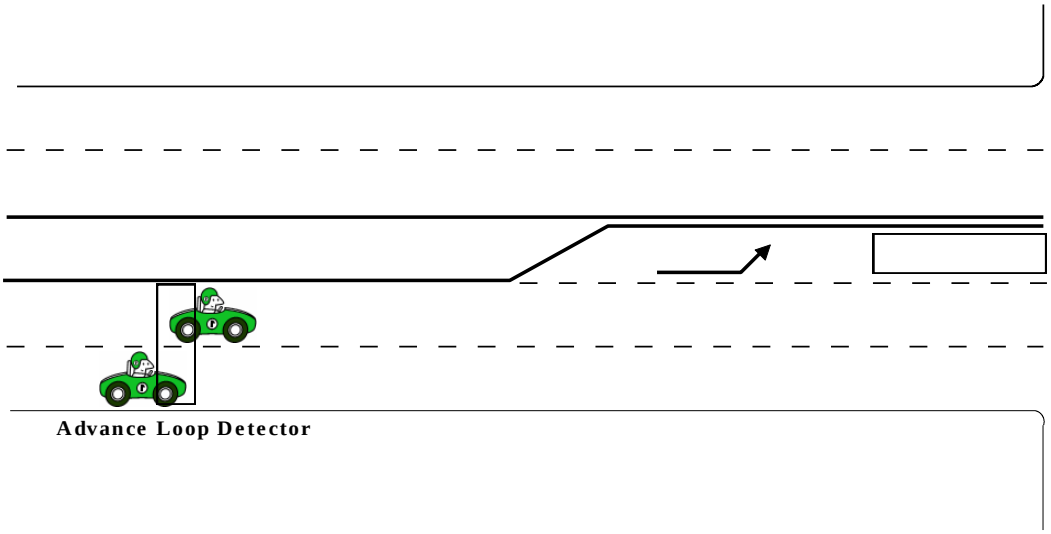

Figure 3.26: Missing Count Problem at Advance Loop Detectors.

Figure 3.27 shows missing count problem at left-turn detectors. When two vehicles occupied at the detector waiting for the green phase, i.e., the latter vehicle is on the detector when the left-turn signal is red, the detector will only report one actuation to traffic cabinet and the vehicle count is also under-measured.

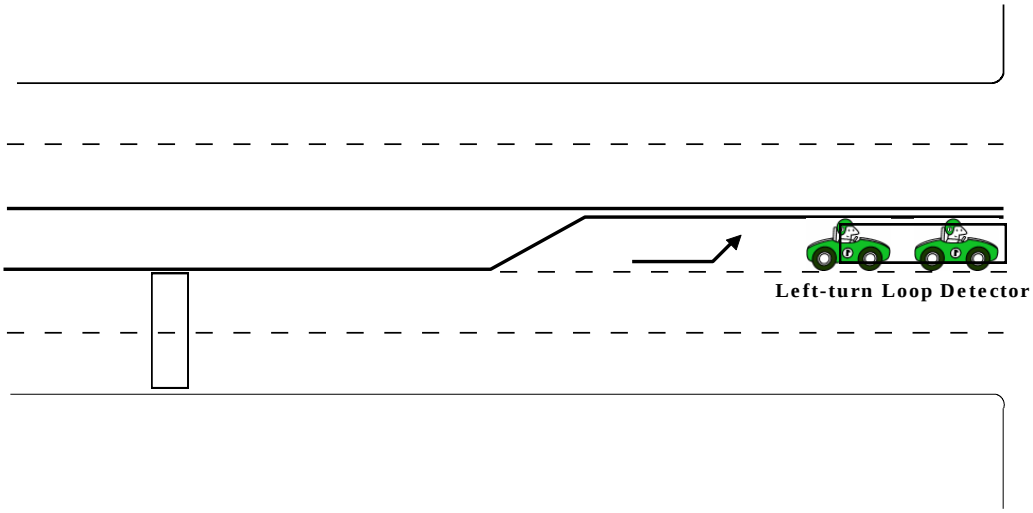

Figure 3.27: Missing Count Problem at Left-turn Loop Detectors.

Missing count problems described above are detected in the field study site at France Avenue. The traffic count measured by the SMART-SIGNAL system is about 8% lower than the actual vehicle count from ground truth video data. However, the performance measures generated from the SMART-SIGNAL system are not significantly impacted by the missing count problem (the results are presented in the following chapters). We believe that the SMART-SIGNAL system will do better job if lane-based detectors are available, corresponding testing and research work are being investigated by the colleague of the author in another corridor with lane-based detector systems.

Chapter 4. Intersection Performance Measurement

Queue length and turning movement proportion (TMP) are arguably the most important performance measures at isolated intersections. They provide important traffic information for advanced traffic management systems, and have been used as input data for many adaptive control systems. They are not only used to evaluate the operation of traffic signal systems, but also used to generate some other intersection measures, such as intersection delay and level of service. In the following, proposed mathematical models for the estimation of queue length and turning movement proportions are discussed, and results from field implementation are also presented.

4.1 Queue Estimation

4.2.1 Definition of Queue

The definitions of queue and queue length need to be clarified before we discuss the queue length estimation model. According to the Highway Capacity Manual 2000, queue is defined as:

- "*a line of vehicles, bicycles, or persons waiting to be served by the system in which the flow rate from the front of the queue determines the average speed within the queue. Slowly moving vehicles or people joining the rear of the queue are usually considered part of the queue.* "

The above definition indicates that a queue contains not only stacked vehicles but also approaching vehicles that are affected. Therefore, a queue is divided into two parts: the standing queue which is composed of motionless stacked vehicles behind the stop-line, and the moving queue which is composed of moving vehicles that are impacted (i.e., forced to decelerate) by the signal or the standing queue. Since both standing queue and moving queue will affect the driving behavior of the virtual probe, they both need to be included in queue estimation.

The definition of queue length is mixed up with queue size by some researchers. Strictly speaking, queue length should be the physical length from intersection stop-line to the queue rear, i.e. the distance between the stop-line and the back of the last queued vehicle. However, traffic engineers often use the number of vehicles in the queue as the so-called "queue length" instead of the physical queue length. They usually simplify the variation of vehicle composition with passenger cars, trucks, buses and etc as uniform vehicles. The difference of vehicle types and models is less considered. In this project, we define queue length as the physical length of the queue, and queue size the number of queued vehicles.

Vehicles in a standing queue are usually assumed stacking uniformly with jam density and discharging with saturation flow rate. However, the concept of "moving queue" is difficult to define: queued vehicles are approaching the standing queue with various speeds. Queue length and queue size in a moving queue are difficult to measure because it is hard to identify the rear of the moving queue. However, the purpose of studying intersection queue is to investigate the impact of the queue to new arrival vehicles. The speed and location of the last queued vehicle are the key factors that will affect driver activities of the new arrival vehicles. Here, the last queued vehicle is the rear-end vehicle of the standing queue if there is no moving queue, or the rear-end vehicle of the moving queue if it exists.

To overcome the difficulty for the estimation of moving queue, "dummy vehicles" are added behind the rear of the original standing queue to represent the effect of the moving queue. As shown in Figure 4.1, assuming Vehicle *Q* is the last queued vehicle of the moving queue, and it would stop at the location of Vehicle *Q'*. Therefore, Vehicle *Q'* is the representative vehicle of Vehicle *Q* because they have the similar impact to the following vehicles in terms of maneuver decisions. In the following of this report, the definition of the queue is the "equivalent standing queue", which includes both standing queue and additional dummy vehicles representing moving queue. Queue length is the distance from the stop-line to the rear of the "equivalent standing queue", and queue size is the number of vehicles in the "equivalent standing queue".

This project proposes a model to estimate intersection queue length based on the traffic data collected from the SMART-SIGNAL data collection system. Queue estimation models for both short queue and long queue are discussed next.

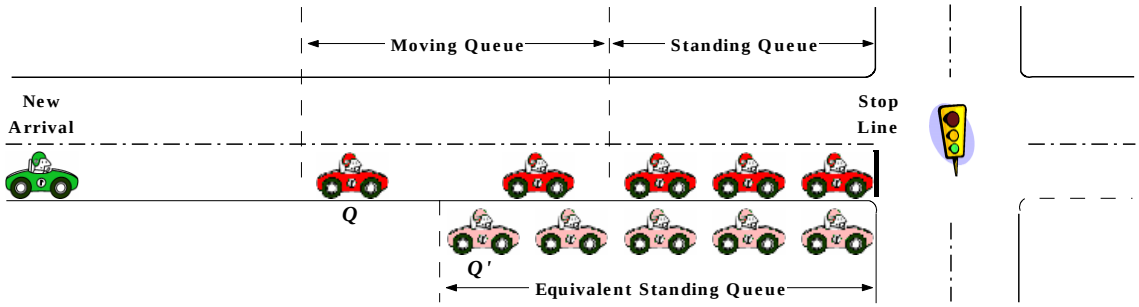

Figure 4.1: Queue at a Signalized Intersection.

4.2.2 Queue Discharge Process

Figure 4.2 shows the development of a single-lane queue along the time-distance coordinates. Usually, input (i.e. the arrival counts $N_A(\tau)$) and output (i.e. the departure counts $N_D(\tau)$) can be used to calculate the queue length. However, queue length may not be simply calculated as $h \times \left(N_A(\tau) - N_D(\tau)\right)$, where h is the saturated space headway. As Stephanopoulos and Michalopoulos (1979) pointed out, shortly after the commencement of green time, the queue length would not decrease regardless the net difference of $N_A(\tau)$ and $N_D(\tau)$, until the discharging wave reaches the rear of the queue. The queue length increases until the shock wave reaches the last queued vehicle, i.e., when the queue is cleared.

Figure 4.2 shows the development of a single-lane queue along the time-distance coordinates. During the red time, vehicles arrived at the intersection are queued behind the stop-line and queue length is increasing along with time. At time point T_g, green light for this approach is on. After the reaction time t_r, the first queued vehicle starts to move and the discharge shockwave propagates backward. During the queue clearing process, newly arrived vehicles will be joining the queue and the queue length will be still increasing. At time T_D the last queued vehicle starts to move and queue length begins to decrease. When the last queued vehicle passes the stop-line, the queue is cleared. How to estimate the time dependent queue length, represented by the dark black line in the figure, is crucial to other performance measures for both individual intersection and arterial corridor.

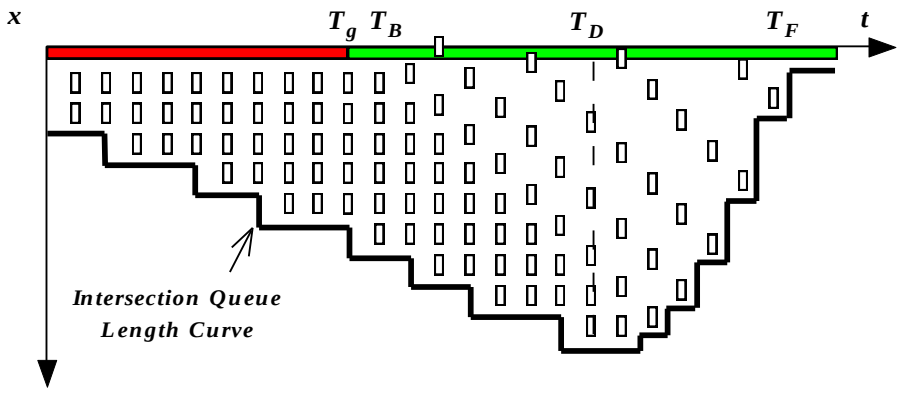

Figure 4.2: Demonstration of Queue Development at a Signalized Intersection.

Essentially, the discharge of queue is determined by four time instants as depicted in Figure 4.2: T_B is the time when the first queued vehicle starts to move, i.e., the starting time of queue discharge; T_D is the time when the discharge wave propagates to the rear of the queue, when the last queued vehicle starts to move; T_F is the time when the last queued vehicle passes the stop-line; and T_G is the time when the last queued vehicle accelerates to the desired speed. It can be seen that the intersection queue length keeps increasing until time T_D, and then decreases after the discharge wave reaches the rear of the queue.

Figure 4.3 shows the discharge trajectories of a single-lane queue along the time-distance coordinates. If there is stop-line detector available, the queue discharge pattern could be measured; otherwise, it could be estimated based on assumed queue discharge pattern. Assuming t_s is the uniform starting time difference between two adjacent queued vehicles, then the queue discharge propagates from the front to the rear as shown in the figure: the first vehicle starts at time $T_g + t_r$, the second vehicle starts at time $T_g + t_r + t_s$, …, and the n^{th} vehicle in the queue starts at time T_n^s, which can be calculated as Equation 4.1:

$$T_n^s = T_g + t_r + (n-1)t_s \tag{4.1}$$

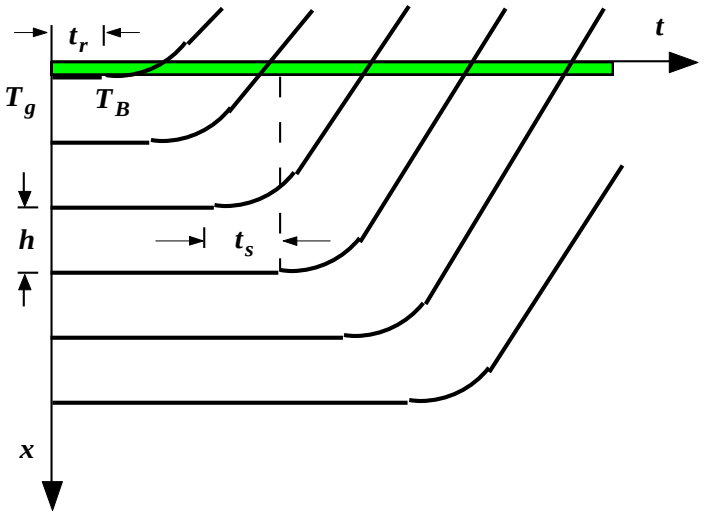

Figure 4.3: Demonstration of Queue Discharge at a Signalized Intersection.

The rationality of the queue discharging assumption can be validated by a time headway analysis at the stop-line. According to the above queue discharging pattern, the first vehicle passes the stop-line at time $T_g + t_r$ (here we use the time when vehicle's front bumper passes the stop-line); the second vehicle passes the stop-line at time $T_g + t_r + t_s + \sqrt{2h/\gamma_a}$ (here h is the saturated space headway and γ_a is the acceleration rate) ; the third vehicle passes the stop-line at time $T_g + t_r + 2t_s + \sqrt{2h/\gamma_a} \cdot \sqrt{2}$; ...; and the n^{th} vehicle passes the stop-line at time T_n^l, which can be calculated as Equation 4.2:

$$T_n^l = T_g + t_r + (n-1)t_s + \sqrt{2h/\gamma_a} \cdot \sqrt{(n-1)} \qquad (4.2)$$

Therefore, the first measured time headway at the stop-line should be $t_s + \sqrt{2h/\gamma_a}$; the second measured time headway at the stop-line should be $t_s + \sqrt{2h/\gamma_a} \cdot (\sqrt{2}-1)$; and the n^{th} measured time headway at the stop-line t_n^h can be calculated as Equation 4.3:

$$t_n^h = t_s + \sqrt{2h/\gamma_a} \cdot (\sqrt{n} - \sqrt{n-1}) \qquad (4.3)$$

The time headway of the discharging queue is then shown as Figure 4.4(a). As vehicles released from the stop-line, the time headway captured at the stop-line becomes stable to a constant value t_s. A similar figure (Figure 4.4(b)) can be found as Figure 17.1 in the Traffic Engineering textbook (Roess, *et al.* 2004). This demonstrates that the queue discharge assumption made in this project is reasonable.

4.2.3 Short Queue Estimation Model

Depending on the availability of vehicle arrival information, the queue estimation model can be divided into two categories: short queue estimation and long queue estimation. If vehicle arrivals can be measured using advance loop detector and queue length is less than the distance between

the advance loop detector and the stop-line, it is a short queue by our definition. Otherwise, it is a long queue when the rear of the queue is beyond the advance loop detector. As shown in Figure 4.5, vehicle arrivals can be directly measured from the advance loop detector when queue is short and vehicles are not accumulated to spill over the detector. Short queue can be estimated according to the queue development demonstrated in Figure 4.2, which is described in the following.

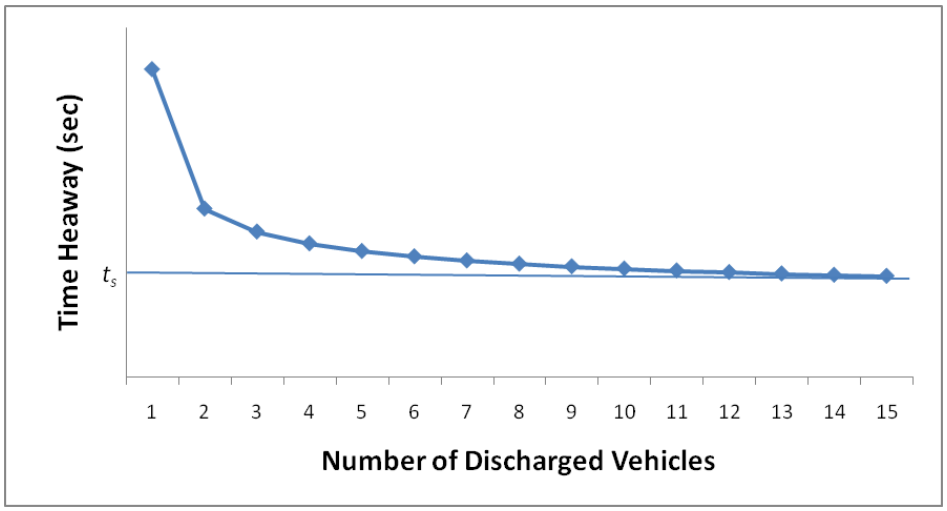

a) Concluded from Equation 4.3

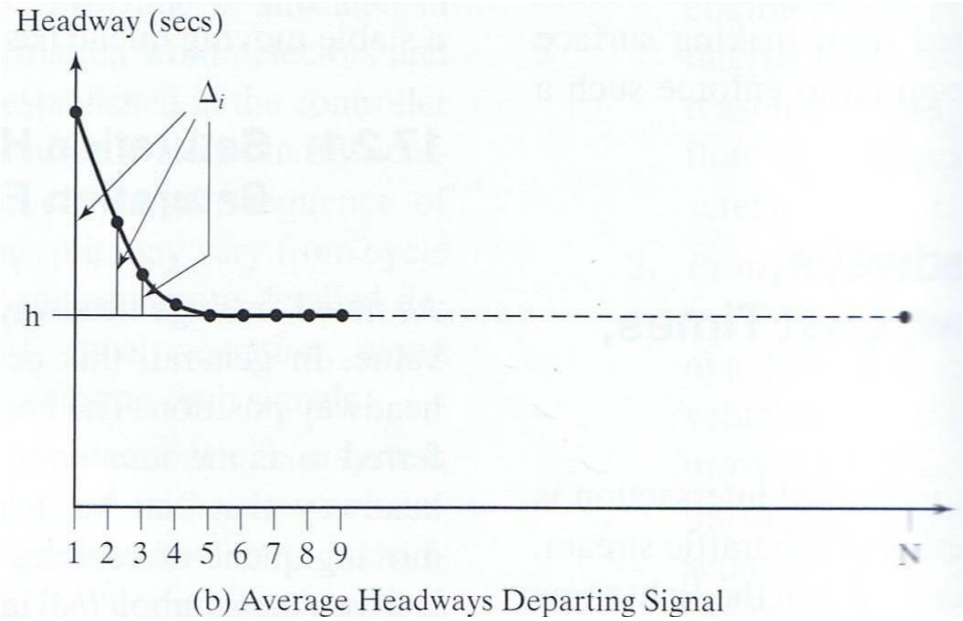

b) In Figure 17.1 of the Traffic Engineering Textbook

Figure 4.4: Queue Discharge Time Headway at a Signalized Intersection.

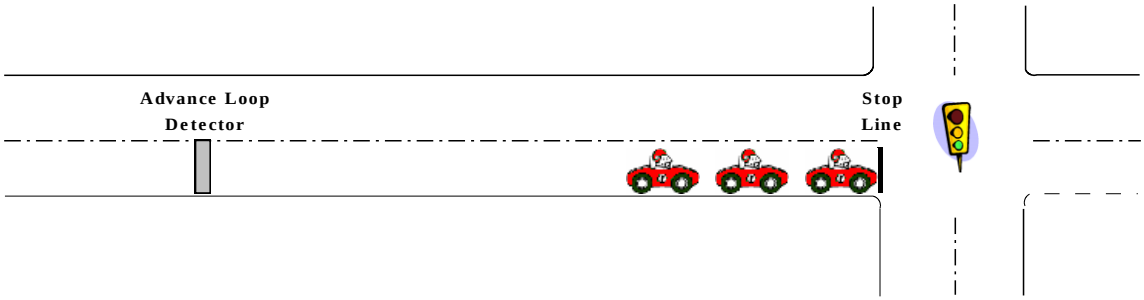

Figure 4.5: Demonstration of Short Queue at a Signalized Intersection.

As shown in Figure 4.2, T_D is an inflexion point of the intersection queue length curve: the time dependent queue length $L_q(\tau)$ increases before T_D and decreases after T_D. T_B is equal to the green starting time T_g plus a first vehicle reaction time t_r; T_D is equal to T_B plus the time queue discharge shockwave propagates to the rear of the queue; and T_G is equal to T_D plus the acceleration time. They can be calculated as in Equation 4.4 ~ Equation 4.6:

$$T_B = T_g + t_r \tag{4.4}$$

$$T_D = T_B + t_s \cdot \left(n_q(\tau) - 1\right) \tag{4.5}$$

$$T_G = T_D + \frac{u_f}{\gamma_a} \tag{4.6}$$

where $n_q(\tau)$ is the maximum number of queued vehicles accumulated behind the stop-line from the starting of last red time T_r to time τ within a cycle. The calculation of T_F is a little bit complex, which will be presented later in this section.

The calculation of $n_q(\tau)$ is based on time τ: from the red starting time T_r to time T_D, queue size keeps increasing, and $n_q(\tau)$ is equal to the residual queue from last cycle plus vehicle arrivals during the time interval [T_r, τ]; after time T_D, discharge propagates to the rear and queue size decreases, $n_q(\tau)$ is equal to the maximum number it reaches in the cycle at time T_D. Assuming $n(t)$ is the number of vehicles passing the advance loop detector within time period [t, $t+\Delta t$], $n_q(\tau)$ can be calculated as in Equation 4.7:

$$n_q(\tau) = \begin{cases} N_A(T_r) - N_D(T_r) + \sum_{t=T_r}^{\tau-\Delta t} n(t), & T_r \le \tau \le T_D \\ n_q(T_D), & otherwise \end{cases} \tag{4.7}$$

where $N_A(T_r) - N_D(T_r)$ is the net difference between the arrival counts and the departure counts at the beginning of last red time T_r, i.e., the residual queue from last cycle. $N_A(\tau)$ can be obtained from the advance loop detector, and $N_D(\tau)$ can be calculated based on an assumed discharging rate if no stop-line detector is available.

The calculation of T_F depends on if the last queued vehicle accelerates to the desired speed u_f first or passes the stop-line first, which is described as following.

- **Queue Rear Passes Stop-line First**

When $h \cdot n_q(T_D) \leq u_f^2/2\gamma_a$, the last queued vehicle passes the stop-line first, (i.e., $T_F \leq T_G$), and T_F is equal to T_D plus its travel time from the rear to the stop-line, which can be calculated as in Equation 4.8:

$$T_F = T_D + \sqrt{\frac{2h \cdot n_q(T_D)}{\gamma_a}} \tag{4.8}$$

Correspondingly, the calculation of queue length $L_q(\tau)$ has three cases: before time T_D, queue length is equal to headway times queue size; between time T_D to T_F, queue length is equal to the maximum queue length within the cycle ($h \cdot n_q(T_D)$) minus the travelled distance of the last queued vehicle; and afterwards when the last queued vehicle has been discharged from the stop-line, queue is cleared and the queue length is equal to zero. $L_q(\tau)$ can be calculated as in Equation 4.9:

$$L_q(\tau) = \begin{cases} h \cdot n_q(\tau), & T_r \leq \tau \leq T_D \\ h \cdot n_q(T_D) - \frac{1}{2}\gamma_a(\tau - T_D)^2, & T_D < \tau \leq T_F \\ 0, & T_F < \tau \end{cases} \tag{4.9}$$

The speed of the last queued vehicle $u_q(\tau)$ is a measure that will be used later to calculate travel time. Its calculation involves two cases: before time T_D, it is equal to zero; between time T_D to T_F, it is linearly increasing with the travel time of the last queued vehicle; and it does not exist after T_F since when the queue length is then equal to zero. $u_q(\tau)$ can be calculated as in Equation 4.10:

$$u_q(\tau) = \begin{cases} 0, & T_r \leq \tau \leq T_D \\ \gamma_a \cdot (\tau - T_D), & T_D < \tau \leq T_F \end{cases} \tag{4.10}$$

- **Queue Rear Accelerates to u_f First**

If $h \cdot n_q(T_D) > u_f^2/2\gamma_a$, the last queued vehicle accelerates to u_f first, (i.e., $T_F > T_G$), and the travel time of the last queued vehicle to the stop-line can be decomposed into two components: the time it accelerates from zero to the desired speed and the time it travels with the desired speed until it arrives the stop-line. T_F can be calculated as Equation 4.11:

$$T_F = T_D + \frac{u_f}{2\gamma_a} + \frac{h \cdot n_q(T_D)}{u_f} \tag{4.11}$$

Correspondingly, queue length calculation has four cases based on time τ: before time T_D, it is equal to the space headway multiplies queue size; between time T_D to T_G, it is equal to the maximum queue length minus the travelled distance of the last queued vehicle, which is in

acceleration state; between time T_G to T_F, it is equal to the maximum queue length minus the travelled distance of the last queued vehicle, which travels with the desired speed; and afterwards, queue is cleared and the queue length is equal to zero. $L_q(\tau)$ can be calculated as Equation 4.12:

$$L_q(\tau) = \begin{cases} h \cdot n_q(\tau), & T_r \le \tau \le T_D \\ h \cdot n_q(T_D) - \frac{1}{2}\gamma_a(\tau - T_D)^2, & T_D < \tau \le T_G \\ h \cdot n_q(T_D) + \frac{u_f^2}{2\gamma_a} - u_f(\tau - T_D), & T_G < \tau \le T_F \\ 0, & T_F < \tau \end{cases} \quad (4.12)$$

The calculation of $u_q(\tau)$ involves three cases: before time T_D, it is equal to zero; between time T_D to T_G, it is linearly increasing with the travel time of the last queued vehicle; between time T_G to T_F, the vehicle travels with the desired speed; and $u_q(\tau)$ does not exist after T_F since when the queue length is equal to zero. $u_q(\tau)$ can be calculated as in Equation 4.13:

$$u_q(\tau) = \begin{cases} 0, & T_r \le \tau \le T_D \\ \gamma_a \cdot (\tau - T_D), & T_D < \tau \le T_G \\ u_f, & T_G \le \tau \le T_F \end{cases} \quad (4.13)$$

4.2.4 Long Queue Estimation Model

- **Demonstration of Long Queue**

When queues spill over the advance loop detector or even back to the upstream intersections under congestion, the proposed model is still valid as long as we know $n_q(\tau)$. However, the queue estimation model becomes more complicated under such traffic conditions. As shown in Figure 4.6, the advance detector is occupied by a queued vehicle and $n_q(\tau)$ cannot be directly measured using the volume data from the detector. Additional information, beyond the vehicle count provided by the advance loop detector, is apparently needed. When queues extend over the detector, high values of detector occupancy will be observed. There is a relationship between queue length and detector occupancy. In this project, we propose an approach for long queue estimation by investigating the relationship between queue length and detector occupancy values.

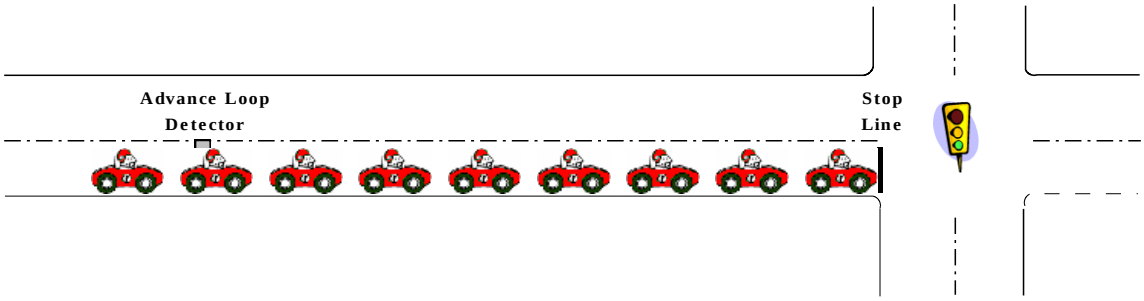

Figure 4.6: Demonstration of Long Queue at a Signalized Intersection.

- **Relationship of Queue Development and Occupancy Profile**

Before describing the proposed long queue estimation model, we first analyze the relationship between queue length and occupancy profile from loop detector based on shockwave theory. As shown in Figure 4.7, the queue is accumulated behind the stop-line after red time starts. The detector measures vehicle arrivals and the occupancy profile represents the vehicle arrival pattern. When queue extends over the detector at time T_A, the occupancy value δ jumps to 1.0 because the detector is occupied. At time T_g, the green light is on and discharge shockwave begins to propagate upstream at time T_B (after a reaction time t_r of the first queued vehicle). The occupancy δ keeps 1.0 until the discharge shock wave propagates to the detector at time T_C. As has been discussed previously, the queue length still increases until time T_D, when the last queuing vehicle starts to accelerate. Assume that the last queued vehicle passes the advance detector at time T_E. If the green time is long enough, the last queued vehicle is going to reach the stop-line before green time end, and the queue is cleared; otherwise, the residual queue is going to stack at and forms a queue to the next cycle.

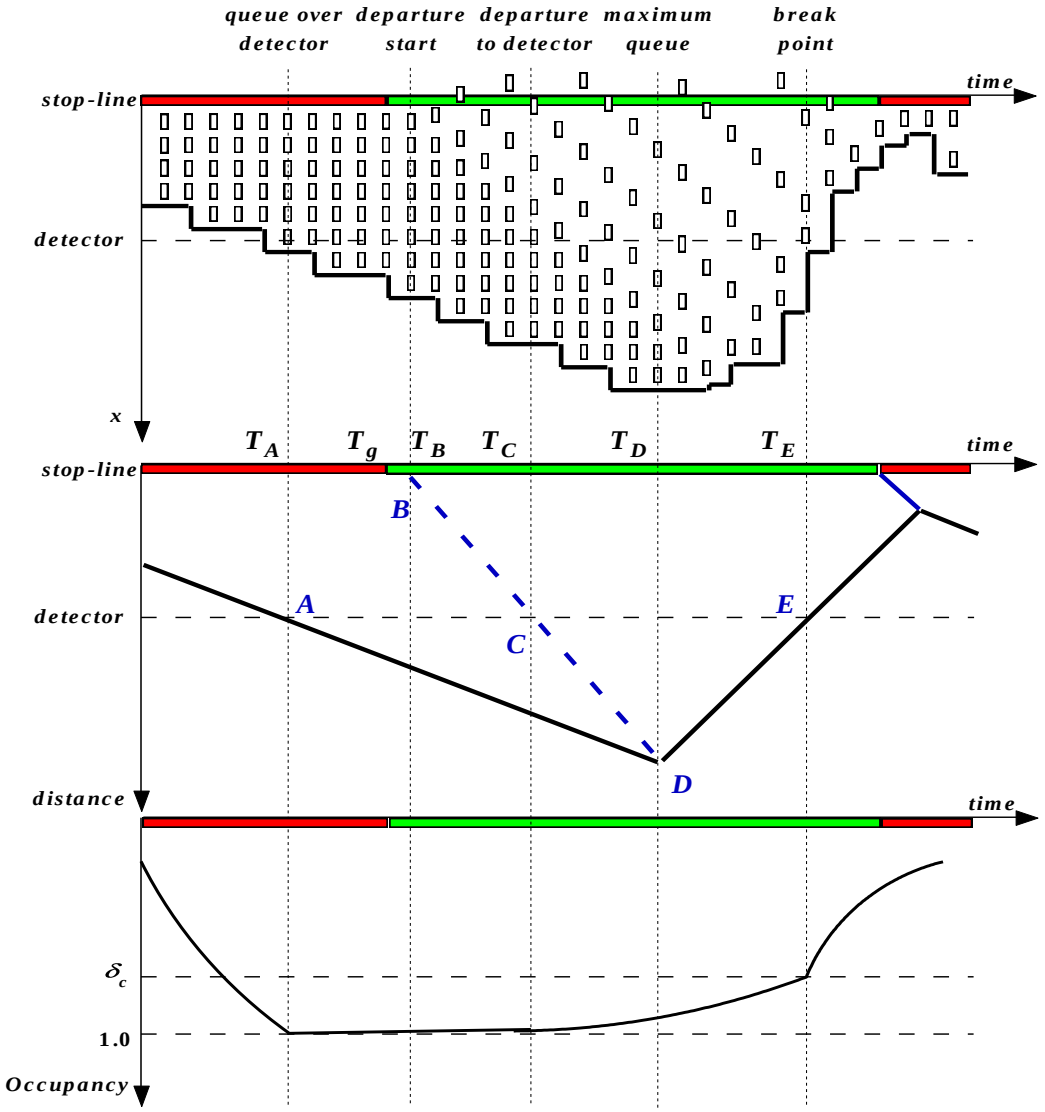

Figure 4.7: Relationship of Queue Development and Occupancy Profile at a Signalized Intersection.

Successfully identifying points *A*, *B*, *C*, *D*, and *E* through the occupancy profile is necessary for the long queue estimation. As shown in the figure, Point *B* is the moments when green starts, which can be easily obtained from the signal status data archived by the SMART-SIGNAL system. Point *A* is the time when the detector is occupied by a motionless vehicle and Point *C* is the time when the detector is "released", so the occupancy δ between Point *A* and Point *C* is always 1.0, which can be easily identified from the occupancy profile. Between Point *C* and Point *E*, saturated traffic from the queue discharging process passes the detector. The occupancy δ during time interval $[T_C, T_E]$ is usually not 1.0, but still keeps higher than a critical value δ_c since queue discharges at capacity flow rate (by forming a vehicle platoon). The traffic pattern detected at the detector should be different before and after Point *E*. After Point *E* the traffic flow pattern is dependent on the vehicle arrival process from upstream, which most likely is different with the traffic flow pattern during queue discharge. Correspondingly, the occupancy

δ drops after Point *E*. Therefore, δ_c can be used as a threshold to identify Point *E* (which is named as "break point" in this project). In the following, we describe how the queue length can be estimated once Point *E* is identified.

- **Maximum Queue Length Estimation**

Maximum queue length is the maximum length that the queue accumulated during a cycle, which is the distance from the stop-line to Point *D* as shown in Figure 4.7. To estimate time-dependent intersection queue length during a cycle, we need to first estimate the maximum queue length of the cycle.

Figure 4.8 demonstrates the proposed maximum queue length estimation model. Unlike the shockwave curve (with the assumption of constant arrival flow and infinity acceleration and deceleration rates) shown in Figure 4.7, the queue length curve depicted in the figure is not a straight line, which considers the variation of the arrival flows and the acceleration / deceleration activities of the queued vehicles. Before the queue reaches its maximum value at Point *D*, the queue length is an unknown irregular curve varies with uncertain vehicle arrivals. After Point *D*, the queue length curve coincides with the moving trajectory of the last queued vehicle. When the arterial link is short or vehicles arrive at the intersection as a platoon, assumptions of infinite acceleration / deceleration speed may give rise to large errors in the queue length estimation. In this project, microscopic analysis that considers vehicles' acceleration / deceleration behaviors during queue development and discharge is implemented.

Once Points A, B, C, and E are identified, the maximum queue length L_q^{max} during the last cycle can be estimated as shown in Figure 4.8. Denote the distance between the advance detector and the stop-line as d_l, and the travel time for the last queued vehicle to pass the advance loop detector as t_l. The relationship of the variables can be formulated as in Equation 4.14:

$$L_q^{max} - d_l = \begin{cases} \frac{1}{2}\gamma_a t_l^2, & L_q^{max} \leq \frac{u_f^2}{2\gamma_a} + d_l \\ u_f t_l - \frac{u_f^2}{2\gamma_a}, & \text{otherwise} \end{cases} \tag{4.14}$$

Additionally denote the maximum queue size at time T_D as $n_q(T_D)$, then L_q^{max} can be calculated as Equation 4.15:

$$L_q^{max} = h \cdot n_q(T_D) \tag{4.15}$$

Considering that we assume uniform starting time difference between two adjacent queued vehicles, and

$$T_E = T_g + t_r + (n_q(T_D) - 1)t_s + t_l \tag{4.16}$$

Equations 4.14, 4.15, and 4.16 can be solved if T_E can be detected from the detector occupancy profile, and the maximum queue length L_q^{max} is thus generated.

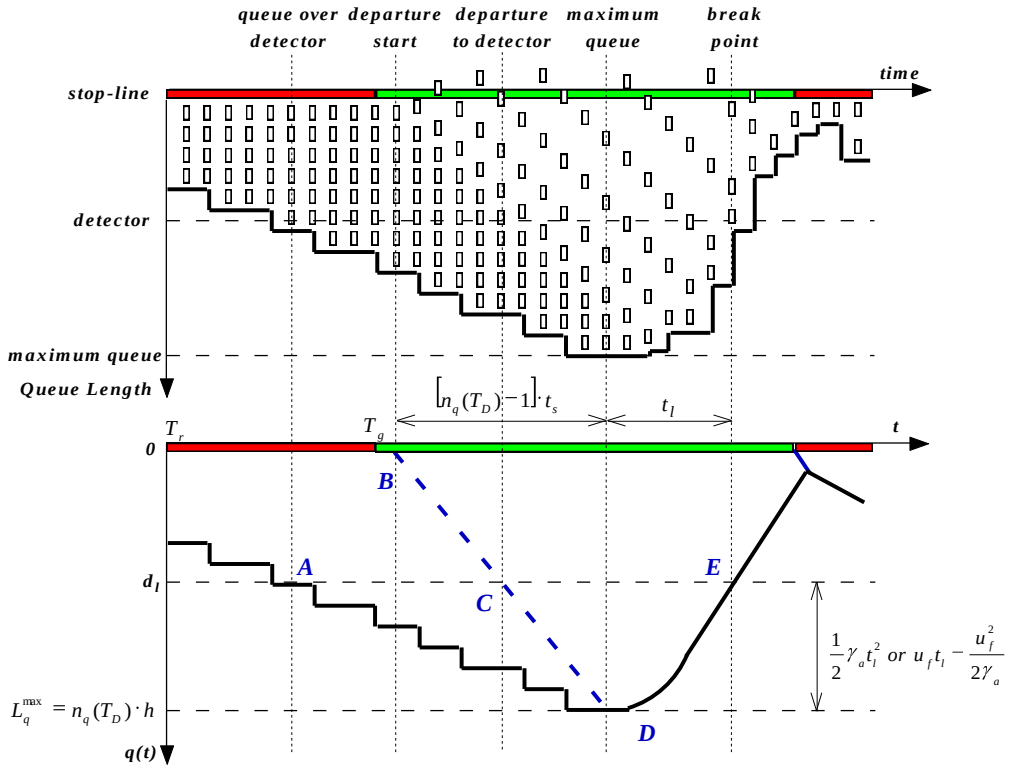

Figure 4.8: Maximum Queue Length Estimation for Long Queues.

- **Time-Dependent Queue Length Curve Estimation**

Maximum queue length curve is an irregular curve because of the fluctuation of vehicle arrivals. The queue length curve in a long queue case can be divided into three parts along the time axis: before the detector is occupied at time T_A, after the queue discharge wave propagates to the last queued vehicle at time T_D, and that within time period [T_A, T_D]. The queue length curve can be generated once the maximum queue length is calculated. Queue length before time T_A and after time T_D can be easily calculated; however, queue length within time period [T_A, T_D] is difficult to estimate because the arrival pattern is unknown after the detector being occupied.

Before the queue accumulates to the advance detector, vehicle arrival data is still available from the detector and queue length can be calculated as linearly with queue size. After the last queued vehicle starts to move forward, the distance of its current position to the stop-line is the queue length. The estimation of queue length curve can be obtained by calculating the trajectory of the last queued vehicle.

When the detector is occupied by a queued vehicle, the maximum queue length L_q^{max} (i.e. $L_q(T_D)$) can be estimated as we discussed above; however, the queue length curve between time T_A and T_D cannot be accurately estimated without vehicle arrival data. The trajectory that how the queue is developed is unknown: a queued vehicle could be accumulated in the queue at anytime during the period. Therefore, reasonable hypothesis is necessary to be made to estimate the queue length curve. In this project, we propose two possible queue length formulation hypotheses: a triangle curve or a trapezoid curve, which are described following.

Figure 4.9 demonstrates the triangle curve queue length formulation hypothesis. Vehicles are assumed constantly arrive at the intersection and accumulate at the rear of the queue, until the discharge shockwave reaches the rear. The vehicle arrival pattern at the intersection is uniform and the queue length curve between time T_A and T_D is a straight line. The queue length can be calculated as in Equation 4.17:

$$L_q(\tau) = L_q^{max} \cdot \frac{\tau - T_A}{T_D - T_A} \tag{4.17}$$

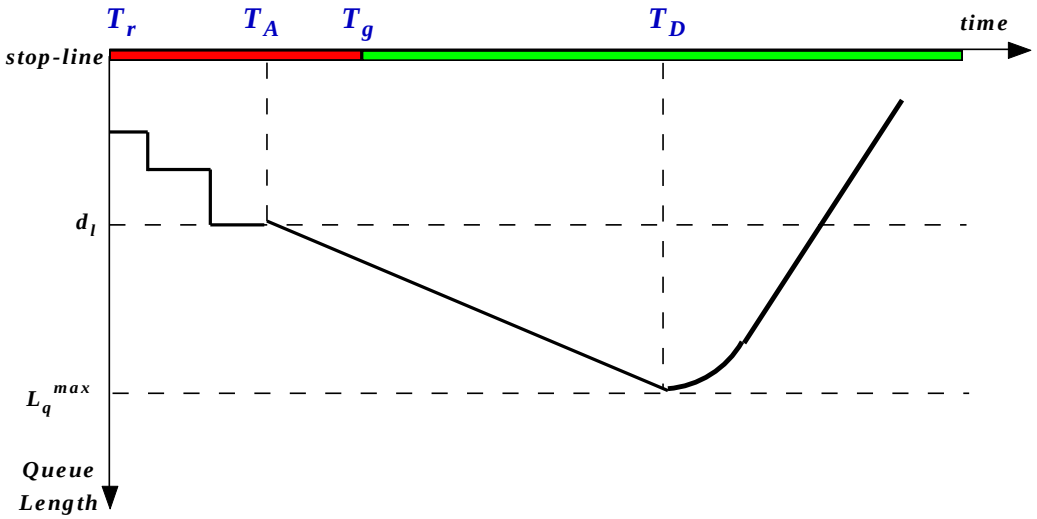

Figure 4.9: Queue Length Formulation Hypothesis — Triangle Curve.

Similarly as in short queue estimation, there are two cases after time T_D depending on if the last queued vehicle accelerates to u_f first or passes the stop-line first. If the last queued vehicle passes the stop-line first, the time-depend queue length $L_q(\tau)$ within the cycle can be calculated as in Equation 4.18:

$$L_q(\tau) = \begin{cases} h \cdot n_q(\tau), & T_r \le \tau \le T_A \\ L_q^{max} \cdot \frac{\tau - T_A}{T_D - T_A}, & T_A < \tau \le T_D \\ L_q^{max} - \frac{1}{2}\gamma_a(\tau - T_D)^2, & T_D < \tau \le T_F \\ 0, & T_F < \tau \end{cases} \tag{4.18}$$

If the last queued vehicle reaches u_f first, the time-depend queue length $L_q(\tau)$ within the cycle can be calculated as in Equation 4.19:

$$L_q(\tau) = \begin{cases} h \cdot n_q(\tau), & T_r \le \tau \le T_A \\ L_q^{max} \cdot \frac{\tau - T_A}{T_D - T_A}, & T_A < \tau \le T_D \\ L_q^{max} - \frac{1}{2}\gamma_a(\tau - T_D)^2, & T_D < \tau \le T_G \\ L_q^{max} + \frac{u_f^2}{2\gamma_a} - u_f(\tau - T_D), & T_G < \tau \le T_F \\ 0, & T_F < \tau \end{cases} \quad (4.19)$$

When the links between intersections are short, vehicles arrivals to an intersection are more likely in a platoon mode than with a constant rate. The queue length curve between time T_A and T_D can be also assumed as a piece-wise linear curve as shown in Figure 4.10. In this case, vehicles constantly arrive at the intersection between time T_A and T_D', and no vehicles would join the queue between time T_D' and T_D. In such cases, the through movement vehicles and left-turn movement vehicles from upstream intersection form the queue at the beginning of the red time, and no vehicle would arrive at the intersection once the right-of-way from upstream intersection to the subject intersection is prohibited. The queue reaches its maximum length before time T_D (at time T_D') so the queue length during the time interval [T_D', T_D] is a constant value L_q^{max}. Here we still assume that between time T_A and T_D', vehicle arrivals are uniform as a straight line. The time that vehicle reaches its maximum value can be calculated as in Equation 4.20:

$$T_D' = T_r + \frac{L_q^{max}}{d_l} \cdot (T_A - T_r) \quad (4.20)$$

The queue length can be calculated as in Equation 4.21:

$$L_q(\tau) = \begin{cases} L_q^{max} \cdot \frac{\tau - T_A}{T_D' - T_A}, & T_A < \tau \le T_D' \\ L_q^{max}, & T_D' < \tau \le T_D \end{cases} \quad (4.21)$$

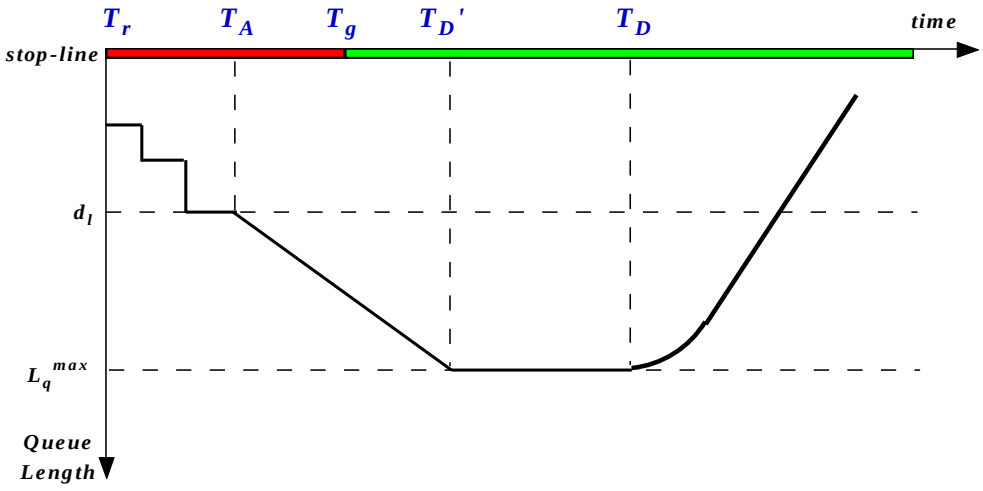

Figure 4.10: Queue Length Formulation Hypothesis — Trapezoid Curve.

Correspondingly as the calculation with the triangle hypothesis, here time-dependent queue length $L_q(\tau)$ within the cycle can be calculated as in Equation 4.22 if the last queued vehicle passes the stop-line first:

$$L_q(\tau) = \begin{cases} h \cdot n_q(\tau), & T_r \le \tau \le T_A \\ L_q^{max} \cdot \frac{\tau - T_A}{T_D' - T_A}, & T_A < \tau \le T_D' \\ L_q^{max}, & T_D' < \tau \le T_D \\ L_q^{max} - \frac{1}{2}\gamma_a(\tau - T_D)^2, & T_D < \tau \le T_F \\ 0, & T_F < \tau \end{cases} \quad (4.22)$$

and as in Equation 4.23 the last queued vehicle reaches u_f first:

$$L_q(\tau) = \begin{cases} h \cdot n_q(\tau), & T_r \le \tau \le T_A \\ L_q^{max} \cdot \frac{\tau - T_A}{T_D' - T_A}, & T_A < \tau \le T_D' \\ L_q^{max}, & T_D' < \tau \le T_D \\ L_q^{max} - \frac{1}{2}\gamma_a(\tau - T_D)^2, & T_D < \tau \le T_G \\ L_q^{max} + \frac{u_f^2}{2\gamma_a} - u_f(\tau - T_D), & T_G < \tau \le T_F \\ 0, & T_F < \tau \end{cases} \quad (4.23)$$

The calculation of the speed of the last queued vehicle $u_q(\tau)$ is as same as in Equation 4.10 and Equation 4.13.

4.2.5 Case Study

- **Study Site**

To validate the proposed queue estimation model, a field study is conducted to compare the estimated queue length and the ground truth. We select the southbound approach at the intersection of 76th Street and France Avenue as the study site because the Hennepin County Transportation Department operates a monitor camera at this intersection, which can provided video data for the ground truth queue estimation. Figure 4.11 shows the bird's eye view of the approach. In order identify queue length from the videos, the distances to the stop-line are marked in the picture. The advance loop detector is 250 ft to the stop-line. Other land markers, such as trees, traffic signs, the entrance and the exit are also used to help identifying the location of the queue.

Two sample snapshots from the videos of the study approach are shown as in Figure 4.12. The red diamond in the snapshot indicates the location of the advance detector. It can be seen from the picture that queues are spilled back over the advance detector. Occupancy profile is therefore needed to estimate queue length with the proposed long queue estimation model.

Figure 4.11: Bird's-eye View of the Study Approach.

a) Sept. 27th, 2008 11:55:58 am **a) Sept. 27th, 2008 12:03:31 pm**

Figure 4.12: Sample Video Snapshots at the Study Approach.

- **Occupancy Profiles Selection**

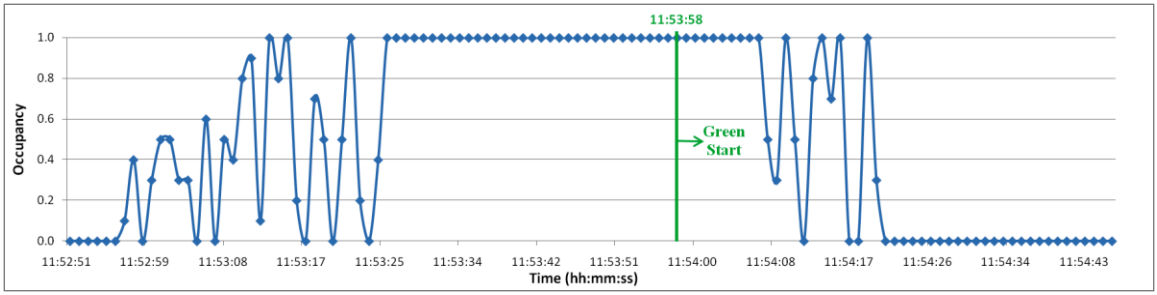

a) Occupancy Profile with 1 Second Interval

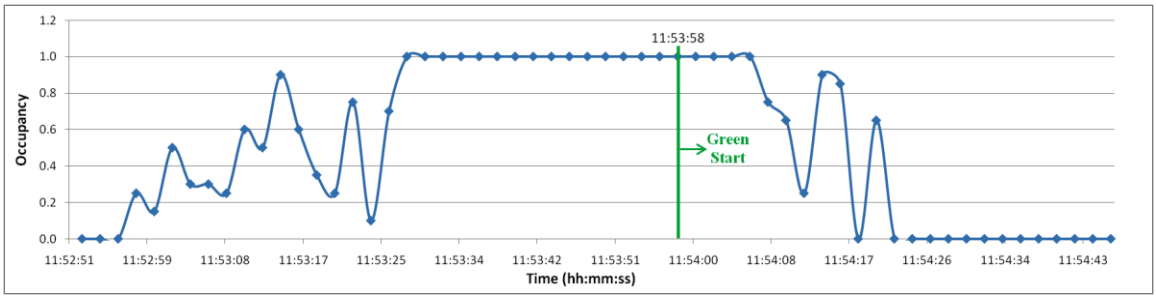

b) Occupancy Profile with 2 Seconds Interval

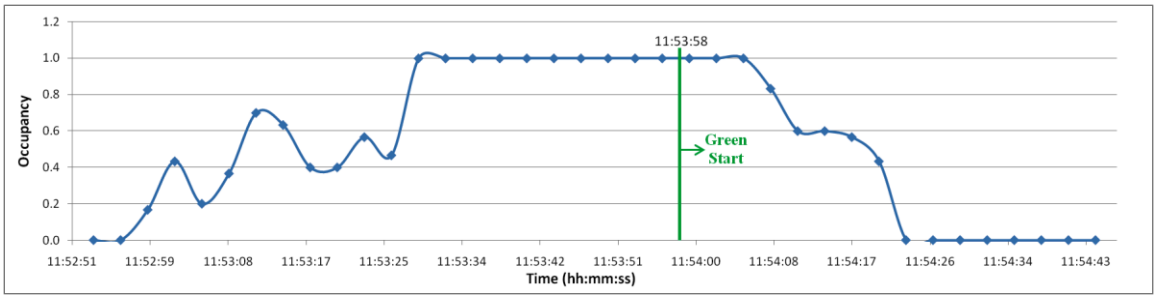

c) Occupancy Profile with 3 Seconds Interval

Figure 4.13: Cyclic Occupancy Profiles at the Advance Loop Detector.

Figure 4.13 shows cyclic occupancy profiles of the advance detector at the southbound approach of the intersection of 76th Street and France Avenue. The occupancy profiles of the same cycle are compared with different resolutions: 1 second, 2-seconds, and 3-seconds. The cycle begins with the red time of the southbound through traffic at time 11:52:51 am. The start of green time is 11:53:58 am, which is indicated with a green line in the figures. Both green time and cycle end at time 11:54:46 am. The length of the cycle is 115 seconds, and the red time and green time for the traffic are 67 seconds and 38 seconds, respectively. (Yellow time counts as green time in this figure.)

It can be clearly seen that the occupancy profile fluctuates at the beginning of the red time, which indicates the queue formulation process before the queue reached the detector. At time 11:53:26, the occupancy becomes a constant value 1.0, when the detector is occupied. The

queue starts to discharge from the stop-line as the green light starts. The discharge shockwave reaches the detector after 9 seconds at time 11:54:07, and then the occupancy profile becomes fluctuated but with a similar trend until time 11:54:22, when the rear of the queue passed the detector, which is the break point discussed previously.

Although all of the three occupancy profiles in Figure 4.13 can identify "break points" at the intersection, they are not all straightforward. The occupancy profile shown in Figure 4.13(a) is very fluctuated; the occupancy profile shown in Figure 4.13(b) is better; and the one shown in Figure 4.13(c) clearly demonstrates the trend of the detector occupancy. Therefore, in this project, we use the occupancy profile with 3-second interval to identify break points.

As shown in Table 4.1, the break points that identified from the detector occupancy files are very close to those observed from the field videos. Seventy long queue samples are obtained from the videos of six weekdays during the noon peak-hour (11:00 am ~ 13:00 pm). Three of the traffic state change points described in Section 4.2.4 are compared. The three points are Point *A* when queue is spilled over the detector, Point *C* when queue discharge wave is propagated to the detector, and Point *E* when the last queued vehicle passed the detector. For the three identified points in the seventy samples, 98.6% have errors less than 10 seconds, 95.2% have errors less than 5 seconds, and 91.4% have errors less than 3 seconds. The average errors for the seventy samples of identifying Point *A*, Point *C* and Point *E* are 1.5 seconds, 1.6 seconds and 1.8 seconds. Identification the traffic change points from occupancy profile is reasonable and doable.

Table 4.1: Comparisons of Observed vs. Identified Traffic State Change Points.

Date	No.	Queue Over Det. (A)			Discharge to Det. (C)			Last Veh. to Det. (E)			MQ Form	Discharge to MQ	Diff.
		Obs.	Est.	Err	Obs.	Est.	Err	Obs.	Est.	Err			
09/27/2007 Thu	1	11:55:11	11:55:12	1	11:56:09	11:56:12	3	11:56:31	11:56:31	0	11:56:04	11:56:20	0
	2	12:03:11	12:03:10	1	12:03:45	12:03:49	4	12:03:58	12:03:58	0	12:03:32	12:03:50	1
	3	12:05:01	12:05:00	1	12:05:46	12:05:47	1	12:06:05	12:06:05	0	12:05:55	12:05:55	1
	4	12:31:38	12:31:41	3	12:32:35	12:32:36	1	12:32:53	12:32:53	0	12:32:07	12:32:40	4
	5	12:36:03	12:36:03	0	12:36:29	12:36:30	1	12:36:36	12:36:37	1	12:36:17	12:36:31	1
	6	12:37:48	12:37:49	1	12:38:22	12:38:22	0	12:38:31	12:38:31	0	12:38:07	12:38:25	1
	7	12:39:22	12:39:21	1	12:40:03	12:40:03	0	12:40:20	12:40:21	1	12:40:10	12:40:10	1
	8	12:41:12	12:41:14	2	12:41:58	12:41:57	1	12:42:09	12:42:09	0	12:42:02	12:41:43	17
	9	12:43:36	12:43:36	0	12:44:03	12:44:04	1	12:44:21	12:44:22	1	12:43:51	12:44:10	1
	10	12:45:34	12:45:34	0	12:45:34	12:45:47	13	12:45:55	12:45:55	0	12:45:42	12:45:48	0
	11	12:49:13	12:49:12	1	12:49:55	12:49:54	1	12:50:30	12:50:22	8	12:50:10	12:50:19	12
	12	12:51:03	12:51:03	0	12:51:40	12:51:38	2	12:51:49	12:51:50	1	12:51:37	12:51:44	3
10/02/2007 Tue	13	11:51:24	11:51:24	0	11:52:12	11:52:13	1	11:52:24	11:52:26	2	11:51:56	11:52:18	1
	14	11:53:24	11:53:26	2	11:54:10	11:54:08	2	11:54:20	11:54:21	1	11:53:37	11:54:14	1
	15	11:55:30	11:55:31	1	11:56:09	11:56:08	1	11:56:13	11:56:13	0	11:55:57	11:56:10	2
	16	11:57:19	11:57:18	1	11:58:11	11:58:13	2	11:58:37	11:58:38	1	11:58:26	11:58:28	4
	17	11:59:13	11:59:31	18	12:00:00	12:00:01	1	12:00:20	12:00:11	9	11:59:46	12:00:13	11
	18	12:03:12	12:03:13	1	12:03:50	12:03:49	1	12:04:04	12:04:09	5	12:03:54	12:03:55	1
	19	12:05:17	12:05:18	1	12:05:46	12:05:47	1	12:06:02	12:06:03	1	12:05:51	12:05:52	1
	20	12:33:39	12:33:38	1	12:34:32	12:34:31	1	12:34:45	12:34:50	5	12:34:37	12:34:39	0
	21	12:37:24	12:37:25	1	12:38:13	12:38:13	0	12:38:21	12:38:22	1	12:37:57	12:38:16	1
	20	12:39:28	12:39:29	1	12:40:04	12:40:05	1	12:40:13	12:40:14	1	12:39:41	12:40:09	2
	23	12:41:34	12:41:35	1	12:42:03	12:42:05	2	12:42:12	12:42:13	1	12:41:57	12:42:08	1
	24	12:43:21	12:43:21	0	12:44:08	12:44:08	0	12:44:09	12:44:09	0	12:43:21	12:44:08	1
	25	12:45:19	12:45:23	4	12:46:03	12:46:06	3	12:46:22	12:46:15	7	12:45:52	12:46:15	8

	26	12:47:14	12:47:17	3	12:47:44	12:47:44	0	12:47:55	12:47:59	4	12:47:37	12:47:49	1
	27	12:49:15	12:49:16	1	12:49:50	12:49:51	1	12:50:22	12:50:23	1	12:50:00	12:50:12	5
	28	12:53:06	12:53:06	0	12:53:31	12:53:34	3	12:53:39	12:53:40	1	12:53:25	12:53:35	2
	29	11:53:35	11:53:33	2	11:54:27	11:54:24	3	11:54:43	11:54:44	1	11:54:20	11:54:31	2
	30	11:55:47	11:55:52	5	11:56:20	11:56:20	0	11:56:33	11:56:41	8	11:56:22	11:56:28	1
	31	11:59:42	11:59:42	0	12:00:16	12:00:16	0	12:00:35	12:00:35	0	12:00:20	12:00:26	3
	32	12:03:37	12:03:34	3	12:04:06	12:04:04	2	12:04:21	12:04:24	3	12:04:11	12:04:14	1
10/03/	33	12:09:28	12:09:28	0	12:09:45	12:09:47	2	12:09:59	12:10:01	2	12:09:42	12:09:52	1
2007	34	12:24:33	12:24:31	2	12:25:12	12:25:09	3	12:25:33	12:25:33	0	12:25:21	12:25:23	3
Wed	35	12:35:39	12:35:38	1	12:36:40	12:36:40	0	12:37:00	12:37:01	1	12:36:30	12:36:53	4
	36	12:39:34	12:39:32	2	12:40:16	12:40:15	1	12:40:39	12:40:44	5	12:40:04	12:40:30	1
	37	12:41:35	12:41:35	0	12:42:25	12:42:24	1	12:42:37	12:42:38	1	12:41:50	12:42:31	2
	38	12:47:46	12:47:44	2	12:48:11	12:48:09	2	12:48:26	12:48:24	2	12:48:19	12:48:19	5
	39	12:49:18	12:49:17	1	12:49:58	12:49:56	2	12:50:07	12:50:06	1	12:49:34	12:50:02	2
	40	11:51:49	11:51:49	0	11:52:35	11:52:33	2	11:52:42	11:52:42	0	11:52:26	11:52:38	2
	41	11:57:40	11:57:38	2	11:58:03	11:58:00	3	11:58:08	11:58:08	0	11:57:50	11:58:04	1
	42	12:28:03	12:28:04	1	12:28:49	12:28:50	1	12:28:51	12:28:50	1	12:28:03	12:28:49	1
	43	12:38:09	12:38:10	1	12:38:36	12:38:37	1	12:38:43	12:38:44	1	12:38:27	12:38:38	1
10/04/	44	12:39:31	12:39:29	2	12:40:20	12:40:18	2	12:40:33	12:40:35	2	12:40:24	12:40:27	1
2007	45	12:41:50	12:41:50	0	12:42:26	12:42:25	1	12:42:41	12:42:43	2	12:42:34	12:42:34	2
Thu	46	12:47:43	12:47:43	0	12:48:05	12:48:07	2	12:48:24	12:48:24	0	12:47:59	12:48:14	2
	47	12:49:09	12:49:07	2	12:50:04	12:50:07	3	12:50:10	12:50:11	1	12:49:23	12:50:05	0
	48	12:51:34	12:51:35	1	12:51:59	12:52:02	3	12:52:14	12:52:16	2	12:52:03	12:52:07	1
	49	12:55:19	12:55:19	0	12:55:40	12:55:39	1	12:55:58	12:55:59	1	12:55:32	12:55:44	4
	50	11:51:33	11:51:42	9	11:52:23	11:52:20	3	11:52:30	11:52:31	1	11:52:01	11:52:24	0
	51	11:55:48	11:55:50	2	11:56:25	11:56:25	0	11:56:34	11:56:34	0	11:56:03	11:56:28	0
	52	11:57:40	11:57:40	0	11:58:05	11:58:03	2	11:58:08	11:58:07	1	11:57:50	11:58:09	5
	53	12:01:31	12:01:28	3	12:02:02	12:02:00	2	12:02:10	12:02:14	4	12:02:02	12:02:06	0
10/08/	54	12:29:56	12:30:00	4	12:30:45	12:30:45	0	12:30:58	12:30:58	0	12:30:44	12:30:52	3
2007	55	12:31:55	12:31:53	2	12:32:35	12:32:35	0	12:32:43	12:32:43	0	12:32:11	12:32:37	1
Mon	56	12:39:37	12:39:37	0	12:40:17	12:40:18	1	12:40:39	12:40:39	0	12:40:07	12:40:28	2
	57	12:41:35	12:41:37	2	12:42:18	12:42:20	2	12:42:25	12:42:24	1	12:42:17	12:42:20	1
	58	12:45:50	12:45:51	1	12:46:13	12:46:14	1	12:46:22	12:46:22	0	12:46:05	12:46:17	3
	59	12:49:27	12:49:28	1	12:50:01	12:49:59	2	12:50:15	12:50:21	6	12:50:01	12:50:08	1
	60	11:49:43	11:49:43	0	11:50:26	11:50:25	1	11:50:41	11:50:41	0	11:50:30	11:50:31	1
	61	11:53:39	11:53:39	0	11:54:22	11:54:23	1	11:54:34	11:54:34	0	11:54:21	11:54:28	2
	62	11:59:48	11:59:47	1	12:00:14	12:00:16	2	12:00:21	12:00:20	1	12:00:01	12:00:17	1
	63	12:05:28	12:05:28	0	12:05:52	12:05:53	1	12:06:10	12:06:11	1	12:06:05	12:06:05	4
10/09/	64	12:30:20	12:30:19	1	12:30:47	12:30:46	1	12:30:49	12:30:49	0	12:30:10	12:30:47	1
2007	65	12:41:58	12:41:59	1	12:42:17	12:42:17	0	12:42:31	12:42:32	1	12:42:21	12:42:23	1
Tue	66	12:45:32	12:45:32	0	12:46:04	12:46:01	3	12:46:10	12:46:16	6	12:46:02	12:46:07	0
	67	12:47:32	12:47:33	1	12:47:57	12:47:59	2	12:48:10	12:48:10	0	12:48:03	12:48:03	0
	68	12:49:46	12:49:45	1	12:50:07	12:50:06	1	12:50:14	12:50:14	0	12:50:08	12:50:09	1
	69	12:51:34	12:51:33	1	12:51:49	12:51:51	2	12:52:25	12:52:09	16	12:52:00	12:52:17	20
	70	12:53:29	12:53:28	1	12:53:57	12:53:59	2	12:54:18	12:54:19	1	12:54:08	12:54:07	0
Average				**1.5**			**1.6**			**1.8**			**13.9**

- **Queue Length Curve Hypothesis**

The last three columns in Table 4.1 shows the comparison of the time queue reached maximum queue length and the time discharge wave propagated to the rear of the queue. The data are all observed data from the videos. If the queue met the triangle queue length curve hypothesis, the errors between the two observed time points should be small; otherwise, the trapezoid queue length curve hypothesis is better for the filed case. Table 4.1 shows that the average error is 13.9

seconds, which means that the queue reached its maximum value is 14 seconds earlier than the discharge propagated to its rear. The 14 seconds time difference cannot be omitted in a cycle. Therefore, the trapezoid queue length curve hypothesis is made for our case study at the corridor of France Avenue in Minneapolis, MN.

- **Results of Maximum Queue Estimation**

The values of the parameters for the estimation of the queue length are obtained either from published sources (Institute of Transportation Engineers, 1999) or field experiences. In this report, the desired speed u_f is 40 mph, the acceleration rate γ_a is 3.6 ft/s^2, the deceleration rate γ_d is 10 ft/s^2, the jammed space headway h is 30 ft, the reaction time t_r is 1 second, the starting time difference between two adjacent queued vehicles t_s is 1.2 second, and the vehicle tracing step Δt is 1 second.

The results of the proposed maximum queue estimation model are depicted in Table 4.2. The observed and estimated maximum queue length, maximum queue size and the time of queue discharge propagated to the rear of the queue (i.e. time T_D) are compared. As can be seen, the average estimation error of time T_D is 2.4 seconds, and 92.9% of the errors are less than 5 seconds. The average maximum queue length estimation error is 31.9 ft, which is 7.5% off the average of the ground truth. 78.6% estimated maximum queue lengths have errors within 10 percent. The average error of maximum queue size is 1.4 vehicles, which is 9.4% of the observed maximum queue size. Considering the limited information we can use, the estimation results are very encouraging.

Table 4.2: Comparisons of Observed vs. Estimated Maximum Queue.

Date	No.	Discharge to MQ (Tb)			Max. Queue Length (ft)				Max. Queue Size			
		Obs.	Est.	Err	Obs.	Est.	Err	%	Obs.	Est.	Err	%
09/27/ 2007 Thu	1	11:56:20	11:56:20	0	470	472	2	0.5%	17	15.7	1	7.4%
	2	12:03:50	12:03:49	1	400	384	16	4.0%	13	12.8	0	1.5%
	3	12:05:55	12:05:54	1	480	472	8	1.6%	17	15.7	1	7.4%
	4	12:32:40	12:32:44	4	400	413	13	3.1%	14	13.8	0	1.8%
	5	12:36:31	12:36:30	1	360	344	16	4.4%	12	11.5	1	4.4%
	6	12:38:25	12:38:24	1	330	332	2	0.5%	12	11.1	1	7.9%
	7	12:40:10	12:40:11	1	390	427	37	9.5%	14	14.2	0	1.7%
	8	12:41:43	12:42:00	17	390	384	6	1.5%	13	12.8	0	1.5%
	9	12:44:10	12:44:11	1	440	472	32	7.3%	16	15.7	0	1.6%
	10	12:45:48	12:45:48	0	290	332	42	14.4%	12	11.1	1	7.9%
	11	12:50:19	12:50:07	12	700	635	65	9.3%	25	21.2	4	15.4%
	12	12:51:44	12:51:41	3	400	384	16	4.0%	16	12.8	3	20.0%
10/02/ 2007 Tue	13	11:52:18	11:52:17	1	400	398	2	0.4%	15	13.3	2	11.5%
	14	11:54:14	11:54:13	1	360	357	3	0.8%	12	11.9	0	0.8%
	15	11:56:10	11:56:08	2	290	297	7	2.5%	10	9.9	0	1.0%
	16	11:58:28	11:58:24	4	600	618	18	3.0%	23	20.6	2	10.5%
	17	12:00:13	12:00:02	11	440	384	56	12.7%	17	12.8	4	24.7%
	18	12:03:55	12:03:56	1	520	535	15	2.9%	18	17.8	0	0.9%
	19	12:05:52	12:05:51	1	490	519	29	6.0%	16	17.3	1	8.2%
	20	12:34:39	12:34:39	0	420	457	37	8.8%	14	15.2	1	8.8%
	21	12:38:16	12:38:15	1	330	332	2	0.5%	13	11.1	2	15.0%
	20	12:40:09	12:40:07	2	330	344	14	4.3%	12	11.5	1	4.4%

	23	12:42:08	12:42:07	1	320	320	0	0.1%	12	10.7	1	11.2%
	24	12:44:08	12:44:07	1	280	256	24	8.7%	9	8.5	0	5.3%
	25	12:46:15	12:46:07	8	440	357	83	18.8%	15	11.9	3	20.6%
	26	12:47:49	12:47:50	1	390	413	23	5.8%	15	13.8	1	8.3%
	27	12:50:12	12:50:07	5	720	703	17	2.3%	24	23.4	1	2.3%
	28	12:53:35	12:53:33	2	330	332	2	0.5%	11	11.1	0	0.5%
	29	11:54:31	11:54:33	2	420	457	37	8.8%	15	15.2	0	1.5%
	30	11:56:28	11:56:29	1	440	503	63	14.4%	16	16.8	1	4.9%
	31	12:00:26	12:00:23	3	480	503	23	4.9%	18	16.8	1	6.8%
10/03/ 2007 Wed	32	12:04:14	12:04:13	1	430	488	58	13.4%	15	16.3	1	8.4%
	33	12:09:52	12:09:51	1	410	427	17	4.2%	14	14.2	0	1.7%
	34	12:25:23	12:25:20	3	560	535	25	4.4%	19	17.8	1	6.1%
	35	12:36:53	12:36:49	4	470	503	33	7.1%	18	16.8	1	6.8%
	36	12:40:30	12:40:29	1	540	635	95	17.5%	20	21.2	1	5.8%
	37	12:42:31	12:42:29	2	400	384	16	4.0%	15	12.8	2	14.6%
	38	12:48:19	12:48:14	5	420	442	22	5.2%	16	14.7	1	7.9%
	39	12:50:02	12:50:00	2	380	320	60	15.9%	14	10.7	3	23.9%
	40	11:52:38	11:52:36	2	340	320	20	6.0%	12	10.7	1	11.2%
	41	11:58:04	11:58:05	1	280	269	11	3.9%	10	9.0	1	10.4%
	42	12:28:49	12:28:48	1	280	256	24	8.7%	11	8.5	2	22.5%
	43	12:38:38	12:38:37	1	350	344	6	1.7%	13	11.5	2	11.7%
10/04/ 2007 Thu	44	12:40:27	12:40:26	1	430	398	32	7.4%	15	13.3	2	11.5%
	45	12:42:34	12:42:32	2	450	488	38	8.4%	17	16.3	1	4.4%
	46	12:48:14	12:48:12	2	430	503	73	17.1%	16	16.8	1	4.9%
	47	12:50:05	12:50:05	0	350	308	42	12.0%	12	10.3	2	14.4%
	48	12:52:07	12:52:06	1	420	442	22	5.2%	18	14.7	3	18.2%
	49	12:55:44	12:55:48	4	450	488	38	8.4%	16	16.3	0	1.6%
	50	11:52:24	11:52:24	0	350	344	6	1.7%	12	11.5	1	4.4%
	51	11:56:28	11:56:28	0	350	320	30	8.7%	12	10.7	1	11.2%
	52	11:58:09	11:58:04	5	310	262	48	15.6%	10	8.7	1	12.8%
	53	12:02:06	12:02:06	0	340	370	30	9.0%	13	12.3	1	5.0%
10/08/ 2007 Mon	54	12:30:52	12:30:49	3	380	413	33	8.6%	14	13.8	0	1.8%
	55	12:32:37	12:32:38	1	320	297	23	7.1%	12	9.9	2	17.5%
	56	12:40:28	12:40:26	2	560	535	25	4.4%	19	17.8	1	6.1%
	57	12:42:20	12:42:19	1	300	287	13	4.4%	11	9.6	1	13.1%
	58	12:46:17	12:46:14	3	330	357	27	8.2%	13	11.9	1	8.4%
	59	12:50:08	12:50:09	1	440	503	63	14.4%	16	16.8	1	4.9%
	60	11:50:31	11:50:32	1	440	398	42	9.5%	15	13.3	2	11.5%
	61	11:54:28	11:54:26	2	360	370	10	2.9%	13	12.3	1	5.0%
	62	12:00:17	12:00:16	1	330	277	53	15.9%	11	9.2	2	15.9%
	63	12:06:05	12:06:01	4	460	427	33	7.2%	16	14.2	2	11.0%
10/09/ 2007 Tue	64	12:30:47	12:30:46	1	300	269	31	10.4%	12	9.0	3	25.3%
	65	12:42:23	12:42:22	1	450	427	23	5.1%	16	14.2	2	11.0%
	66	12:46:07	12:46:07	0	330	384	54	16.4%	14	12.8	1	8.5%
	67	12:48:03	12:48:03	0	380	344	36	9.4%	14	11.5	3	18.0%
	68	12:50:09	12:50:08	1	360	308	52	14.4%	12	10.3	2	14.4%
	69	12:52:17	12:51:57	20	720	503	217	30.1%	24	16.8	7	30.1%
	70	12:54:07	12:54:07	0	560	519	41	7.3%	16	17.3	1	8.2%
Average				**2.4**			**31.9**	**7.5%**			**1.4**	**9.4%**

Figure 4.14 and Figure 4.15 demonstrate the comparison of observed and estimated maximum queue length and maximum queue size with figures. For each data point, the horizontal axis value is the observed data from videos and the vertical axis value is the estimated

result from the proposed model. The data points should fall on the red lines when the estimation is perfect. The figures indicate that the estimation values are very close to the ground truth observations. The estimation errors are insignificant, and the proposed model is promising.

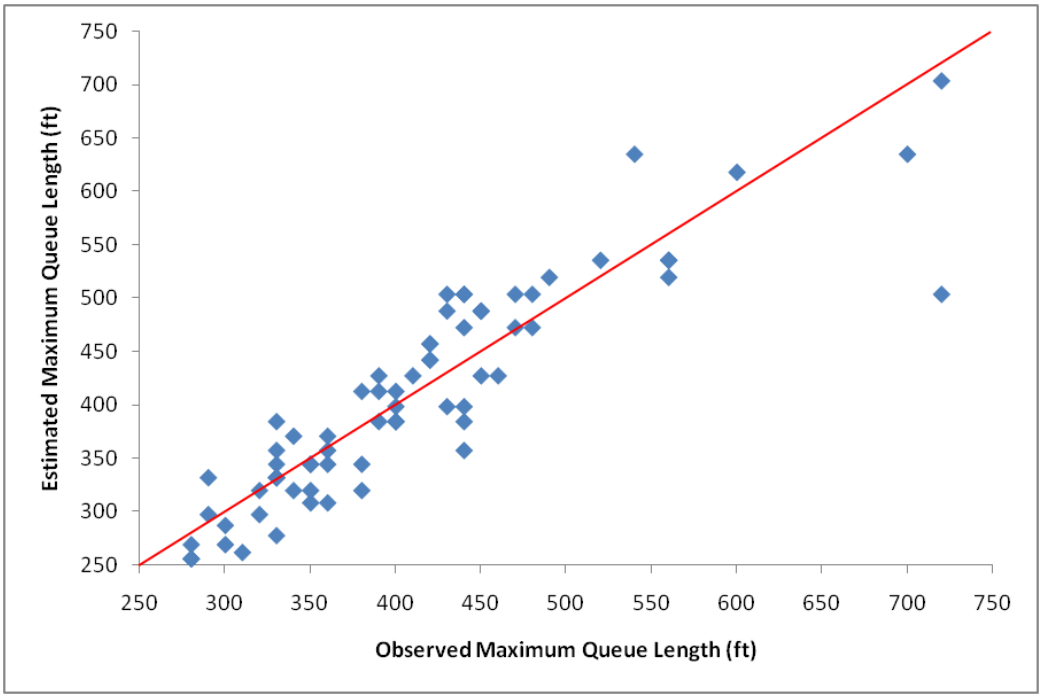

Figure 4.14: Comparisons of Observed vs. Estimated Maximum Queue Length.

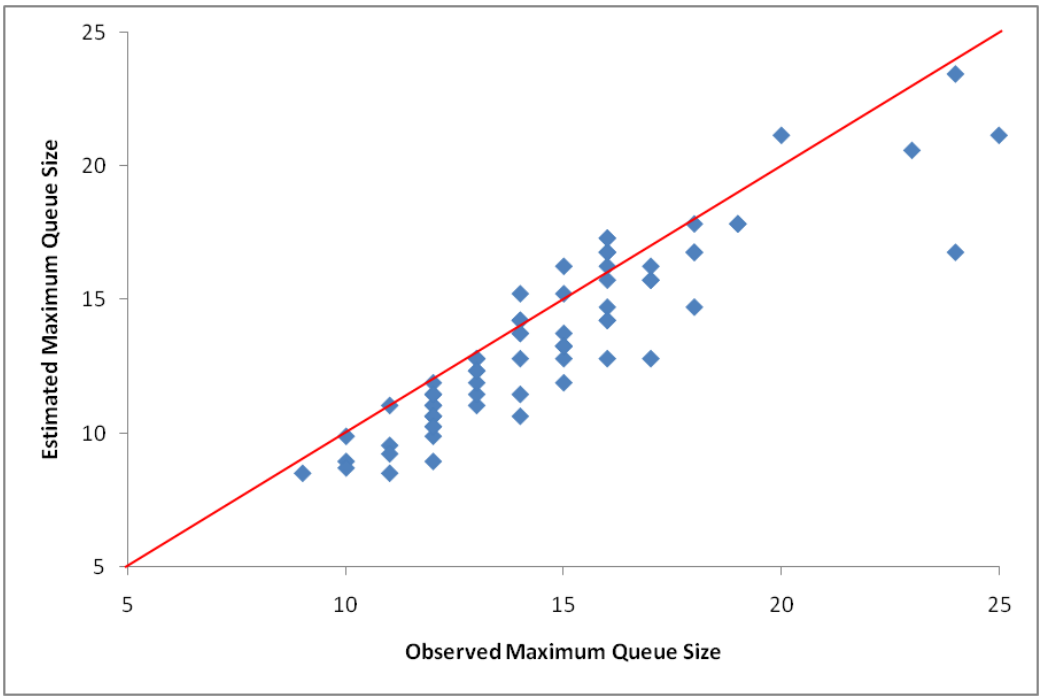

Figure 4.15: Comparisons of Observed vs. Estimated Maximum Queue Size.

- **Results of Cyclic Queue Length Curve**

The trapezoid queue length curve hypothesis is selected for this study site to estimate real-time intersection queue length, which also reflects the platoon arrival pattern shown from the videos. Figure 4.16 shows the comparison of a cyclic queue length curve from one of the seventy samples. The blue line is the queue length captured from the video. It is jagged before the maximum queue is reached because the ground truth queue length is calculated based on the observed queue size. After the discharge propagated to the rear of the queue, the queue length curve is just the trajectory of the last queued vehicle. The red line is the queue length estimated from Equation 4.22. It can be seen that the two lines are close, which indicates that proposed model has good estimation on real-time queue length curve.

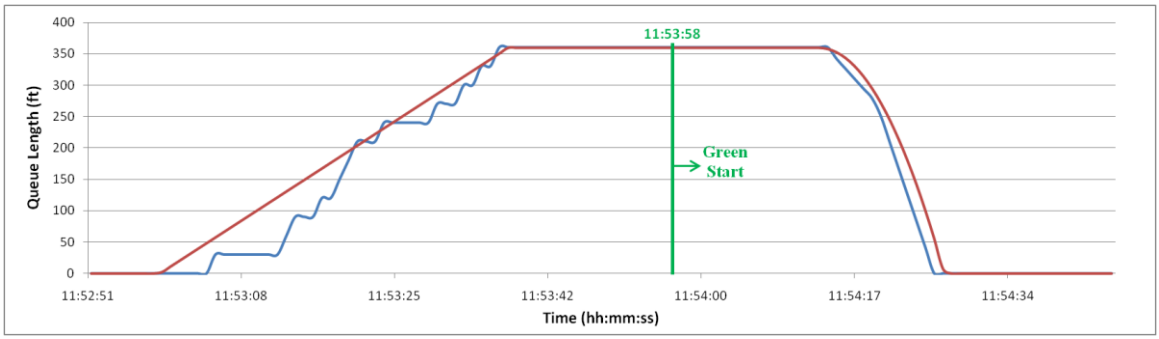

Figure 4.16: Comparison of Observed vs. Estimated Cyclic Queue Length Curve.

4.2 Turning Movement Proportion Estimation

4.2.1 Problem Description

Turning movement proportion (TMP) is another important intersection performance measure, which is often used as input data for signal control systems. However, TMPs at arterial intersections cannot be directly measured, because full-set detector configuration is rare in the field and right-turn detectors are usually not available. Right-turn traffic does not have protected phases at the majority of the intersections in the United States; they are usually designed to share detectors with through movement traffic. The problem in obtaining TMPs is how to distinguish the right-turn traffic from the through traffic using measured detector counts.

Figure 4.17 shows the typical movements at a dual ring actuated signalized intersection. The solid-line arrows with numbered circles indicate the eight protected through and left-turn traffic movements at the intersection. The dashed-line arrows illustrate the four permitted right-turn traffic movements. The rectangles in the figure indicate the location of the detectors. Assuming the eastbound and westbound are the major approaches, which have advance through and right-turn detectors and stop-line left-turn detectors; the northbound and southbound are the minor approaches, which have all detectors deployed at the stop-lines. The dual-ring signal control guarantees protected phasing time for the through and left-turn traffic. The right-turn traffic has permitted right-of-way at all approaches during the cycle. They need to yield to any conflicting traffic movements, but they are not prohibited in any phase.

4.2.2 Proposed Model

In this project, a simple turning movement proportion estimation model that relies only on short-term detector counts is proposed. The model classifies the traffic counts into groups according to signal phases and directions. The relationship of the groups is analyzed and a uniform right-turn traffic assumption is made to calculate TMPS at the intersection. Here, the southbound and westbound approaches shown in the figure are selected as demo approaches to depict the proposed model. The northbound and eastbound approaches can be examined with the same logic.

As shown in Figure 4.17, we denote the number of westbound through movement vehicles during time t as $V_T^W(t)$, the number of northbound left-turn movement traffic during time t $V_L^N(t)$, the number of southbound right-turn movement traffic during time t $V_R^S(t)$, the number of vehicles measured at the eastbound downstream detector D_d during time t $V_D^E(t)$. The traffic movements are indicated in the figure as red-line arrows, and their relationship can be formulated as in Equation 4.24:

$$V_D^E(t) = V_T^W(t) + V_L^N(t) + V_R^S(t) \tag{4.24}$$

Here, it is assumed that the travel times for the traffic from the detectors D_t, D_l, D_r to the downstream detector D_d are known and stable.

Equation 4.24 can be further expressed in terms of different phases, which have different combinations since some of the movements are prohibited in various phases during the cycle. For example, the westbound through movement traffic is not allowed in Phases 1, 3, 5, 6, 7, and 8; the northbound left-turn movement traffic is not allowed in Phases 1, 2, 3, 4, 7, and 8. Equation 4.24 can be extended into 8 equations corresponding to the 8 signal phases, which are formulated as in Equation 4.25 ~ Equation 4.27:

$$V_D^E(p) = V_R^S(p) \tag{4.25}$$

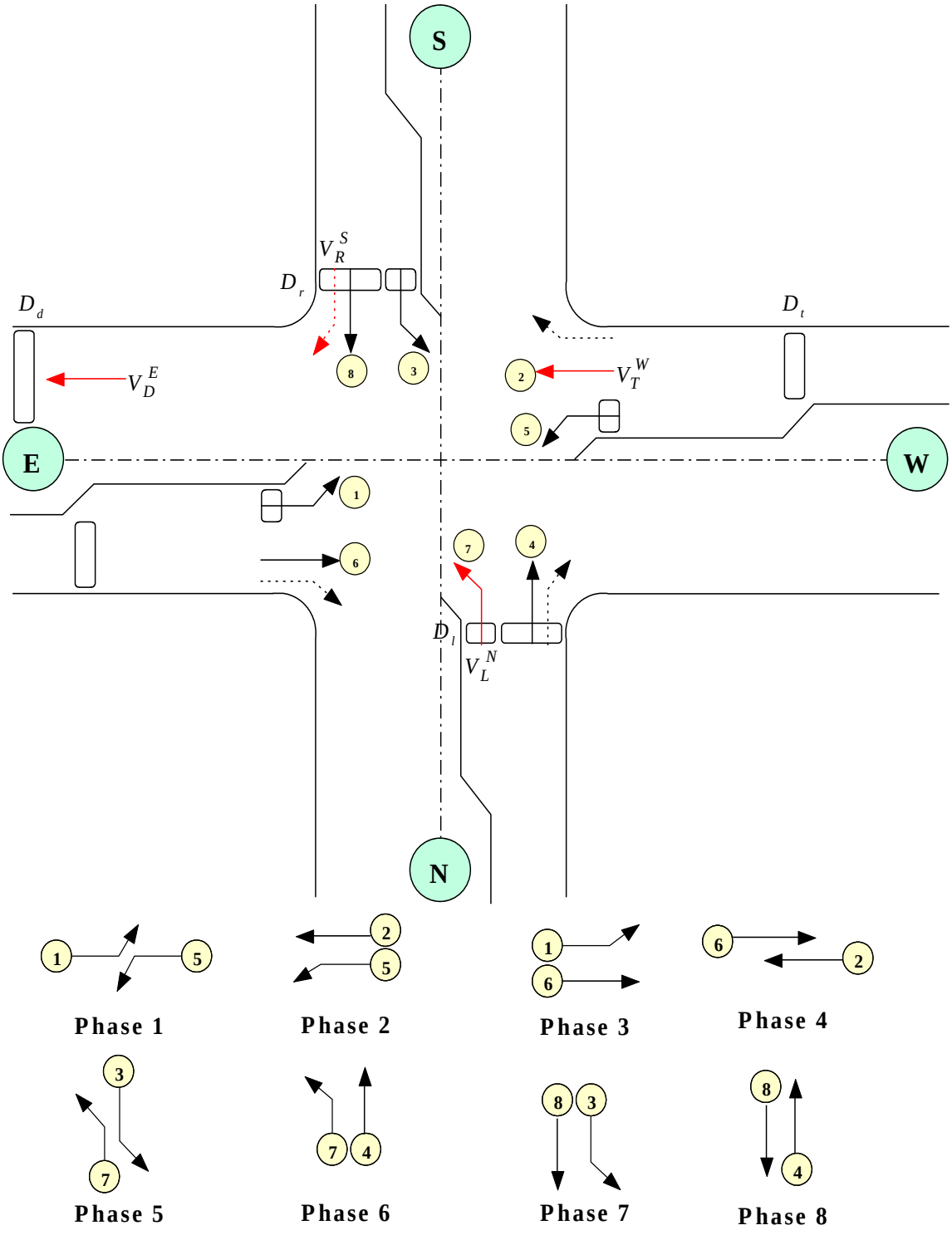

Figure 4.17: Typical Movements at a Dual-ring Actuated Signalized Intersection.

where p is the phase number, p = 1, 3, 7, and 8;

$$V_D^E(p) = V_T^W(p) + V_R^S(p) \tag{4.26}$$

where p = 2 and 4;

$$V_D^E(p) = V_L^N(p) + V_R^S(p) \tag{4.27}$$

where p = 5 and 6.

There are total 20 variables in the eight equations listed above. Amongst them, $V_D^E(p)$ (l = 1~8) and $V_L^N(p)$ (p = 5 and 6) are known, which can be directly measured from the downstream detector D_d and the northbound left-turn detector D_l. Therefore, Equation 4.25 and Equation 4.27 can be solved and $V_R^S(p)$ (p = 1, 3, 5, 6, 7, and 8) can be obtained accordingly. On the other hand, Equation 4.26 cannot be solved because $V_T^W(p)$ (p = 2 and 4) are unknown. The traffic counts measured at the westbound detector D_t during phase time p (denoted it as $V_{TR}^W(p)$) are combinations of $V_T^W(p)$ and $V_R^W(p)$ (i.e., the number of westbound right-turn vehicles during phase time p). The relationship can be formulated as in Equation 4.28:

$$V_{TR}^W(p) = V_T^W(p) + V_R^W(p) \tag{4.28}$$

where p = 1~8.

Although $V_{TR}^W(p)$ are known variables, the introduction of Equation 4.28 does not help solve the problem since new unknown variables $V_R^W(p)$ are also introduced. A reasonable assumption is needed to distinguish the right-turn movement traffic and through movement traffic from the detectors. Therefore, the so-called uniform right-turn volume pattern assumption is applied in this project to solve the problem. It is assumed the right-turn movement traffic in a cycle is continuous and uniform. Based on this assumption, the right-turn traffic counts in the phases with unknown conflicting traffic movements can be produced from the phases with known right-turn traffic counts. For instance, the unknown right-turn traffic counts $V_R^S(p)$ (p = 2 and 4) is assumed have the same distribution as the known right-turn traffic counts $V_R^S(p)$ (p = 1, 3, 5, 6, 7, and 8), which can be calculated as in Equation 4.29:

$$V_R^S(j) = \frac{\sum_i V_R^S(i)}{\sum_i t(i)} \times t(j) \tag{4.29}$$

where $t(p)$ is the duration of Phase p; i = 1, 3, 5, 6, 7, and 8; and j = 2 and 4.

With the right-turn traffic counts at all phases known, the turning movement proportion for the southbound can thus be calculated as in Equation 4.30:

$$\begin{cases} P_R^S = \frac{\sum_{p=1}^{8} V_R^S(p)}{\sum_{p=1}^{8} V_{TR}^S(p) + V_L^S(p)} \\ P_L^S = \frac{\sum_{p=1}^{8} V_L^S(p)}{\sum_{p=1}^{8} V_{TR}^S(p) + V_L^S(p)} \\ P_T^S = 1 - P_R^S - P_L^S \end{cases} \tag{4.30}$$

where P_R^S, P_L^S, and P_T^S are the right-turning, left-turning and through movement proportions respectively at the southbound approach; $V_{TR}^S(p)$ are the traffic counts measured at the southbound detector D_r during Phase p; and $V_L^S(p)$ are the traffic counts measured at the southbound left-turn detector during Phase p (which should only have measures during Phase 5 and 7).

With the southbound right-turn traffic counts at Phase 2 and 4, the westbound through movement counts at the phases can also be calculated according to Equation 4.26; then the westbound right-turn counts at Phase 2 and 4 can be calculated according to Equation 4.28; thus, based on the same uniform right-turn volume pattern assumption, the westbound right-turn counts at all other phases can be calculated as in Equation 4.31:

$$V_R^W(j) = \frac{\sum_i [v_{TR}^W(i) - (v_D^E(i) - v_R^S(i))]}{\sum_i t(i)} \times t(j) \tag{4.31}$$

where i = 2 and 4; and j = 1, 3, 5, 6, 7, and 8.

Similarly, the turning movement proportion at the westbound can be calculated as in Equation 4.32:

$$\begin{cases} P_R^W = \frac{\sum_{p=1}^{8} V_R^W(p)}{\sum_{p=1}^{8} V_{TR}^W(p) + V_L^W(p)} \\ P_L^W = \frac{\sum_{i=1}^{8} V_L^W(p)}{\sum_{p=1}^{8} V_{TR}^W(p) + V_L^W(p)} \\ P_T^W = 1 - P_R^W - P_L^{SW} \end{cases} \tag{4.32}$$

where P_R^W, P_L^W, and P_T^W are the right-turning, left-turning and through movement proportions, respectively, at the westbound approach; and $V_L^W(p)$ are the traffic counts measured at the westbound left-turn detector during Phase p (which should only have measures during Phase 1 and 2).

Based on the described model, the cyclic turning movement proportions at the intersection can be generated. The model only requires cyclic traffic counts from the detectors at the subject intersection and downstream detectors at major approaches. If the downstream detectors are not available, then the advance detectors of the downstream intersections can be used instead. It should be noted that when the downstream detectors are occupied under congested traffic conditions, the method cannot be applied directly because the traffic counts at the downstream detectors are not available.

4.2.3 Results Analysis

To validate the proposed queue estimation model, a field study is implemented to compare the estimated turning movement proportion with the ground truth turning movement proportions. The selected intersection is the same study site located at the intersection of 76th Street and France Avenue at Minneapolis, MN. Northbound right-turning proportion is calculated based on

the proposed model. The ground truth data are obtained from the videos recorded during noon peak hours at the intersection.

Figure 4.18 shows the comparisons of the observed northbound cyclic right-TMPs and estimated right-TMPs. The blue line is shows the observed measures from the videos and the red line shows the estimated ones. As can be seen, the proposed model generates quite fair estimations of the right-turning movement proportions. There are in total 56 sample cycles compared and eighty-five percentiles have errors less than 15%. The average error is 8.9%.

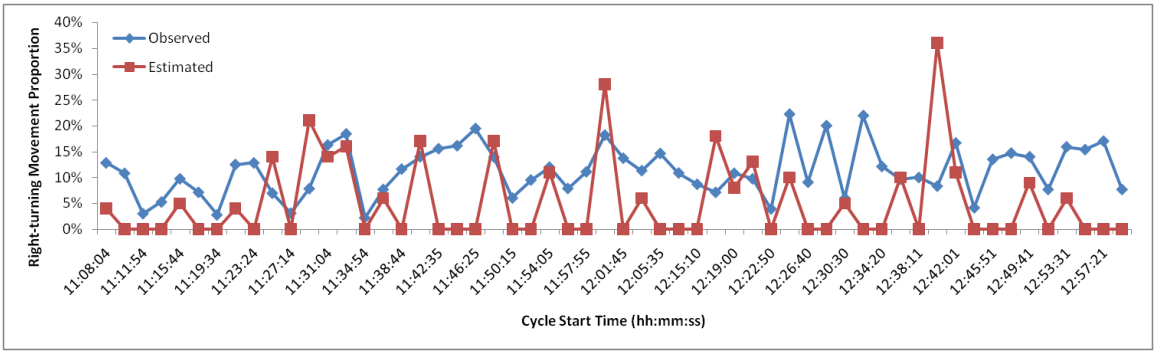

Figure 4.18: Comparisons of Observed vs. Estimated Northbound Cyclic Right-turning Movement Proportion at the Study Intersection.

4.3 Summary

This chapter describes the models to estimate two important arterial performance measures at intersection level: one is intersection queue estimation and the other is turning movement proportion estimation. The proposed queue estimation model analyzes queue development from microscopic view: driver behaviors are examined, and acceleration / deceleration activities are considered. Long queue estimation when queues spill over the advance detectors is investigated. The occupancy profiles during the queue development and discharge is utilized to identify traffic state change point. Two different queue length curve hypotheses are offered to accommodate different vehicle arrival pattern.

The proposed turning movement proportion estimation model is based on the relationships of the entering traffic volumes and exiting traffic volumes during different signal phases. The model is only relies on short-term traffic counts from the detectors deployed in field.

The input data for the two models are collected by the SMART-SIGNAL system described in Chapter 3. Field studies have been implemented at the intersection of 76th Street and France Avenue at Minneapolis, MN. Although the data can be collected from the study site is limited due to the detector configurations, the proposed models can generate good estimation of queue length and TMPs under various traffic conditions. For example, the detectors deployed at the France Avenue are link-based detectors, which cause missing traffic counts problem, especially under congested traffic condition. Our study found the through movement is under-measured by 8% at the major approaches of the study intersection. However, the proposed

models can still hold most of the estimation errors within 10%. We are doing the best job based upon limited resources.

The outputs of the models, i.e., queue length and turning movement proportions, can be used to evaluate the operation of the intersection. Following in Chapter 6, more intersection performance measures will be demonstrated. The queue length and TMP can also be used as input for estimating other arterial performance measures. The estimated intersection queue length is needed information for the arterial travel time estimation model, which will be discussed next in Chapter 5.

Chapter 5. Arterial Performance Measurement

5.1 Background

The arterial performance measurement focused in this project is travel time estimation. Travel time is one of the most important arterial performance measures for evaluating the operation of traffic network and accurate and reliable travel time information becomes increasingly important for traffic engineers. Travel time is also one of the most understood measures for road users, helping them to make informed decisions on travel choices, hence avoid unnecessary delay. In the last few years, measuring and monitoring performance of traffic management systems has become one of the priorities of Federal Highway Administration (FHWA) as indicated in the recent transportation bill SAFETEA-LU (Federal Highway Administration, 2006).

This project aims to develop an effective time-dependent arterial travel time estimation algorithm utilizing event-based traffic data from existing infrastructure. The proposed model is data-intensive, which utilizes both vehicle-actuation and signal phase change data in a synchronized manner. The high-resolution event-based detector and signal status data are retrieved from the SMART-SIGNAL system described in Chapter 3, which has been successfully implemented in the field. The availability of time-stamped signal status and loop detector data essentially allows us to reconstruct the history of traffic signal events along the arterial street.

The proposed model estimates the time-dependent travel time by tracing the virtual probe and determining its next maneuver based on estimated traffic states. At each time step, the virtual probe has three possible maneuvers: acceleration, deceleration and no-speed-change. The maneuver decision is determined by its own status and its surrounding traffic conditions. State variables of the virtual probe include its position, speed and acceleration rate. Surrounding traffic states include the status of the queue ahead of the virtual probe and the signal status. The traffic states are examined to make maneuver selection, and thus determine the speed and position of the probe in the next time step. All of the traffic states can be calculated based on the availability of event-based traffic data at the intersections. The step-by-step maneuver selection continues until the virtual probe "*arrives*" at the destination, and the difference between the starting time and the ending time is the arterial travel time. It should be noted that since we are tracing a virtual vehicle, the number of stops can be also estimated as a by-product of the travel time estimation.

An interesting property of the proposed model is that travel time estimation errors can be self-corrected when the virtual probe is delayed due to queuing or red phasing. The travel time difference between a virtual probe vehicle and a real one will be reduced at those times because the faster one will always wait for the later since queue accumulation speed is generally slower than queue discharging speed. This property will be explained in detail after the presentation of the virtual probe model.

5.2 Virtual Probe Vehicle Approach

5.2.1 Problem Statement

The proposed arterial travel time estimation model utilizes both surveillance and signal status data collected from the traffic data collection system. Figure 5.1 represents the geometric layout of an arterial network. There are *n* signalized intersections, i.e. Intersection 1, Intersection 2, till Intersection *n*, along the corridor from origin *O* to destination *D*. All intersections adopt vehicle-actuated signal timing plans, in either a synchronized or non-synchronized mode. Each approach of an intersection should have at least one advance loop detector (indicated as D_1, D_2 … D_n in Figure 5.1) placed sufficiently upstream from the intersection stop-line (advance detectors are typically placed 200 to 400 ft upstream from the intersection). The existence of stop bar detector would be helpful in the travel time estimation, but is not required. Event-based traffic data are collected at each intersection between *O* and *D*. Now the problem is how to derive the arterial travel time at time τ using the achieved data. Since many notations will be used in the following, we provide a list of all notations in the appendix.

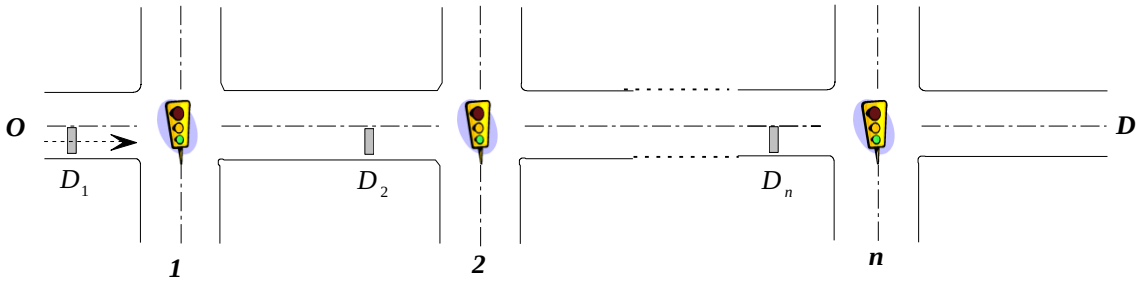

Figure 5.1: Geometric Layout of a Signalized Arterial Street.

5.2.2 States of the Virtual Probe

The maneuver decision of a virtual probe depends on a set of traffic state variables, which is demonstrated in Figure 5.2. As shown in the figure, the virtual probe approaches Intersection *i* with speed $u^p(\tau)$ at time τ, when the queue length ahead of the virtual probe, i.e., the distance from the back of the last queued vehicle in front of the virtual probe to the stop-line, is $L_q^p(\tau)$. We should also note that $L_q^p(\tau)$ is not necessary equal to the current intersection queue length $L_q(\tau)$, it simply represents the queue length in front of the virtual probe. The intersection queue length $L_q(\tau)$ is always equal or greater than $L_q^p(\tau)$. We denote the position (*x*-coordinate) of the virtual probe as $x^p(\tau)$, the position of the rear of the queue ahead of the probe $x_q^p(\tau)$ and the position of the stop-line of Intersection *i* x_s^i, respectively.

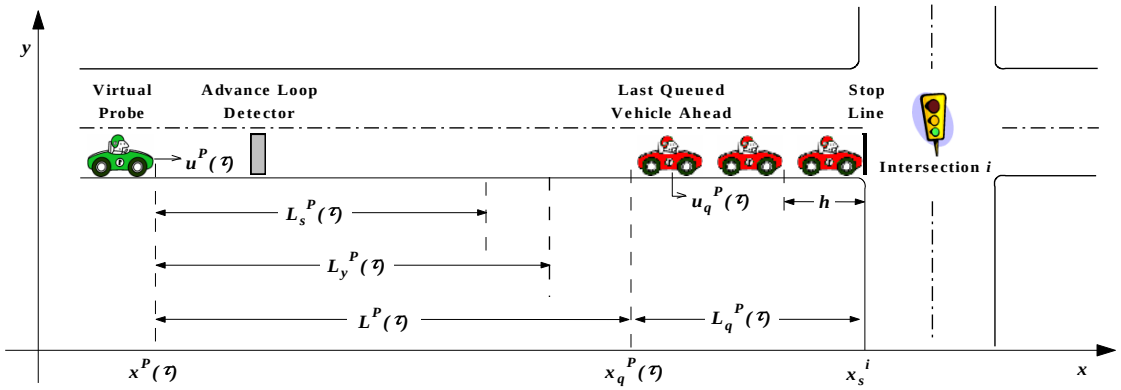

Figure 5.2: State Variables of the Virtual Probe.

$L^P(\tau)$ is the distance between the virtual probe and a "*barrier*" at time τ. The "*barrier*" is either the last queued vehicle in front of the virtual probe or the stop-line of the intersection when no queue is present in front of the virtual probe. $L^P(\tau)$ can be calculated as in Equation 5.1:

$$L^P(\tau) = x_s^i - x^P(\tau) - L_q^P(\tau) \tag{5.1}$$

$L_s^P(\tau)$ is the safe space headway of the virtual probe at time τ. It is the minimum headway required for the virtual probe which can either stop before the stop-line to avoid violation (i.e. $u^P(\tau + t_d) = 0$), or decelerate to $u_q^P(\tau)$ to avoid collision (i.e. $u^P(\tau + t_d) = u_q^P(\tau)$) where $u_q^P(\tau)$ is the speed of the last queued vehicle in front of the virtual probe and t_d is the deceleration time. $L_s^P(\tau)$ is calculated based on a constant deceleration rate γ_d. If no queue exists, $L_s^P(\tau)$ is the deceleration distance of the virtual probe from $u^P(\tau)$ to zero; if queue exists and the virtual probe is faster than the last queued vehicle ahead, $L_s^P(\tau)$ is the difference of the travel distances during time interval t_d between the virtual probe and the last queued vehicle ahead; otherwise, if the virtual probe is slower than or has the same speed as the last queued vehicle ahead, there is no potential collision risk at the moment and $L_s^P(\tau)$ is equal to zero. $L_s^P(\tau)$ can be calculated as in Equation 5.2:

$$L_s^P(\tau) = \begin{cases} u^P(\tau) \cdot t_d - \frac{1}{2}\gamma_d t_d^2, & if\ L_q^P(\tau) = 0 \\ u^P(\tau) \cdot t_d - \frac{1}{2}\gamma_d t_d^2 - u_q^P(\tau) \cdot t_d, & if\ L_q^P(\tau) > 0\ and\ u^P(\tau) > u_q^P(\tau) \\ 0, & otherwise \end{cases} \tag{5.2}$$

Considering that $t_d = \frac{u^P(\tau)}{\gamma_d}$ when no queue exists and $t_d = \frac{u^P(\tau) - u_q^P(\tau)}{\gamma_d}$ when queue appears, Equation 5.2 can be further derived as in Equation 5.3:

$$L_s^P(\tau) = \begin{cases} \frac{\left(u^P(\tau)\right)^2}{2\gamma_d}, & if\ L_q^P(\tau) = 0 \\ \frac{\left(u^P(\tau) - u_q^P(\tau)\right)^2}{2\gamma_d}, & if\ L_q^P(\tau) > 0\ and\ u^P(\tau) > u_q^P(\tau) \\ 0, & otherwise \end{cases} \tag{5.3}$$

$L_y^P(\tau)$ is the yellow-time travel distance of the virtual probe at time τ. It is the maximum travel distance of the virtual probe during the remaining yellow time if the signal was yellow at time τ. $L_y^P(\tau)$ is introduced to determine if the remaining yellow time is sufficient for the virtual probe to enter the intersection. The calculations of $L_y^P(\tau)$, $u_q^P(\tau)$ and $L_q^P(\tau)$ will be discussed further later in this section.

5.2.3 Virtual Probe Maneuver Decision Tree

The virtual probe has three maneuvers, i.e. acceleration, deceleration and no-speed-change, in terms of the speed change in the next time step. Figure 5.3 shows the maneuver decision tree of the virtual probe at each time step. The states of the probe are examined to select the maneuver. There are generally 11 cases (*C1* ~ *C11*). The decision procedures are depicted as follows:

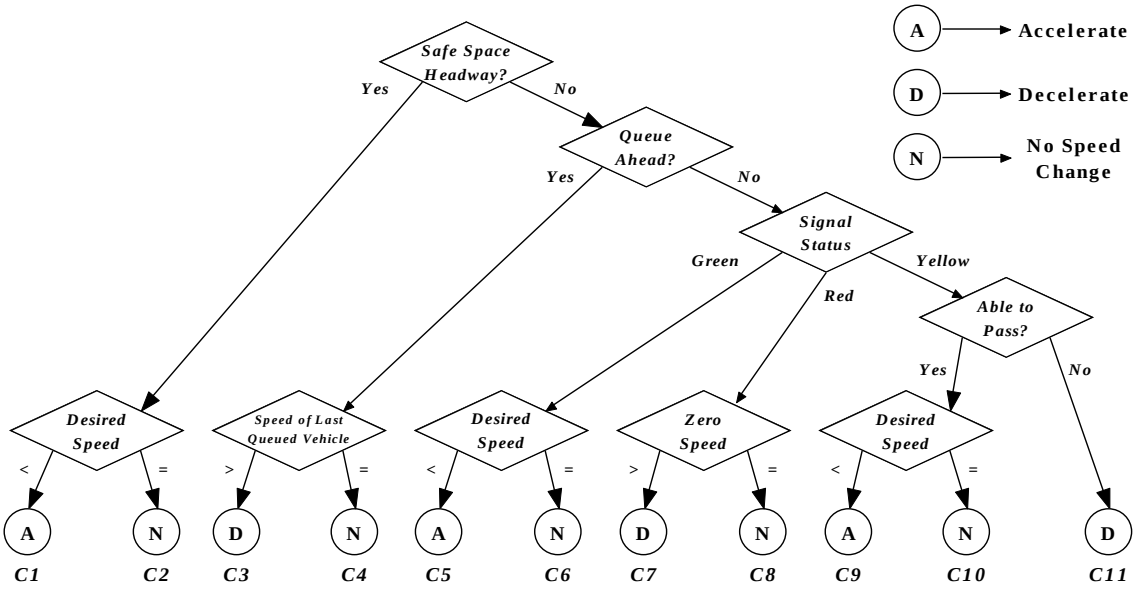

Figure 5.3: Maneuver Decision Tree of a Virtual Probe.

1) At each time step, the position of the virtual probe is examined first. If there is sufficient deceleration distance between its current position and the "*barrier*", i.e. $L^P(\tau) > L_s^P(\tau)$, the virtual probe will not need to slow down. No matter what the queue and signal states are, the virtual probe either accelerates when it does not reach the desired speed u_f yet (Case *C1*), or continues without speed change when the speed is already u_f (Case *C2*). Otherwise, the queue ahead is examined next.
2) If there is a queue stacked between the virtual probe and the stop-line when $L^P(\tau) \leq L_s^P(\tau)$, then according to Equation 5.3, either the virtual probe is faster than the last queued vehicle ahead, i.e. $u^P(\tau) > u_q^P(\tau)$ (Case *C3*), or both vehicles are motionless and $L^P(\tau) = L_s^P(\tau) = 0$ (Case *C4*). No matter the signal state, the virtual probe attempts to decelerate to $u_q^P(\tau)$ in Case *C3*, or keeps the stop status in Case *C4*. Otherwise, if no queue is in front of the virtual probe, the signal state is examined next.

3) The signal has three different states: green, red and yellow. If the signal is green, the virtual probe either accelerates when the speed is not u_f (Case *C5*), or keep its speed u_f (Case *C6*). If the signal is red, the virtual probe attempts to decelerate to a stop (Case *C7*), or keeps the stopped status (Case *C8*). The situation of yellow time is more complicated, and an additional examination of $L_y^P(\tau)$ is required to make the maneuver decision.
4) If the signal is yellow, the virtual probe needs to examine $L_y^P(\tau)$, which is the maximum travel distance within the remaining yellow time $y(\tau)$. If $L^P(\tau) < L_y^P(\tau)$, which means $y(\tau)$ is sufficient for the virtual probe to at least cross the stop-line, then the virtual probe utilizes $y(\tau)$ to enter the intersection with either acceleration (Case *C9*) or speed u_f (Case *C10*); otherwise, $y(\tau)$ is not sufficient and the virtual probe decelerates to a stop (Case *C11*). In Case *C11*, because $L_s^P(\tau) \geq L^P(\tau) \geq L_y^P(\tau) > 0$, it can be concluded that $u^P(\tau) > 0$ according to Equation 5.3; therefore, there is no speed examination needed in this case. $L_y^P(\tau)$ can be calculated as in Equation 5.4:

$$L_y^P(\tau) = \begin{cases} u^P(\tau) \cdot y(\tau) + \frac{1}{2}\gamma_a y^2(\tau), \ if\ y(\tau) \leq y^P(\tau) \\ u^P(\tau) \cdot y^P(\tau) + \frac{1}{2}\gamma_a \left(y^P(\tau)\right)^2 + u_f\left(y(\tau) - y^P(\tau)\right), \ otherwise \end{cases} \quad (5.4)$$

where γ_a is a constant acceleration rate, and $y^P(\tau)$ is the acceleration time required for the virtual probe to reach u_f, which is equal to $\left(u_f - u^P(\tau)\right)/\gamma_a$.

5.2.4 Virtual Probe Position and Speed Calculation

The position and speed of the virtual probe at the next time step can be calculated once the maneuver is selected. From the decision tree, it can be seen that an acceleration maneuver is selected in cases *C1*, *C5* and *C9*; a deceleration maneuver is selected in cases *C3*, *C7* and *C11*; and a no-speed-change maneuver is selected in the remaining cases. The detailed calculations of the position and speed of the virtual probe are discussed next.

- **Acceleration**

Figure 5.4 shows the three cases of the acceleration maneuver selection. Figure 5.4(a) shows Case *C1* where the distance between the virtual probe and the "*barrier*", i.e. $L^P(\tau)$, is longer than the safe space headway $L_s^P(\tau)$, and the speed has not reached u_f yet. The solid line in the figure shows the possible trajectory of the virtual probe in Case *C1*, and the dashed line shows the deceleration trajectory of the virtual probe starting from time τ. Usually, *C1* happens either at the time when the virtual probe is away from the "*barrier*" (because $L^P(\tau) > L_s^P(\tau)$), or at the green time when the virtual probe accelerates within a queue. Figure 5.4(b) shows Case *C5* that $L^P(\tau)$ is shorter than or equal to $L_s^P(\tau)$, no queue is in front of the virtual probe, the signal is green and the virtual probe runs with speed lower than u_f. Figure 5.4(c) shows Case *C9* that is similar to Case *C5*, except it happens during the yellow and the remaining yellow time is sufficient for the virtual probe to enter the intersection. Both *C5* and *C9* happen when the virtual probe is near the stop-line without queue ahead. In all three cases, the virtual probe accelerates with γ_a in the next time step, and the position and speed of the virtual probe at time $\tau + \Delta t$ can be calculated as in Equation 5.5:

$$\begin{cases} x^P(\tau+\Delta t) = x^P(\tau) + u^P(\tau)\cdot\Delta t + \frac{1}{2}\gamma_a \Delta t^2 \\ u^P(\tau+\Delta t) = u^P(\tau) + \gamma_a \Delta t \end{cases} \quad (5.5)$$

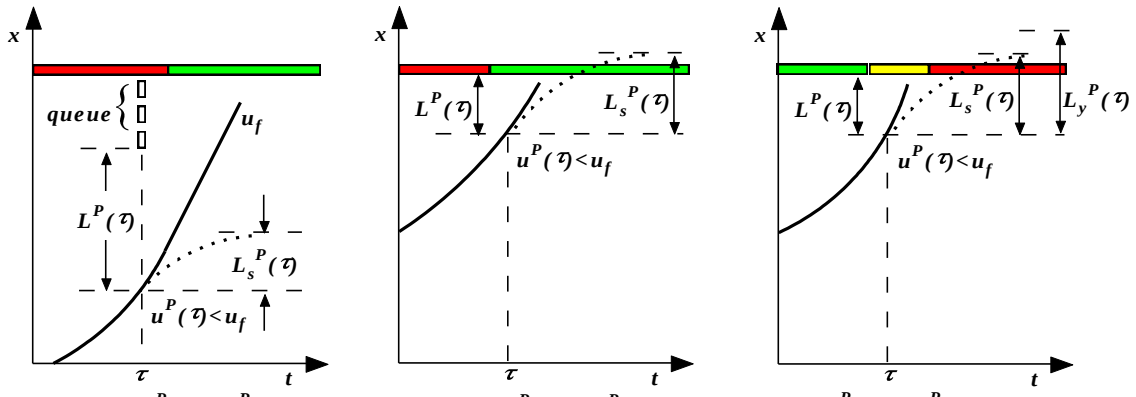

a) C1: $L^P(\tau)>L_s^P(\tau)$, $u^P(\tau)<u_f$

b) C5: $L^P(\tau)\leq L_s^P(\tau)$, No Queue, Green, $u^P(\tau)<u_f$

c) C9: $L^P(\tau)\leq L_s^P(\tau)$, No queue, Yellow, $L^P(\tau)<L_y^P(\tau)$, $u^P(\tau)<u_f$

Figure 5.4: Acceleration Maneuver Selection.

- **Deceleration**

Figure 5.5 shows the three cases of the deceleration maneuver selection. Figure 5.5(a) shows Case *C3* that $L^P(\tau)$ is shorter than or equal to $L_s^P(\tau)$, a queue is stacked between the virtual probe and the stop-line, and the virtual probe runs faster than the last queued vehicle ahead. Usually, *C3* happens when the virtual probe is approaching the queue with higher speed ($u^P(\tau) > u_q^P(\tau)$). Figure 5.5(b) shows Case *C7* that $L^P(\tau)$ is shorter than or equal to $L_s^P(\tau)$,, no queue exists, the signal is red and the virtual probe is moving. Figure 5.5(c) shows Case *C11* that is similar to Case *C7*, except it happens at yellow time and the remaining yellow time is not sufficient for the virtual probe to enter the intersection. Both *C7* and *C11* happen when the virtual probe is near the stop-line without a queue ahead. In the three cases, the virtual probe decelerates with recalculated deceleration rate $\gamma_d^P(\tau)$ in the next time step, and the position and speed of the virtual probe at time $\tau + \Delta t$ can be calculated as in Equation 5.6:

$$\begin{cases} x^P(\tau+\Delta t) = x^P(\tau) + u^P(\tau)\cdot\Delta t - \frac{1}{2}\gamma_d^P(\tau)\Delta t^2 \\ u^P(\tau+\Delta t) = u^P(\tau) - \gamma_d^P(\tau)\Delta t \end{cases} \quad (5.6)$$

Where $\gamma_d^P(\tau) = \begin{cases} \frac{\left(u^P(\tau)\right)^2}{2L^P(\tau)}, & if\ L_q^P(\tau) = 0 \\ \frac{\left(u^P(\tau)-u_q^P(\tau)\right)^2}{2L^P(\tau)}, & otherwise \end{cases}$.

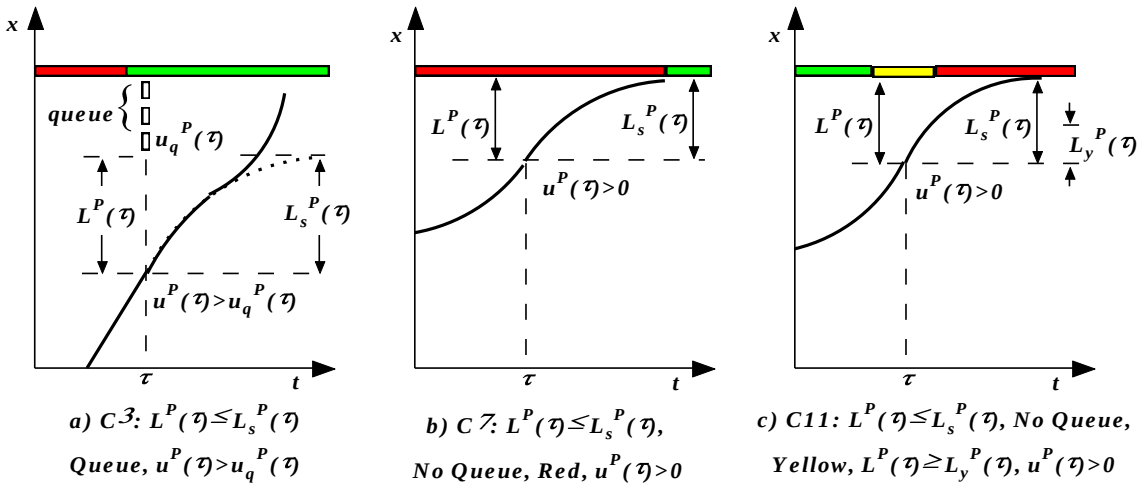

Figure 5.5: Deceleration Maneuver Selection.

- **No-speed-change**

Figure 5.6 shows the remaining five cases of the no-speed-change maneuver selection. The virtual probe either continues with speed u_f or keeps the stopped status. Cases *C2*, *C6* and *C10* (shown in Figure 5.6(a~c)) are similar to cases *C1*, *C5* and *C9*, except the virtual probe reaches the desired speed and does not need to accelerate; Cases *C4* and *C8* (shown in Figure 5.6(d) and Figure 5.6(e)) are similar to cases *C3* and *C7*, except the virtual probe is already motionless and cannot further decelerate. The position and speed of the virtual probe at time $\tau + \Delta t$ can be calculated as in Equation 5.7:

$$\begin{cases} x^P(\tau + \Delta t) = x^P(\tau) + u^P(\tau) \cdot \Delta t \\ u^P(\tau + \Delta t) = u^P(\tau) \end{cases} \tag{5.7}$$

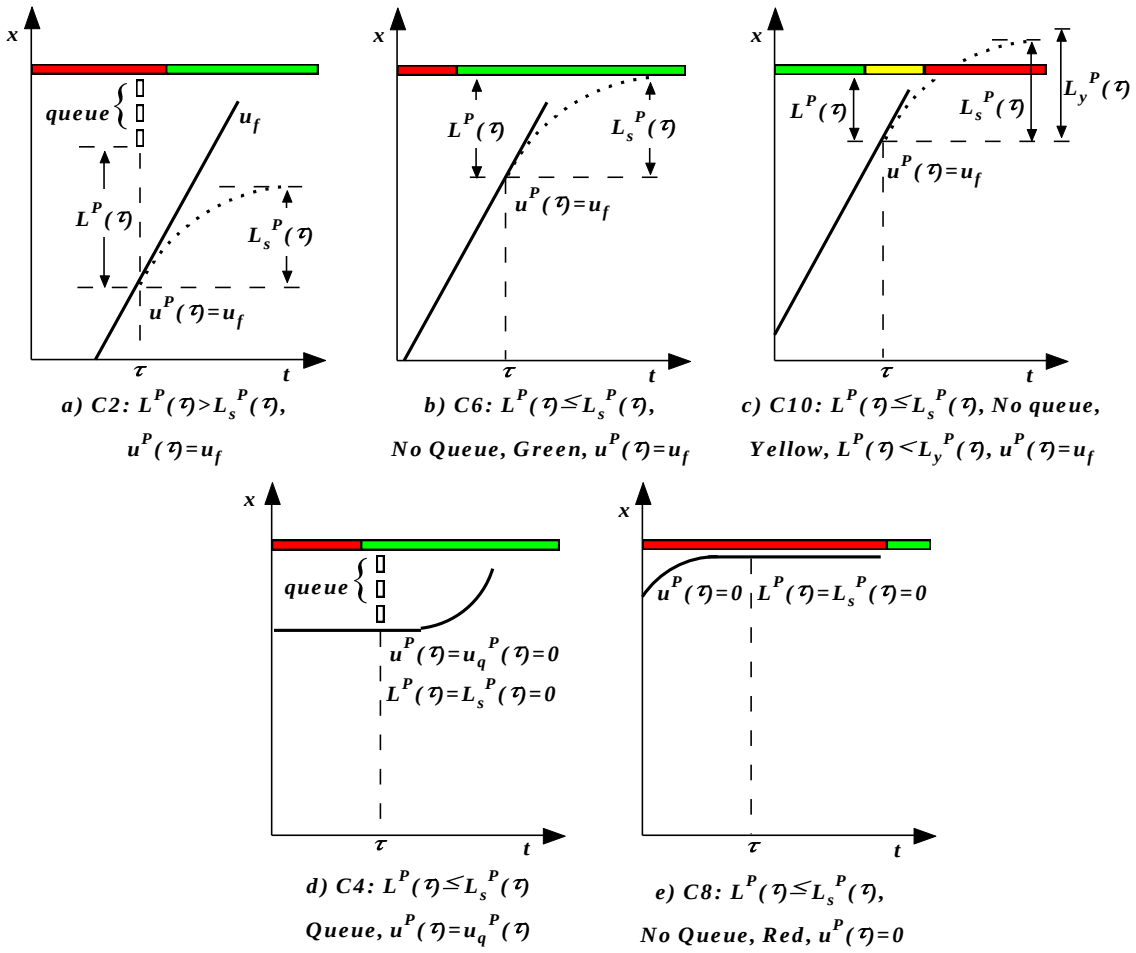

Figure 5.6: No-speed-change Maneuver Selection.

5.2.5 Self-correction Property

With the high-resolution traffic signal data, the proposed virtual probe model can self-correct the travel time estimation error, and the error will not propagate. Imagine that there exists a real vehicle probe running simultaneously with the virtual probe, and the difference in terms of their trajectory is the estimation error. If the two vehicles are stopped by a red signal or a queue, the error accumulated from previous tracing steps would be self-corrected to some extent as demonstrated in Figure 5.7. In the figure, the red and blue lines represent the trajectories of the faster and slower vehicles, respectively. Note that either the real vehicle probe or the virtual one could be running faster. We denote x_f and x_s as the locations and T_a and T_b the time instants when they join the queue. The difference between T_a and T_b, i.e., $T_b - T_a$, is the travel time estimation error. If no queue exists during the red signal time, x_f and x_s will overlap at the stop-line, therefore the estimation error will become zero. Otherwise, when the signal turns green and these two vehicles are released from the queue, their travel time difference, $T_d - T_c$, become smaller, comparing with $T_b - T_a$. The reason is that the queue formation speed (the slope of the line *ab*) is generally slower than the queue discharge speed (the slope of the line *cd*). As a result, the travel time difference between the real probe and the virtual one will always decrease whenever both vehicles meet the red light or join a queue.

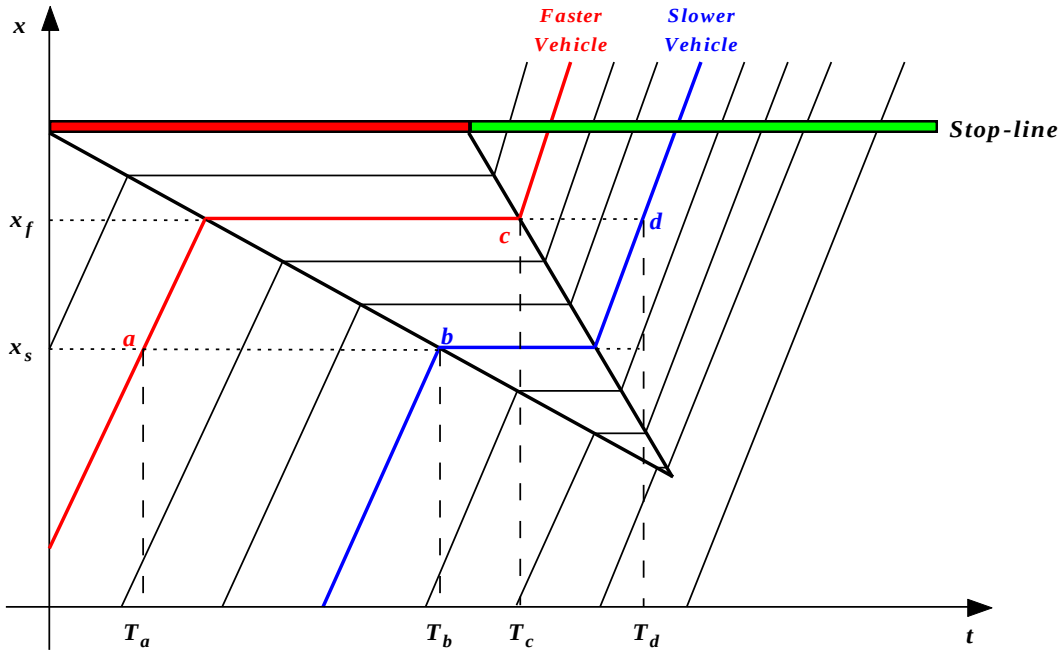

Figure 5.7: Demonstration of Self-correction Property.

It should be noted that the self-correction property occurs only when both the virtual probe and the real one can pass the intersection within one cycle. If they arrive at the intersection at different cycle or they cannot be discharged from the intersection within a cycle, the estimation error cannot be self-corrected. We should further note that self-correction property is independent of traffic condition, either heavy or light. As long as the above condition (i.e., both vehicles can pass the intersection within the same cycle) is met, then the estimation error can be self-corrected.

Figure 5.8 further elaborates an example of the self-correction property by comparing the trajectories of the real vehicle (the blue solid line in the figure) and the virtual probe (the red dashed line in the figure). As shown in the figure, assuming a real vehicle starts the journey at time T_O, the same starting point of a virtual probe (i.e. $T_O = T_O{}'$). The real vehicle arrives at stop-line 1 at time T_1 and the virtual probe arrives at time T'_1, then there is an error $\Delta e_1 = T_1 - T_1{}'$. Assuming $\Delta e_1 < 0$, which means the virtual probe travels faster than the real vehicle due to some estimation errors, the error propagates to the next intersection if the real vehicle does not stop. The absolute value of the error, i.e. Δe_2, becomes larger at intersection 2 as shown in the figure. However, if the vehicle is blocked at an intersection, the faster one would "wait" for the slower one, and they started together with the commencement of the green time. Hence, the aggregated error is self-corrected at the blocked intersection. For example, although the virtual probe arrives at intersection 3 earlier than the real vehicle, it must wait the real vehicle because of the red signal. The absolute value of Δe_3 is then corrected by the red signal. Therefore, the error aggregated through several intersections will be self-corrected at a blocked intersection, and the final estimation error Δe is not aggregated for the full arterial length.

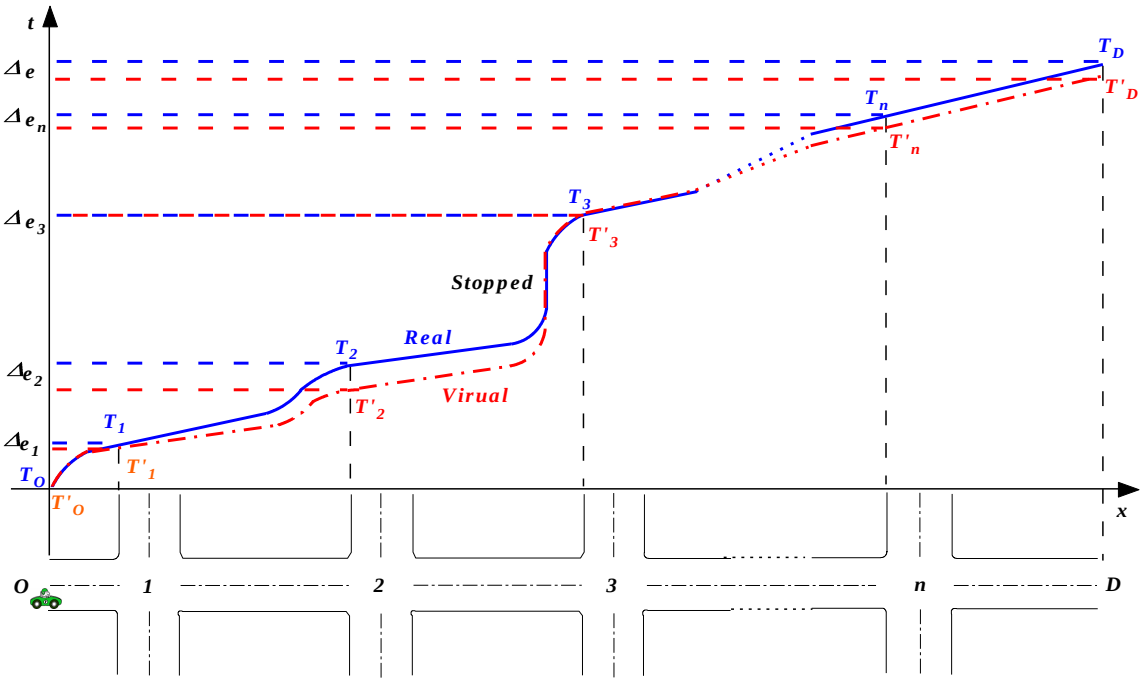

Figure 5.8: An Illustrative Example of the Self-correction Property.

Thanks to the self-correction property, the proposed model is robust and the model is not sensitive to parameters. The error would be self-corrected even if the parameters were not well-calibrated. The model works well under both under-saturated traffic and saturated traffic. When the traffic is light, the impact of queue is not significant, and the error is small; when the traffic is heavy, the vehicle is going to stop frequently, and thus has higher opportunity to self-correct the error. Therefore, the proposed model can be widely adopted due to its robustness.

In addition, we should note that the estimated arterial travel time should be an interval instead of a single value because driver's risk attitude is different. Risk-seeking drivers may have higher desired speeds, acceleration and deceleration rates; while risk-adverse drivers may have lower ones. The corresponding travel times may have large differences especially when vehicles arrive at the intersection at the yellow times. For example, if two identical vehicles arrive at the intersection at yellow time, one is a little bit faster and it can enter the intersection; while the other one is a little bit slower and it must stop for the next green. The proposed model can easily accommodate diverse driver risk attitude and generate an estimated interval of travel times.

5.3 Model Implementation and Testing

5.3.1 Study Site

The proposed model is applied to a 1.83-mile long major arterial corridor named France Avenue in Minneapolis, MN. As shown in Figure 5.9, there are 11 signalized intersections started from 69th Street to 84th Street with link length varying from 510 to 1,470 feet. There are three lanes for both directions from 69th Street to I-494S Ramp, and two lanes thereafter to 84th Street. Additional lanes are available for the turning movements at intersection approaches. The speed

limit is 40 mph. Vehicle-actuated signal timing plans are operated in coordination mode for all intersections. Link-based inductive loop detectors are placed approximately 250 to 300 feet upstream of the intersection stop-lines on France Avenue Stop-bar detectors are also installed on most of the cross street approaches. The data collection system described in Chapter 3 is installed at all 11 intersections of the corridor. Daily event log files are stored in the industrial computers located at the field cabinets, and then transferred back and archived in the database at the University of Minnesota.

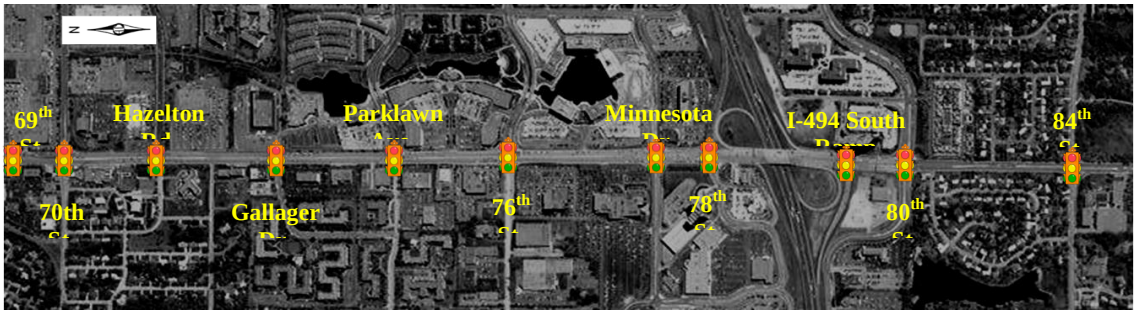

Figure 5.9: Study Site in Minneapolis, MN: France Avenue (69th Street ~ 84th Street).

A field study was undertaken to obtain the ground truth travel time of the arterial corridor. 23 floating car runs were performed on three different weekdays during the afternoon peak hours with a desired speed around 40 mph. The time instants when the floating car passed the stop-lines of the intersections were recorded with a stop watch.

5.3.2 Results Analysis

The Root Mean Squared Percent Error (*RMSP*), a widely used error measure that can provide a good estimate of the degree of fit between the estimated and the observed traffic measurements, is applied to verify the results of the proposed model as in Equation 5.8.

$$RMSP = \sqrt{\frac{1}{n}\sum_{i=1}^{n}\left(\frac{\hat{x}_i - x_i}{x_i}\right)^2} \qquad (5.8)$$

where *RMSP* is the root mean squared percent error, x_i is the i^{th} estimated traffic measurement value, and $\hat{x}_i$ is the i^{th} observed traffic measurement value.

The default values of the parameters for the estimation of the travel time are obtained either from published sources (Institute of Transportation Engineers, 1999) or field data calibration. In this project, the acceleration rate γ_a is 3.6 ft/s^2, the deceleration rate γ_d is 10 ft/s^2, the desired speed u_f is 40 mph, the saturated space headway h is 24 ft, the reaction time t_r is 1 second, the starting time difference between two adjacent queued vehicles t_s is 0.5 second, and the vehicle tracing step Δt is 1 second.

- **Vehicle Trajectory**

Figure 5.10 demonstrates the trajectory of a virtual probe traveling from 84th Street to 69th Street on May 14th, 2007. The solid line in the figure is the trajectory of the virtual probe; the stars in the figure indicate the location and time of the real floating car; the red time durations of the 11 intersections are denoted as the red bars in the figure. It can be seen that the virtual probe approach can estimate the travel time accurately since the virtual probe trajectory matched closely with those of the real floating car. Although the acceleration and deceleration curves can hardly be seen from the figure due to its scale (1.9 miles along y-axis), some other interesting information is apparent from the trajectory. For instances, the queue length in front of the vehicle at each intersection is clear; the vehicle passed through the intersection of I-494 South and France Avenue during the yellow time; the vehicle arrived at the intersection of Minnesota Dr. and France Avenue at the beginning of green but still stopped for a couple of seconds because of the queue at the intersection; all of these are difficult to obtain from traditional arterial performance measurement but become apparent here. Note that on May 14th, 2007, the traffic signals on France Avenue were not coordinated due to a signal retiming effort, therefore the traffic condition was congested and high delay were experienced by the drivers. It can be seen that the proposed model works well under congestion.

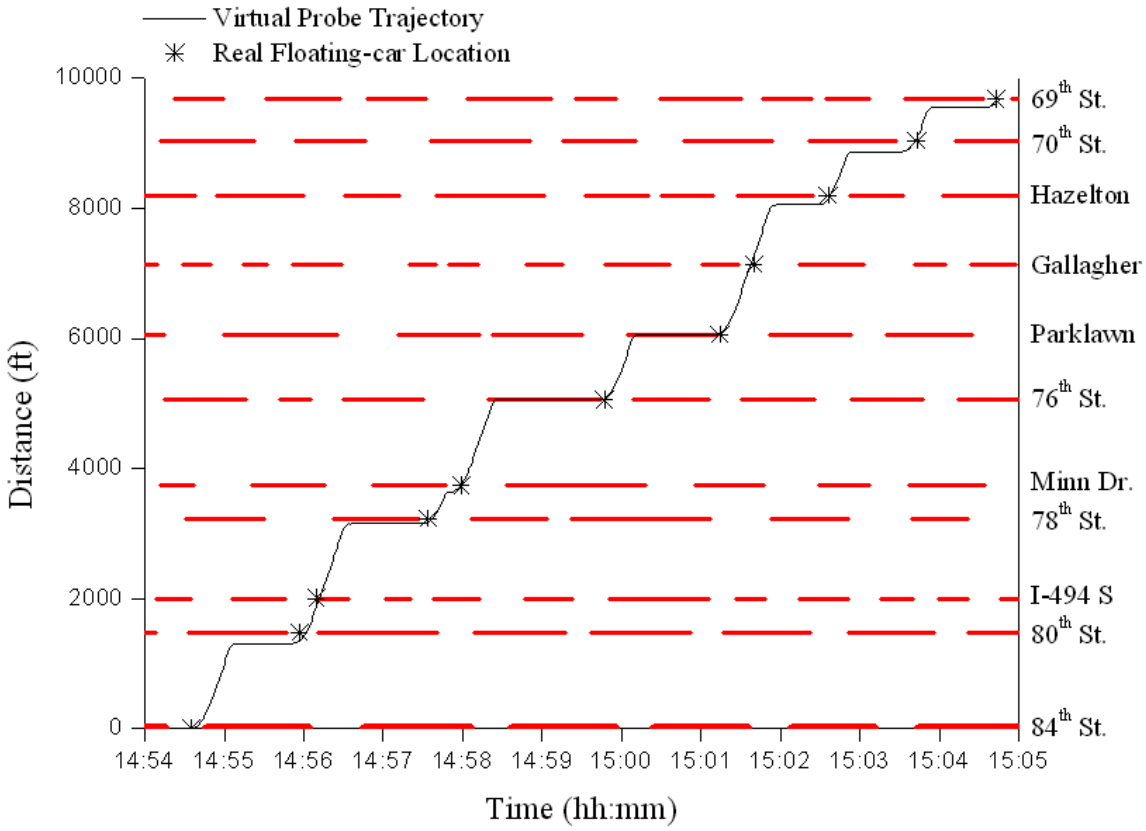

Figure 5.10: Example Virtual Probe Trajectory on May 14th, 2007.

- **Travel Time**

Figure 5.11 compares the northbound corridor travel time estimated by the proposed model and the corridor travel time observed from floating car runs. Each blue diamond data point in the figure represents the observed travel time for the floating car run from 84th Street to 69th Street, and each red rectangle data point in the figure represents the travel time estimated by the proposed model with same direction. The model uses the stop-line of 84th Street as the starting point and the stop-line of the 69th Street as the ending point. Correspondingly, the times when the vehicle passed the two stop-lines were used as the starting and ending times. The figure shows the proposed virtual probe model has good arterial travel time estimation with small errors in most floating car runs. Most runs have errors smaller than 3.5%, except Run 5 (15:50:37) has 45 seconds of error, in which case the estimated value is 13.8% slower than the observed value. The computed statistic measure *RMSP* is 0.0325, which is very small and in an acceptable range.

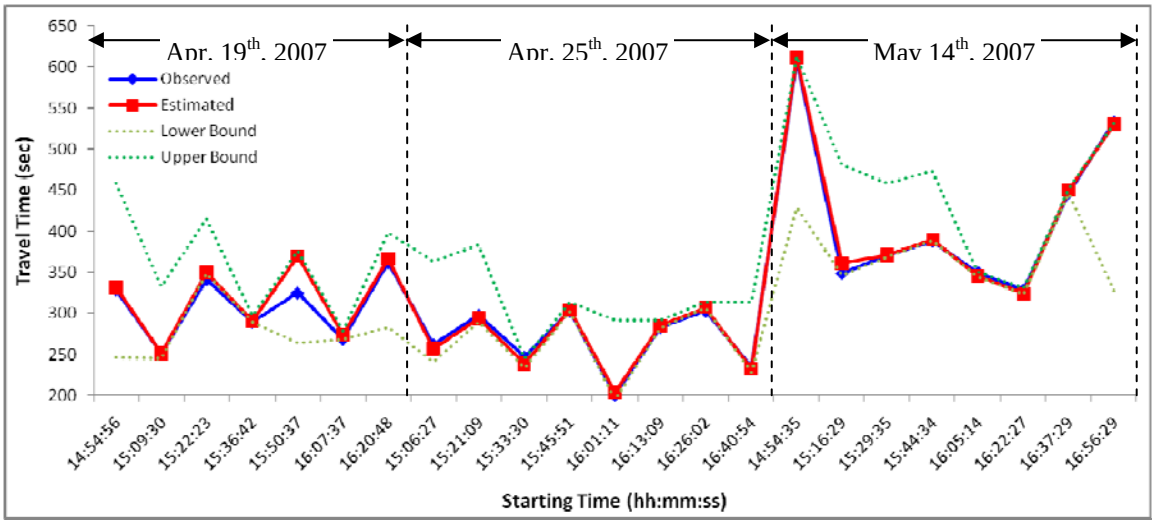

Figure 5.11: Observed vs. Estimated Corridor Travel Time on France Avenue.

A Monte Carlo simulation run is also performed to generate the travel time interval with a variation of drivers' desired speed as shown in Figure 5.11. To obtain the distribution of the desired speed, a sample of 200 field isolated vehicle speed is obtained with a speed gun at the middle link on France Avenue at off-peak hours. One thousand virtual probe runs are generated based on the sample and the results are shown in Figure 5.11. The light green dashed line is the lower bound travel time of 95% percentile vehicles, and the dark green dashed line is the upper bound travel time of 95% percentile vehicles. It can be seen that both the estimated and observed travel times are within the boundaries.

Table 5.1 shows the comparison of the observed and estimated travel times of the 23 runs from 84th Street to all other 10 intersections. The time when vehicle passed the stop-lines are used as the measuring points. The table also shows good estimation of the proposed model except Run 5. The biggest error is 14 seconds if not considering Run 5. The overall statistic measure *RMSP* is 0.0624 even including Run 5, which is also in an acceptable range.

The large error of Run 5 is the result of the vehicle arrival at the boundary time of a phase as discussed in Section 4. It can be seen from the table that the model has a good match until the vehicle passed Parklawn Avenue, both the virtual probe and the floating car passed the stop-line at 15:54:12, which was 215 seconds after the starting time. The floating car passed the stop-line of Gallagher Avenue at 15:54:29, when was the last second of the yellow time according to the signal data. However, due to some estimation errors, the virtual probe "*arrived*" at Gallagher Avenue a little bit slower (maybe just 1 second) at the beginning of the red time. The virtual probe must wait for the next green and there is 25 seconds error. The floating car passed the stop-line of Hazelton Rd. at 15:54:47, which was also the last second of the yellow time, and the following red time was 60 seconds. Therefore the error is propagated to 73 seconds. Both vehicles reached 70th Street at the green time interval, thus the error is still increase but not significant. The floating car had a 54 seconds red time delay at 69th Street, while the virtual probe "*arrives*" at the intersection during green time. The self-correction mechanism plays its role and the error is decreased from 91 seconds to 45 seconds.

Table 5.1: Observed vs. Estimated Travel Time on France Avenue.

Run	Starting Time		84th St.	80th St.	I-494 S Ramp	78th St.	77th St.	76th St.	Parklawn Ave.	Gallagher Dr.	Hazelton Rd.	70th St.	69th St.
1	14:54:56	O	0	72	84	132	142	175	193	213	233	249	329
		E	0	74	86	140	150	184	202	220	239	253	332
2	15:09:30	O	0	43	56	100	111	134	169	198	222	239	252
		E	0	52	62	107	117	140	177	208	227	241	252
3	15:22:23	O	0	104	117	164	175	197	245	271	289	327	341
		E	0	107	119	172	182	205	256	275	293	338	350
4	15:36:42	O	0	94	107	146	161	184	202	223	241	275	290
		E	0	97	111	153	165	188	205	224	242	279	291
5	***15:50:37***	***O***	***0***	***88***	***102***	***157***	***173***	***198***	***215***	***232***	***250***	***266***	***325***
		E	***0***	***94***	***106***	***154***	***175***	***198***	***215***	***257***	***323***	***357***	***370***
6	16:07:37	O	0	61	74	105	130	159	187	205	224	253	269
		E	0	60	72	111	134	166	184	202	220	262	274
7	16:20:48	O	0	101	114	159	192	219	237	255	272	288	362
		E	0	111	122	164	197	222	239	257	275	290	367
8	15:06:27	O	0	84	96	141	157	183	198	217	235	250	262
		E	0	89	99	145	156	178	195	214	232	246	257
9	15:21:09	O	0	43	55	99	121	147	164	184	265	284	298
		E	0	39	53	104	124	147	164	182	267	283	294
10	15:33:30	O	0	25	34	64	84	111	161	185	214	235	247
		E	0	26	35	63	80	105	160	179	213	228	239
11	15:45:51	O	0	89	103	156	168	196	220	242	262	289	303
		E	0	95	106	164	175	200	227	247	265	292	304
12	16:01:11	O	0	31	40	74	86	113	131	150	168	187	201
		E	0	26	35	81	91	114	131	149	168	191	204
13	16:13:09	O	0	31	41	68	99	126	189	213	233	267	283
		E	0	26	35	70	99	122	195	216	234	273	285
14	16:26:02	O	0	55	68	128	147	176	217	240	262	290	303
		E	0	65	75	136	146	178	217	236	255	294	307
15	16:40:54	O	0	37	48	82	119	146	165	185	205	222	235
		E	0	30	40	83	116	139	156	175	193	222	233
16	14:54:35	O	0	82	95	179	204	312	399	425	481	548	608
		E	0	80	92	178	204	310	397	423	484	549	612
17	15:16:29	O	0	28	38	63	107	133	220	264	285	326	349
		E	0	26	35	55	108	131	220	264	284	331	361
18	15:29:35	O	0	95	133	179	192	224	278	301	336	354	371
		E	0	94	142	193	203	232	288	307	343	359	371
19	15:44:34	O	0	88	111	145	158	249	270	289	308	344	388
		E	0	94	120	154	169	264	282	300	318	346	390
20	16:05:14	O	0	40	58	80	125	217	238	258	279	295	350
		E	0	48	59	80	118	212	230	248	266	295	346
21	16:22:27	O	0	40	94	145	156	198	238	262	290	313	329
		E	0	46	94	148	158	193	241	260	296	311	324
22	16:37:29	O	0	31	66	119	208	264	297	342	371	428	447
		E	0	40	72	129	207	268	297	345	365	430	450
23	16:56:29	O	0	117	131	204	223	310	359	409	435	506	533
		E	0	114	131	207	222	309	355	408	429	504	531

* *E represents the estimated travel times and O represents the observed travel times;*

** *the travel time values are all in second.*

- **Parameters Sensitivity Analysis**

Table 5.2 provides the travel time estimation results from a sensitivity analysis by varying the model parameters. The selected parameters include desired speed, acceleration rate and deceleration rate. The parameter values were changed to both lower and higher ones, and the travel time were calculated by varying one-parameter-at-a-time. It can be seen that, although the default parameters value provide the best estimate, the virtual probe model can generate reasonably accurate travel time estimation even by varying the default parameters.

Table 5.2: Results of Parameters Sensitivity Analysis.

Parameters	Value 1	Value 2	Default Value	Value 3	Value 4
Speed (mph)	30	35	40	45	50
Average Error	13.4%	8.1%	1.8%	6.2%	6.7%
Acceleration Rate (ft/s2)	2	3	3.6	4	5
Average Error	12.7%	3.8%	1.8%	2.9%	4.0%
Deceleration Rate (ft/s2)	6	8	10	12	14
Average Error	3.8%	4.5%	1.8%	3.8%	3.7%

We further test the model using infinity acceleration and deceleration rates and zero yellow time (only effective green and effective red), the average estimation will jump from 1.8% to 18.1%. This demonstrates that acceleration and deceleration process needs to be considered in the travel time estimation, especially for signalized arterial, which has higher frequency of stop and go conditions comparing with freeway.

- **Long Queue Estimation Model Improvement**

We also analyze the effects of the queue estimation to travel time estimation. As previously described in Chapter 4, queue length estimation can be divided into two categories as short queue estimation and long queue estimation. When queue spills over advance detector, vehicle arrivals are not available. Long queue estimation should be applied as short queue estimation model cannot represent true traffic conditions. Some of the default parameters were adjusted according to the observation from the field videos. From the seventy sample long queue cycles recorded at the intersection of 76th Street and France Avenue, the saturation headway h is changed to 30 ft, the reaction time t_r is still 1 second, and the starting time difference between two adjacent queued vehicles t_s is changed to 1.2 seconds.

Figure 5.12 shows the travel time model performance without long queue consideration. As can be seen, most of the data points fall on the red line which indicates good estimation; however, some of the data points do not fall close to the red line. The samples without good estimation are from May 14th, 2007, when the traffic condition was congested due to a retiming effort on France Avenue. The average estimation error for the overall 23 samples is 8.6%, which is 29.7 seconds, and the overall *RMSP* is 0.1564. The estimation error for the 15 samples on April 19th and 25th is only 4.2%, which is equal to 13.5 seconds; however, the estimation error on May 14th increases to as large as 16.9%, which is equal to 60.3 seconds. The result indicates although overlooking long queue case can still generate good travel time estimations under

uncongested traffic conditions; it is going to have trouble on the estimation under congested traffic conditions.

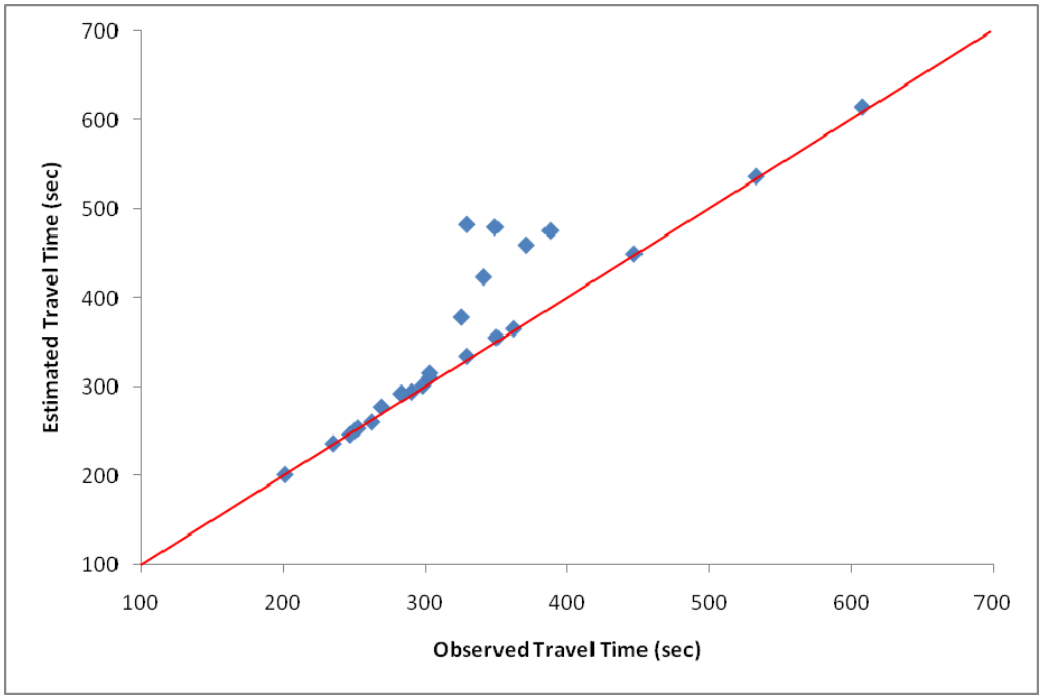

Figure 5.12: Travel Time Estimation Model Performance without Long Queue Consideration.

Figure 5.13 shows the travel time model performance with long queue consideration. As can be seen, the majority of the data points fall on the red line on all of the three days. The average estimation error for the overall 23 samples decreases to 4.1%, which is 13.8 seconds, and the overall *RMSP* is 0.0856. The estimation error for the 15 samples on April 19th and 25th is 3.0%, which is equal to 9.3 seconds; the estimation error on May 14th is 6.1%, which is equal to 22.4 seconds. The result shows with long queue consideration, the error for the 23 samples is half of those without long queue consideration. The performance for the 8 samples on May 14th almost increases three times. Long queue consideration is necessary for travel time estimation under congested traffic conditions. The proposed long queue model can significantly improve the estimation performance.

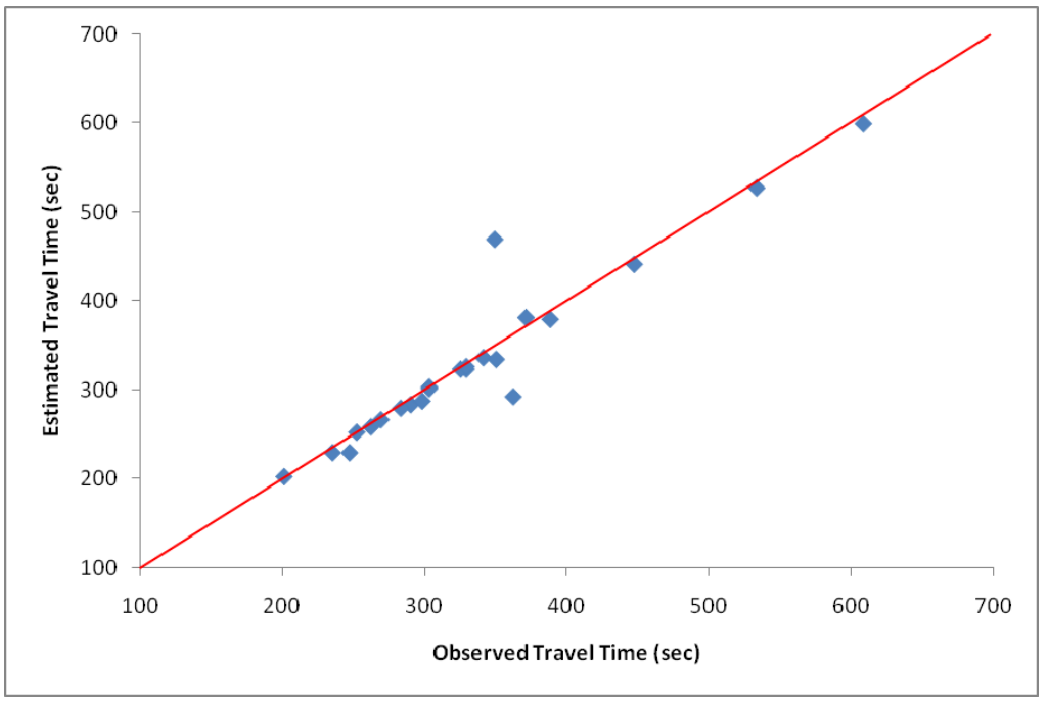

Figure 5.13: Travel Time Estimation Model Performance with Long Queue Consideration.

5.4 Summary

Arterial travel time is an important performance measures for both road travelers and traffic engineers; however, previous research works on arterial travel time estimation do not appropriately account for the needs of a real-time performance measurement system. A virtual probe approach is proposed in this project to calculate the time-dependent arterial travel time based on the data from existing signal controllers and vehicle detection systems. This research fully utilizes all available traffic information, including not only the detector data but also the corresponding signal status data, to conduct the estimation. Unlike most of the previous works that simply aggregate the travel time as the free flow travel time and delays, the proposed model considers the correlations of the states of the vehicle and thus to make the maneuver decision at each time step. Moreover the impact of yellow time, which is usually omitted, is also included. An interesting property of the proposed model is that travel time estimation errors can be self-corrected, because the differences between a virtual probe vehicle and a real one can be reduced when both of them meet a red signal phase and/or a vehicle queue. Therefore the model can be implemented under various traffic conditions, and can generate accurate results even in congested arterials. A field study at an 11-intersections corridor along France Avenue in Minneapolis, MN shows promising results.

Chapter 6. Field Implementation

6.1 Case Study Description

In May 2007, a major signal retiming effort on France Avenue was initiated by the Hennepin County Transportation Department (Alliant Engineering Inc., 2007), in parallel to our project. New signal timing plans were developed and implemented on the 17 intersections along the France Avenue between TH 62 North Ramp and 84th Street, which covers the 11 intersections studied by the authors. The new timing plans were downloaded to the intersection controllers on May 14th, 2007, and have been reviewed during the week of May 14th.

Performance measures generated from SMART-SIGNAL system were used to examine the benefits of the new signal timing plans. We processed the data of two afternoon peak-hours (3 pm to 5 pm) over 10 weekdays before retiming (Apr.19th ~ May 2nd 2007) and after retiming (June 7th, 2007 ~ June 20th, 2007). The comparisons of various "before" and "after" performance measures are discussed next.

6.2 Comparisons of Intersection Performance Measures

In the following, we compare the intersection performance measures before and after signal retiming, using the intersection of 76th Street and France Avenue as an example (the layout of the intersection is shown in Chapter 4). The comparisons of some important intersection performance measures, including arrival type, cyclic volume and occupancy profile, delay, LOS, queue size and queue length, are discussed.

Arrival type is one of the intersection measures to evaluate the signal timing performance at individual intersections (Transportation Research Board, 2000). Arrival type can be indicated by the proportion of all vehicles in movement arriving during green phase, which is noted as P and can be calculated as Equation 6.1.

$$P = \frac{N_g}{N_g + N_r} \tag{6.1}$$

where N_g is the number of vehicles arriving on green time, and N_r is the number of vehicles arriving on red time. Phase 6 (northbound) data over the 10 weekdays at the intersection of 76th Street and France Avenue are calculated and compared. The proportion of vehicles arriving during green phase is 78.9% before retiming, and 83.4% after retiming, and the improvement of the new timing plan is 5.7%.

Figure 6.1 compares vehicle arrival profiles over a full cycle of Phase 6 before and after retiming (Shelby *et al.*, 2007). Both examples are generated from the historical data of the PM peak hours with 140-seconds cycle length. The colors and lengths of the bars in Ring 1 and Ring 2 indicate the active phases and durations in the cycle. The blue bars in the plot indicate northbound vehicle arrival during the cycle (the bar is not scaled with the magnitude of the volume but only shows the occurrence of an arrival event). The figure indicates that the coordination of the corridor before retiming is not good: a group of northbound vehicles arrive at

the intersection during the red time and thus cause high signal delay; on the contrary, the coordination after retiming is better: most northbound vehicles arrive at the intersection during the green time and can pass the intersection with less intersection delay.

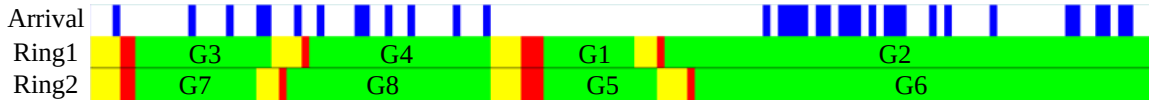

a) Before Retiming: Cycle Start at 4:36:34 pm (Apr. 19th, 2007)

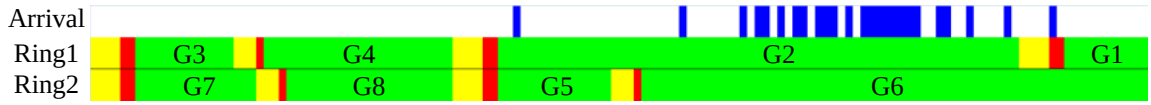

b) After Retiming: Cycle Start at 4:45:33 pm (May 21st, 2007)

Figure 6.1: Comparison of Vehicle Arrivals within One Cycle at the Study Intersection.

Figure 6.2 compares the cyclic volume and occupancy profiles averaged over the two peak hours of 10 weekdays before retiming and after retiming at the intersection of 76th Street and France Avenue. The x-axis is the local cycle time of the controller starts from the end of the recall phase, i.e. Phase 6 in this intersection. The magnitude of the volumes and occupancies are denoted by the height of the corresponding bars in the plots. The height of the green bar indicates the probability that Phase 6 is green at the time in the cycle (Gettman *et al.*, 2007). For example, green probability at local time 0 is always 0 since when Phase 6 is just switched from green to yellow.

Figure 6.2 indicates the signal plans after retiming are better than those before retiming, but still have rooms for improvement. The "after" timing plans have better coordination than the "before" ones. Before retiming, there is high northbound volume arrives at the intersection at the beginning of the cycle when Phase 6 turns to yellow and red, the vehicle arrival is scattered during the cycle; however, after retiming, most northbound traffic arrives at the intersection at the second half of the cycle when Phase 6 has high green probability, the vehicle arrival is concentrated during the green time. The "before" timing plans have the "early return to green" problem that one or more non-synchronized phases gap out earlier than required and the coordinated phase, i.e. Phase 6 in this case, has the green time earlier. Figure 6.2(a) illustrated that starting at local time 97, the probability of green is 100% (meaning that the latest starting time of Phase 6 is time 97); while there are cycles starts Phase 6 as early as local time 60, when Phase 6 traffic is light. The difference of the Phase 6 starting time is 37 seconds. On the contrary, the "after" timing plans alleviate the problem with 22 seconds difference. However, the "after" timing plans still have the "early return to green" problem and they also do not maximally utilize the green time. Figure 6.2(b) shows the green probability is 100% between local time 120 to 140 when the traffic is light, while the traffic is heavier before local time 83 when the green probability is lower than 100%. The "after" timing plans may be further improved by changing the offset and starting Phase 6 earlier.

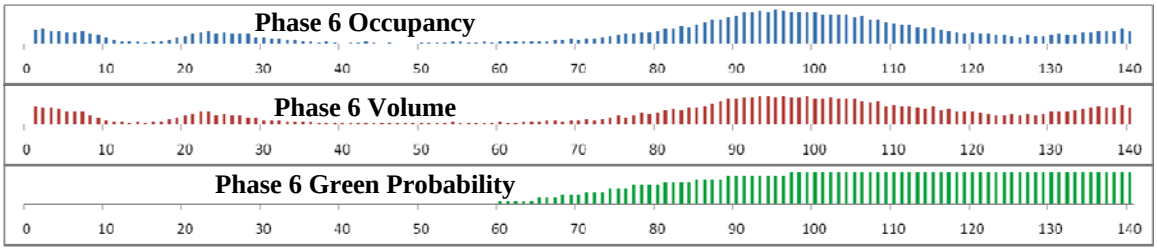

a) Before Retiming: Averaged Over 10 weekdays from 3pm ~ 5pm (Apr.19th ~ May 2nd 2007)

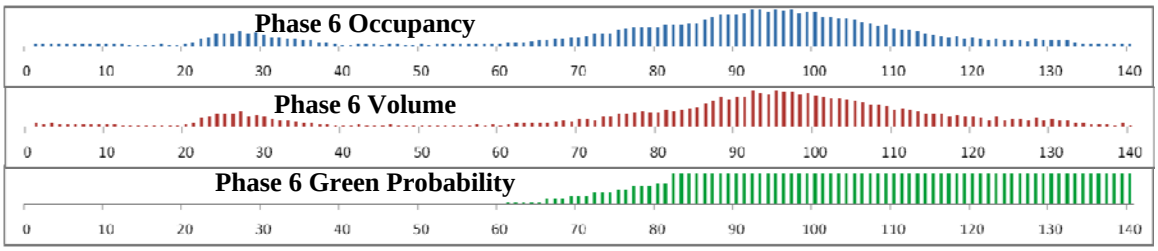

b) After Retiming: Averaged Over 10 weekdays from 3pm ~ 5pm (June 6th ~ June 20th, 2007)

Figure 6.2: Comparisons of Cyclic Volume and Occupancy Profiles at the Study Intersection.

Figure 6.3 and Figure 6.4 compare the intersection delay and LOS averaged over the two peak hours of 10 weekdays before retiming and after retiming at the intersection of 76th Street and France Avenue. The delay is estimated by the proposed virtual probe vehicle approach, and LOS is obtained according to the Highway Capacity Manual (Transportation Research Board, 2000). The figure shows the new timing plan reduced the delay at each 15-minutes interval of the two peak hours. The averaged delay is reduced from 23.0 seconds to 20.9 seconds, and the improvement is 9.3%.

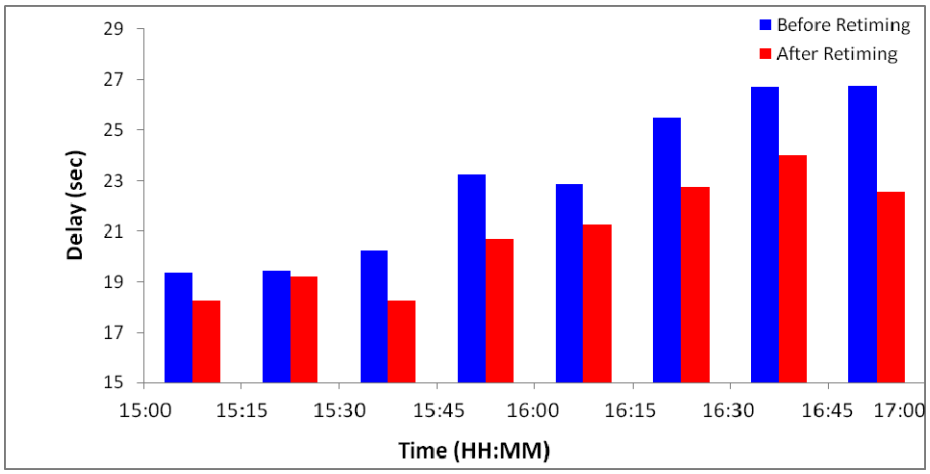

Figure 6.3: Comparisons of Delay at the Study Intersection.

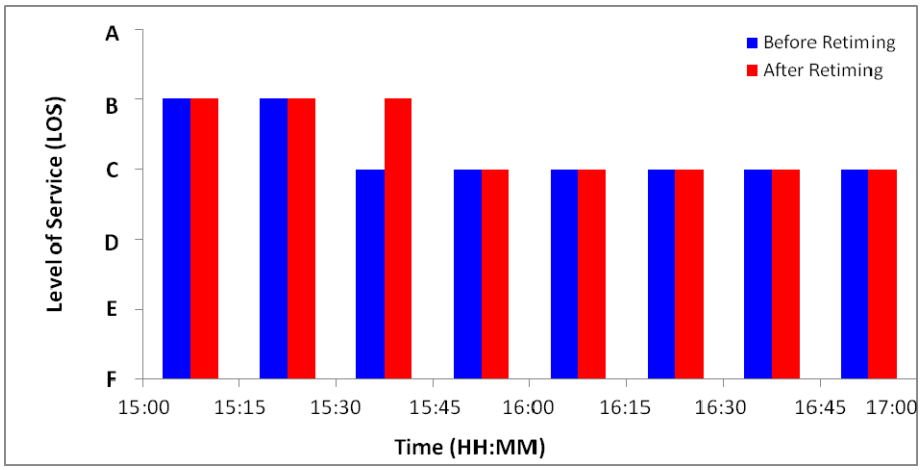

Figure 6.4: Comparisons of LOS at the Study Intersection.

Figure 6.5 and Figure 6.6 compares the queue length and queue size averaged over the two peak hours of 10 weekdays before retiming and after retiming at the intersection of 76th Street and France Avenue. It can be seen that for 7 of 9 intersections, the queue length after retiming is smaller than those before retiming. The overall averaged queue length of the 9 intersections is reduced from 112.9 ft to 98.9 ft. The new timing plans have 12.4% improvement. Similarly, the queue size for the 7 of 9 intersections decreases. The overall averaged queue size of the 9 intersections down from 9.2 vehicles to 8.3 vehicles, and 9.6% improvement is obtained.

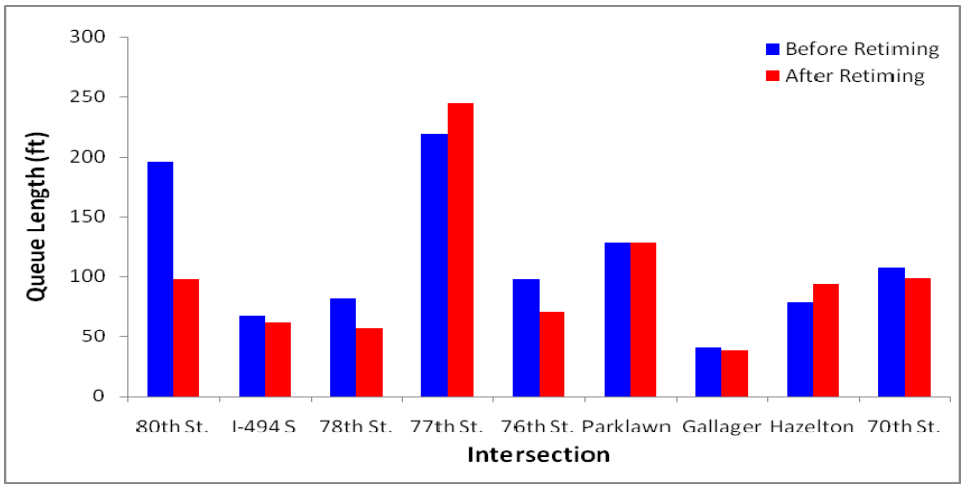

Figure 6.5: Comparisons of Queue Length at the Study Intersection.

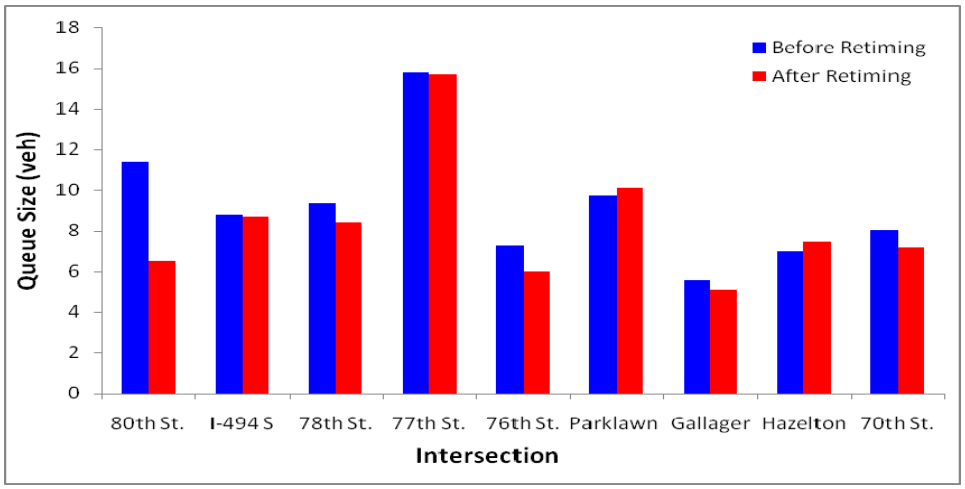

Figure 6.6: Comparisons of Queue Size at the Study Intersection.

6.3 Comparisons of Arterial Performance Measures

The calculations of arterial performance measures in this project are based upon the virtual probe approach mention above. The model has been validated with field investigation on the corridor of France Avenue (the details are described in Chapter 5). The comparisons of some important arterial performance measures, including travel time, delay, number of stops, stop time and vehicle probe trajectory, are discussed.

Figure 6.7 and Figure 6.8 compare the northbound travel time and delay along the France Avenue from 80th Street to 70th Street before and after retiming. The blue bars in the figure are the averaged 15-minutes measures of vehicles traveling during 3 pm to 5 pm at the 10 weekdays before retiming, and the red bars are those after retiming. The figures show both travel time and delay are reduced after the installation of the new timing plans. The averaged travel time was reduced from 226.0 seconds to 217.8 seconds, and the improvement is 3.6%; the averaged delay was reduced from 74.0 seconds to 65.8 seconds, and the benefit is 11.0%.

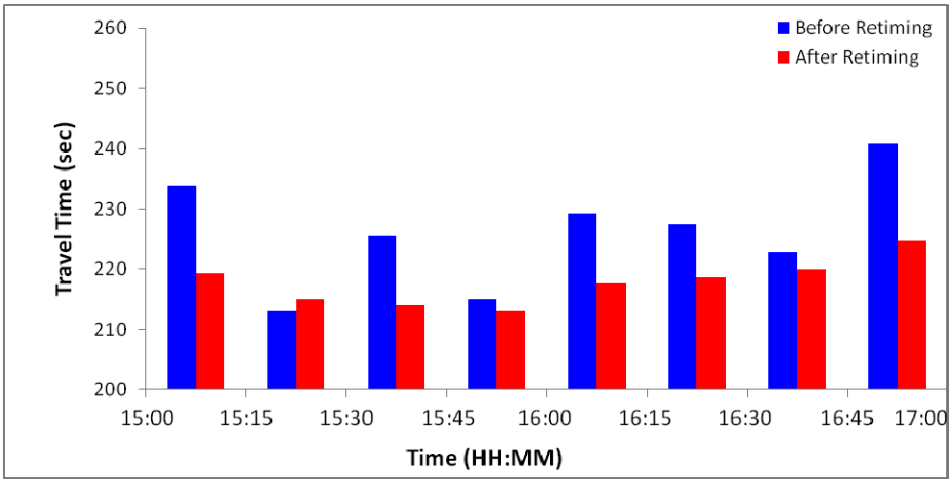

Figure 6.7: Comparisons of Travel Time at the Study Corridor.

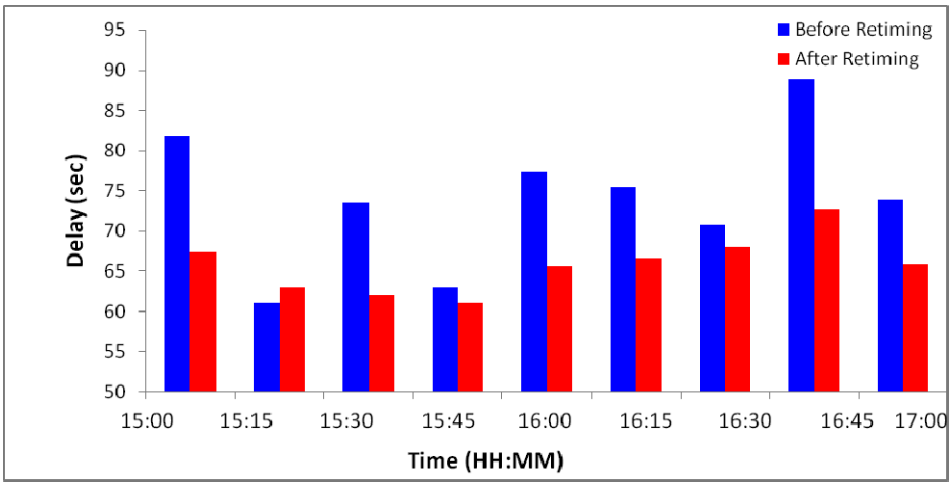

Figure 6.8: Comparisons of Delay at the Study Corridor.

Figure 6.9 and Figure 6.10 compare the northbound number of stops and stop time along the France Avenue from 80th Street to 70th Street before and after retiming. The blue bars in the figure are the averaged 15-minutes measures of vehicles traveling during 3 pm to 5 pm at the 10 weekdays before retiming, and the red bars are those after retiming. The figures show the number of stops is significantly reduced; an average of 35.0% improvement has been obtained with the number of stops has been reduced from 2.8 times to 1.9 times. The stop time, i.e. the time vehicle is motionless, is also reduced during most time intervals; however, the average stop time has been increased from 54.5 seconds to 56.9 seconds, and the lost is 4.4%.

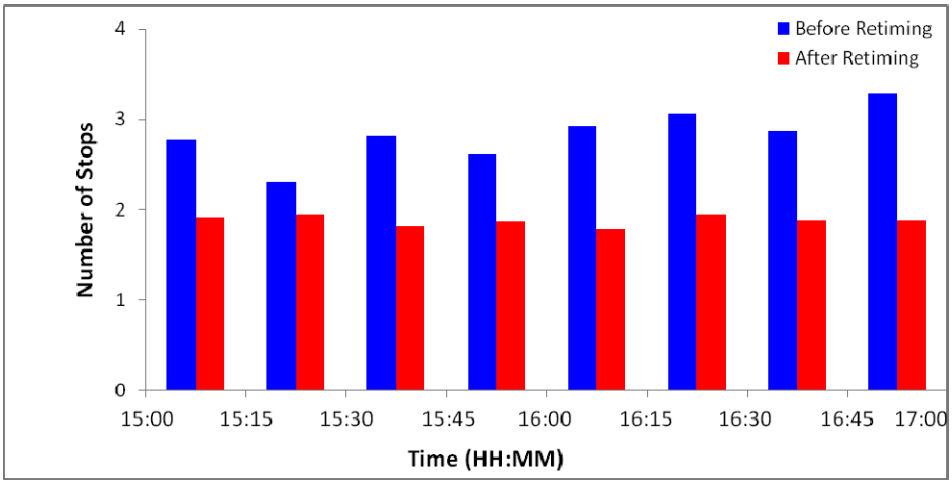

Figure 6.9: Comparisons of Number of Stops at the Study Corridor.

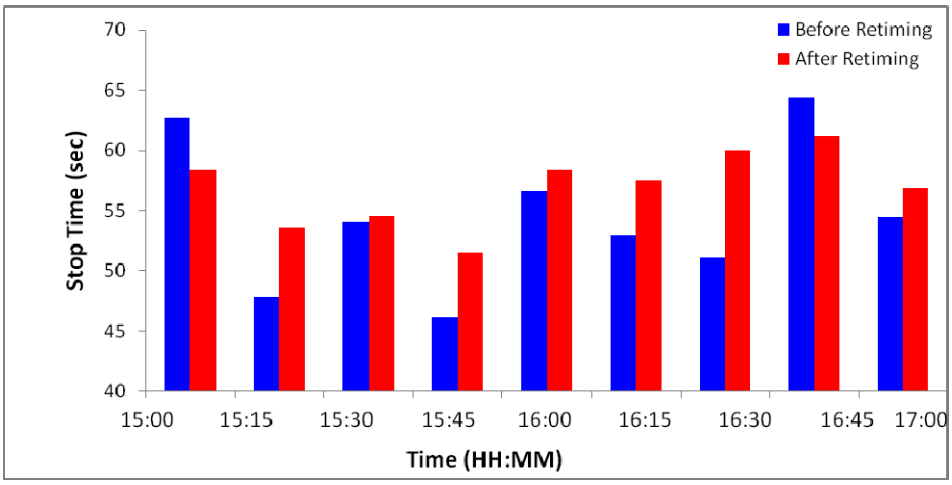

Figure 6.10: Comparisons of Number of Stop Time at the Study Corridor.

It can be seen from Figure 6.7, Figure 6.8 and Figure 6.9 that the measures of travel time, delay and number of stops are significantly improved; however, the stop time does not improve as shown in Figure 6.10. The stop time per stop is increased from 19.2 seconds per stop to 30.2 seconds per stop, which indicates the offsets of some intersections may have problems, and further fine-tune is need. This conclusion is consistent with the one we draw from Figure 6.2.

Figure 6.11 demonstrates the sample trajectories of virtual probes and real floating-cars along the France Avenue from the 80th Street to 70th Street before (journey started at 16:38:20 on Apr.19th, 2007) and after retiming (journey started at 16:44:27 on May 21st, 2007). The blue solid lines in the figures are the trajectory of the virtual probe; the stars in the figures indicate the trajectories of the real floating car; the red time durations of the intersections are denoted as the red bars in the figures. As can be seen, on both days the virtual probe approach can estimate the travel time accurately since the virtual probe trajectories match closely with those of the real probes. The figures shows coordination between signals on France Avenue improved greatly. To demonstrate the difference between the "before" and the "after", we also plot the trajectories of two other virtual probes as the dotted lines in the figures, one started at the beginning of the green phase and the other started at the end of the green phase. The differences, in terms of the number of stops experienced by the virtual probes, are apparent.

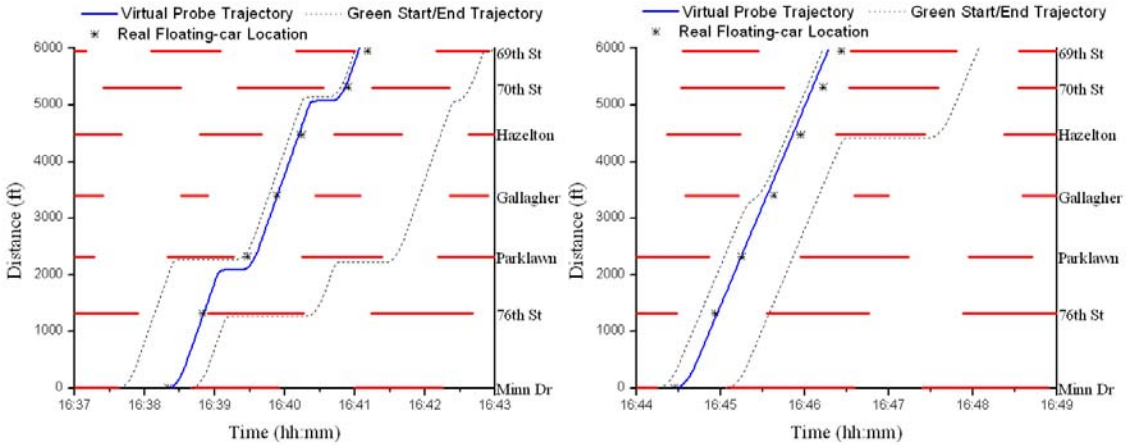

a) Before Retiming: Apr. 19th, 2007 *b) After Retiming: May 21st, 2007*

Figure 6.11: Comparisons of Virtual Probe Trajectories at the Study Corridor.

Figure 6.12 demonstrates the trajectories of virtual probes that depart at the start of green time and end of green ending. The trajectories are averaged from the two afternoon peak-hours over 10 weekdays before retiming and after retiming. It can be seen from Figure 6.12(a) that the averaged green start trajectory has an apparent delay at 78th Street. It indicates the signal setting at this intersection can be improved, which most likely is the offset problem because the trajectory is almost flat near the intersection. From Figure 6.12(b), it can be seen that the problem occurred at 78th Street has been fin-tuned by the new signal timing plans and the bandwidth is apparent; however, the delay has been postponed to the downstream intersection at 76th Street. There are rooms available to improve the signal service by further fine-tuning the signal timing plan at this intersection. Note that the analyses after the problem intersections are useless, because the averaged green start trajectory and the averaged green end trajectory are close to each other, and essentially can be treated as one trajectory.

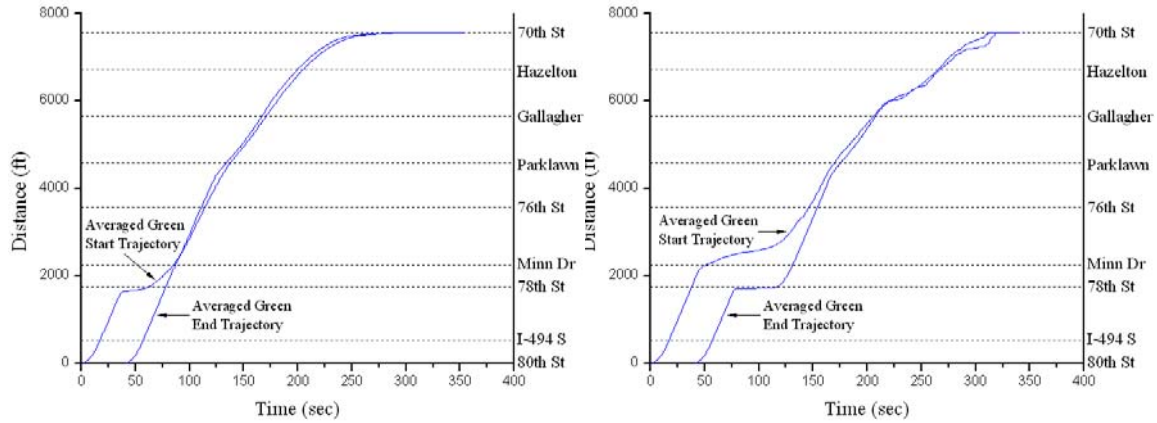

a) Before Retiming: Averaged Over 10 weekdays from 3pm ~ 5pm (Apr.19th ~ May 2nd 2007) *b) After Retiming: Averaged Over 10 weekdays from 3pm ~ 5pm (June 6th ~ June 20th, 2007)*

Figure 6.12: Comparisons of Averaged Northbound Virtual Probe Trajectories at the Study Corridor.

6.4 Summary

From the above analysis, it can be seen that, comparing to the “before” signal timing plan, the “after” one has better performance at both individual intersection level and arterial level. Performance measures, including travel time, delay, number of stops, and LOS, are improved. However, as indicated from Figure 6.2 and Figure 6.10, the “after” timing plans can be still improved and this calls for a data-driven approach to further diagnose and fine-tune the arterial signals.

Chapter 7. Conclusion

Over the past decades, the lack of resources has prevented agencies from collecting high resolution traffic data. Despite the growing needs to improve signalized intersection management, we still see that current data collection efforts for signalized arterial networks are sporadic, both spatially and temporally. Additionally, the aggregate nature of collected data fails to capture the true dynamics at play, and, thus, properly identify problems. The major contributions were two-fold in this project: 1) a system for high-resolution traffic signal data collection, archival, and preprocessing was developed; 2) reliable analytical models were developed to estimate queue length and turning movement proportions at signalized intersections and travel time for arterial corridors under various traffic conditions.

With support from the Transportation Department of Hennepin County, Minnesota, the SMART-SIGNAL arterial data collection system was successfully developed in this project. The system simultaneously collects "event-based" high-resolution traffic data from multiple intersections and generates arterial performance measures in real time. In the SMART-SIGNAL system, a complete history of traffic signal control, including all signal events such as vehicle actuations at detectors and signal phase changes, are archived and preprocessed. The SMART-SIGNAL system has been installed on 11 intersections along France Avenue in Hennepin County, Minnesota since February 2007. The data collection effort with the SMART-SIGNAL system serves as a solid foundation for the proposed theoretic work in this project. Event-based signal data are being collected on a 24/7 basis and then immediately archived in the SMART-SIGNAL system, thus yielding a tremendous amount of field data available for performance measurement research.

Based on the high-resolution data collected, a time-dependent queue length estimation model is proposed that can handle long queues under both under-saturated and over-saturated conditions. We propose a method to account for the long queue situations when queues spill over the advance detector or even back to the upstream intersections under congestion conditions. The model utilizes the detector occupancy profile to identify traffic flow pattern changes during the queue discharging process. A turning movement proportion estimation model was proposed that is based on the relationships of the entering traffic volumes and exiting traffic volumes during different signal phases. The model only relies on short-term traffic counts from the detectors deployed in the field.

A virtual probe approach is proposed in this project to calculate the time-dependent arterial travel time based on the data from existing signal controllers and vehicle detection systems. All available traffic information, including not only the detector data but also the corresponding signal status data, is fully utilized to conduct the estimation. Unlike most of the previous work that simply aggregate the travel time as the sum of free flow travel time and delays, the proposed model considers the correlations of the states of the vehicle and thus to make the maneuver decision at each time step. Moreover, the impact of yellow time, which is usually omitted, is also included. An interesting property of the proposed model is that travel time estimation errors can be self-corrected, because the differences between a virtual probe vehicle and a real one can be reduced when both of them meet a red signal phase and/or a vehicle

queue. Therefore, the model can be implemented under various traffic conditions, and can generate accurate results even on congested arterials.

The field study at an 11-intersections corridor along France Avenue in Minneapolis, MN shows promising results. The proposed mathematical models generated good estimation of intersection queue lengths and arterial travel times.

References

Akçelik, R. (2001). *HCM 2000 Back of Queue Model for Signalised Intersections.* Akcelik & Associates Pty Ltd. Melbourne, Australia.

Akçelik, R. (1988). "The Highway Capacity Manual Delay Formula for Signalized Intersections". *ITE Journal, 58* (3), 23-2.

Akçelik, R. (1980). "Time-Dependent Expressions for Delay, Stop Rate and Queue Length at Traffic Signals". *Internal Report*, AIR 367-1. Australian Road Research Board.

Alliant Engineering Inc. (2007). *France Avenue Signal Optimization and Implementation Project.* Final report to the Hennepin Transportation Department. Minneapolis, MN, 2007.

B&B Electronics Manufacturing Company. (2003). *Port-Powered RS-485 Converter.* Retrieved January 30, 2007, from B&B Electronics Manufacturing Company: http://www.bb-elec.com/product_family.asp?FamilyId=15&TrailType=Sub&Trail=12

Balke, K., & Herrick, C. (2004). *Potential Measures of Assessing Signal Timing Performance Using Existing Technologies.* Texas Transportation Institute. College Station, TX.

Balke, K., Charara, H., & Parker, R. (2005). *Development of a Traffic Signal Performance Measurement System (TSPMS).* Texas Transportation Institute. College Station, TX.

Bang, K. L., & Nilsson, L. E. (1976). "Optimal Control of Isolated Traffic Signals". *Proceedings of the International Federation of Automatic Control/International Foundation for Information Process/International Federation of Oper Research Society International Symposium: Control in Transportation Systems*, (pp. 173-184). Columbus, OH.

Bell, M. (1991). "The Real Time Estimation of Origin-destination Flows in the Presence of Platoon Dispersion". *Transportation Research B, 25*, 115-125.

Bullock, D., & Catarella, A. (1998). "A Realtime Simulation Environment for Evaluating Traffic Signal Systems". *Transportation Research Record, 1634*, 130-135.

Canadian Institute of Transportation Engineers. (1996). *Canadian Capacity Guide for Signalized Intersections*, second edition. Institute of Transportation Engineers, District 7, Canada.

Catling, I. (1977). "A Time Dependent Approach to Junction Delays". *Traffic Engineering and Control, 18*, 520-526.

Chang, G.-L., & Tao, X. (1998). "Estimation of Time-Dependent Turning Fractions at Signalized Intersections". *Transportation Research Record, 1644*, 142-149.

Chang, J., Lieberman, E. B., & Prassas, E. H. (2000). "Queue Estimation Algorithm for Real-Time Control Policy Using Detector Data". *Proceedings of the 79th Annual Meeting of the Transportation Research Board.* Washington, D.C.

Chen, C. (2003). *Freeway Performance Measurement System (PeMS)*. Doctoral Dissertation. University of California. Berkeley, CA.

Cheu, R. L., Lee, D.-H., & Xie, C. (2001). "An Arterial Speed Estimation Model Fusing Data from Stationary and Mobile Sensors". *Proceedings of the IEEE Intelligent Transportation Systems Conference*, (pp. 573-578). Oakland, CA.

Coifman, B., Beymer, D., McLauchlan, P., & Malik, J. (1998). "A Real-Time Computer Vision System for Vehicle Tracking and Traffic Surveillance". *Transportation Research Part C, 6* (4), 271-288.

Courage, K., Showers, R., Harriot, J., Schilling, W., & Godbey, K. (1998). *Improved Methods for Measuring Travel Time on Arterial Streets, Final Report.* University of Florida. Gainesville, FL.

Cremer, M., & Keller, H. (1987). “A New Class of Dynamic Methods for Identification of Origin Destination Flows”. *Transportation Research B, 21*, 117-132.

Cremer, M., & Keller, H. (1981). “Dynamic Identification of OD Flows from Traffic Counts at Complex Intersections”. *Proceedings of the Eighth International Symposium on Transportation and Traffic Theory.* Toronto University. Toronto, Canada.

Cronje, W. B. (1983). “Analysis of Existing Formulas for Delay, Overflow and Stops”. *Transportation Research Record, 905*, 89-93.

Dailey, D., & Cathey, F. (2002). *AVL-Equipped Vehicles as Traffic Probe Sensors*, Final Report. Washington State Transportation Center. Seattle, WA.

Engelbrecht, R., Poe, C., & Balke, K. (1999). “Development of a Distributed Hardware-in-the-loop Simulation for Transportation Networks”. *Proceedings of the 78th Annual Meeting of the Transportation Research Board.* Washington, D.C.

Federal Highway Administration. (2007). *ACS-Lite - Arterial Management Program*. Retrieved May 1, 2008, from Federal Highway Administration: http://ops.fhwa.dot.gov/acs_lite/index.htm

Federal Highway Administration. (1995). *Improving Traffic Signal Operations - A Primer.* Federal Highway Administration, Washington, D.C.

Federal Highway Administration. (2006). *SAFETEA-LU - Legislation.* Retrieved January 30, 2007, from http://www.fhwa.dot.gov/safetealu/legis.htm

Federal Highway Administration. (2008). *The Signal Timing Manual.* Federal Highway Administration, Washington, D.C.

Frechette, L. A., & Khan, A. M. (1998). “Bayesian Regression-based Urban Traffic Models”. *Transportation Research Record, 1644*, 157-165.

Gettman, D., Shelby, S. G., Head, L., & Bullock, D. (2007). “Data-driven Algorithms for Real-time Adaptive Tuning of Offsets in Coordinated Traffic Signal Systems”. *Proceedings of the 86th Annual Meeting of the Transportation Research Board.* Washington D.C.

Gomez, M. (2001). *Hardware-in-the-Loop Simulation.* Retrieved January 30, 2007, from Embedded Systems Design: http://www.embedded.com/story/OEG20011129S0054

Highway Safety Research Center. (1999). The Highway Safety Information System - California Database. University of North Carolina Highway Safety Research Center. Chapel Hill, NC

Illinois Department of Transportation. (2005). *Illinois Traffic Monitoring Program.* Illinois Department of Transportation. Springfield, IL.

Institute of Transportation Engineers. (1999). *Traffic Engineering Handbook.* Washington D.C.: Institute of Transportation Engineers.

Kessaci, A., Farges, J. L., & Henry, J. J. (1989). “On-line Estimation of Turning Movements and Saturation Flows in PRODYN”. *Proceedings of the Sixth IFAC/IFIP/IFORS Symposium on Transportation.* Paris, France.

Kimber, & Hollis. (1979). “Traffic Queues and Delay at Road Junctions”. *Transport and Road Research Laboratory , LR 909*.

Kyte, M., Dixon, M., Nayak, V., Abdel-Rahim, A., & Strong, D. (2008). “Testing the Incremental Queue Accumulation (IQA) Method as a Replacement for the HCM Signalized Intersection Uniform Delay and Queue Method Using the Lankershim Blvd”. NGSIM Data Set. *Proceedings of the 87th Annual Meeting of the Transportation Research Board.* Washington, D. C.

Lan, C.-J., & Davis, G. A. (1999). “Real-time Estimation of Turning Movement Proportions from Partial Counts on Urban Networks”. *Transportation Research Part C, 7*, 305-327.

Lin, F.-B., & Vijayakumar, S. (1988). “Adaptive Signal Control at Isolated Intersections”. *Journal of Transportation Engineering, 114* (5), 555-573.

Lin, W. H., Kulkarni, A., & Mirchandani, P. (2003). “Arterial Travel Time Estimation for Advanced Traveler Information Systems”. *Proceedings of the 82nd Annual Meeting of the Transportation Research Board.* Washington, D.C.

Liu, H. X., & Ma, W. (2008). “A Virtual Vehicle Probe Model for Time-Dependent Travel Time Estimation on Signalized Arterials”. *Transportation Research Part C,* In Press.

Liu, H. X., & Ma, W. (2007). “Time-dependent Travel Time Estimation Model for Signalized Arterial Network”. *Proceedings of the 86th Annual Meeting of the Transportation Research Board.* Washington, D.C.: Transportation Research Board.

Maher, M. J. (1984). “Estimating the Turning Flows at a Junction: A Comparison of Three Models”. *Traffic Engineering and Control, 25*, 19-22.

Miller, A. J. (1968). “Signalised Intersections - Capacity Guide”. *Bulletin No. 4.* Vermont South, Australia: Australian Road Research Board.

Mueck, J. (2002). “Using Detectors near the Stop-line to Estimate Traffic Flows”. *Traffic Engineering and Control,* December, 429-434.

National Cooperative Highway Research Program. (2003). *Synthesis 311: Performance Measures of Operational Effectiveness for Highway Segments and Systems.* Transportation Research Board. Washington, D. C.

National Electrical Manufacturers Association. (2003). *NEMA Standards Publication TS 2.* National Electrical Manufacturers Association. Rosslyn, VA.

National Instruments. (2006). *NI-6528 User Guide and Specifications.* Retrieved January 30, 2007, from National Instruments: http://www.ni.com/pdf/manuals/372124a.pdf

National Transportation Operations Coalition. (2007). *2007 National Traffic Signal Report Card - Technical Report.* National Transportation Operations Coalition. Washington, D.C.

Nee, J., & Hallenbeck, M. E. (2001). *Surveillance Options for Monitoring Arterial Traffic Conditions.* Washington State Transportation Center (TRAC), Washington, D.C.

Newell, G. F. (1989). *Theory of Highway Traffic Signals.* (UCB-ITS-CN-89-1). Institute of Transportation Studies, University of California, Berkeley, CA.

Nihan, N., & Davis, G. A. (1989). “Application of Prediction-error Minimization and Maximum Likelihood to Estimate Intersection O-D Matrices from Traffic Counts”. *Transportation Science, 23*, 77-90.

Nihan, N., & Davis, G. A. (1987). “Recursive Estimation of Origin Destination Matrices from Input/output Counts”. *Transportation Research B, 21*, 149-163.

Nobe, S. (2002). *On-line Estimation of Traffic Split Parameters Based on Lane Counts*. Doctoral Dissertation . University of Arizona. Tucson, AZ.

Ovesen, R. V. (2008). *EIA-485.* Retrieved May 31, 2008, from Wikipedia: http://en.wikipedia.org/wiki/RS-485

Petty, K., Kwon, J., & Skabardonis, A. (2005). A-PeMS: An Arterial Performance Measurement System. 2006 Annual Meeting Workshop. Washington, D.C.

Roberston, D. I. (1969). *TRANSYT: A Traffic Network Study Tool.* Laboratory Report LR 253. Road Research Laboratory, Crowthorne.

Roess, R., Prassas, E., & McShane, W. R. (2004). *Traffic Engineering, Third Edition.* Prentice-Hall. Upper Saddle River, NJ

Rorbech, J. (1968). “Determining the Queue Length of the Approach Lanes Required at Signal Controlled Intersections on Through Highways”. *Transportation Research, 2*, 283-291.

Schrank, D., & Lomax, T. (2007). *The 2007 Urban Mobility Report.* Texas Transportation Institute. College Station, TX.

Sharma, A., Bullock, D. M., & Bonnes, J. A. (2007). “Input–Output and Hybrid Techniques for Real-Time Prediction of Delay and Maximum Queue Length at Signalized Intersections”. *Transportation Research Record 2035*, 69-80.

Shelby, A., Bullock, D. M., & Gettman, D. (2006). “Transition Methods in Traffic Signal Control”. *Proceedings of the 85th Annual Meeting of the Transportation Research Board.* Washington, D.C.

Shuldiner, P., & Upchurch, J. (2001). “Automated Travel Time Data for a Regional Traveler Information System”. *Institute of Transportation Engineers Annual Meeting.* Chicago, IL.

Skabardonis, A., & Geroliminis, N. (2007). “Development of an Arterial Performance Measurement System”. *11th World Congress on Transport Research (WCTR).* Berkeley, CA.

Skabardonis, A., & Geroliminis, N. (2005). “Real-Time Estimation of Travel Times along Signalized Arterials”. *16th ISTTT conference.* College Park, MD.

Smith, L. (2003). *Intelligent Transportation Systems - Archived Data.* Retrieved January 30, 2007, from California Center for Innovative Transportation: http://www.calccit.org/itsdecision/serv_and_tech/Archived_Data/archived_data_report.htm

Stephanopoulos, G., & Michalopoulos, P. G. (1979). “Modeling and Analysis of Traffic Queue Dynamics at Signalized Intersections”. *Transportation Research Part A, 13*, 295-307.

Strong, D. W., Nagui, R. M., & Courage, K. (2006b). “Incorporating the Effects of Traffic Signal Progression into the Proposed Incremental Queue Accumulation (IQA) Method”. *Proceedings of the 85th Annual Meeting of the Transportation Research Board.* Washington, D. C.

Strong, D. W., Nagui, R. M., & Courage, K. (2006a). “New Calculation Method for Existing and Extended HCM Delay Estimation Procedure”. *Proceedings of the 86th Annual Meeting of the Transportation Research Board.* Washington, D. C.

Sunkari, S. (2004). “Benefits of Retiming Traffic Signals”. *ITE Journal* , 26-19.

Takaba, S., Morita, T., Hada, T., Usami, T., & Yamaguchi, M. (1991). “Estimation and Measurement of Travel Time by Vehicle Detectors and License Plate Readers”. *Proceedings of Vehicle Navigation and Information Systems Conference*, *1*, pp. 257-267.

Transportation Research Board. (2000). *Highway Capacity Manual 2000.* Transportation Research Board. Washington, D. C.

Tsekeris, T., & Skabardonis, A. (2004). “Online Performance Measurement Models for Urban Arterial Networks”. *Proceedings of the 82nd Annual Meeting of the Transportation Research Board.* Washington, D.C.

Turner, S., Best, M., & Schrank, D. (1996a). *Measures of Effectiveness for Major Investment Studies.* Texas Transportation Institute. College Station, TX.

Turner, S., Eisele, W. L., Benz, R. J., & Holdener, D. J. (1998). *Travel Time Data Collection Handbook,* Final Report. Federal Highway Administration, Washington, D.C.

Turner, S., Lomax, T. J., & Levinson, H. S. (1996b). “Measuring and Estimating Congestion using Travel Time-based Procedures.” *Transportation Research Record, 1564*, 11-19.

Varaiya, P. (1997). *How to Measure Transportation System Performance.* Retrieved January 30, 2007, from http://paleale.eecs.berkeley.edu/~varaiya/papers_ps.dir/TSperf.pdf

Venglar, S., & Urbanik, T. I. (1995). Advanced Technology Application: The "Smart" Diamond. *Compendium of Technical Papers*. Institute of Transportation Engineers, Washington, D.C.

Viti, F., & Zuylen, H. J. (2006). "Consistency of Random Queuing Models at Controlled Intersections". *Proceedings of the 85th Annual Meeting of the Transportation Research Board.* Washington D.C.: Transportation Research Board.

Viti, F., & Zuylen, H. V. (2005). "Markov Mesoscopic Simulation Model of Overflow Queues at Multilane Signalized Intersections". *Proceedings of the Joint Conference - 10th EWGT Meeting & 16th Mini-EURO Conference.* Poznan, Poland.

Webster, F. V. (1958). "Traffic Signal Settings". *Road Research Technical Paper, 39* . London: Her Majesty's Stationery Office.

Xu, H., Li, K., & Zheng, M. (2006). "An On-line Queue Length Estimation Algorithm for Adaptive Control Strategies at Isolated Signalized Intersections". *Proceedings of the 85th Annual Meeting of the Transportation Research Board.* Washington, D.C.

Zhang, M. H. (1999). "Link-journey-speed Model for Arterial Traffic". *Transportation Research Record, 1676*, 109-115.

Appendix A

LIST OF NOTATIONS

d_l the distance between the advance detector and the stop-line;

D_i the i^{th} detector along the corridor;

D_d the downstream detector;

D_l the detector that detects left-turn traffic;

D_r the detector that detects right-turn traffic;

D_t the detector that detects through traffic;

h the saturated space headway in a queue;

$L_q(\tau)$ the queue length between the back of the last queued vehicle and the stop-line at time τ;

L_q^{max} the maximum queue length within a cycle;

n the n^{th} queued vehicle;

$n_q(\tau)$ the maximum number of queued vehicles accumulated behind the stop-line from time T_r to time τ;

$n(t)$ the number of vehicles passes the advance loop detector within time period $[t, t+\Delta t]$;

$N_A(\tau)$ the vehicle arrival counts at time τ;

$N_D(\tau)$ the vehicle departure counts at time τ;

N_g the number of vehicles arriving on green time;

N_r the number of vehicles arriving on red time;

p the phase number;

P the proportion of all vehicles in movement arriving during green phase;

P_M^A the turning proportion of movement M at approach A during a cycle;

$t(p)$ the duration of phase p;

t_d the deceleration time for the virtual probe to stop or reach the same speed as the last queued vehicle ahead.

t_l the travel time for the last queued vehicle to pass the advance loop detector;

t_n^h the n^{th} measured time headway since green start;

t_n^l the time of the n^{th} vehicle passes the stop-line since green start;

t_r the reaction time of the first queued vehicle;

t_s the uniform discharge starting time difference between two adjacent queued vehicles;

T_A the time when the detector is occupied by a motionless vehicle;

T_B the time when the first queued vehicle starts to move;

T_C the time when the discharge shock wave propagates to the detector;

T_D the time when the discharge shock wave propagates to the rear of the queue;

T_D' the time when the queue reaches maximum;

T_E the time when the last queued vehicle passes the advance detector;

T_F the time when the last queued vehicle passes the stop-line;

T_g the starting time of green;

T_G the time when the last queued vehicle accelerates to the desired speed;

T_n^s the discharge starting time of the n^{th} queued vehicle;

T_r the starting time of red;

u_f a constant desired speed;

$u_q(\tau)$ the speed of the last queued vehicle at time τ;

$V_M^A(t)$ the traffic counts of movement M at approach A during time t;

$V_{MN}^A(t)$ the combination traffic counts of movement M and movement N at approach A during time t;

x_f the time when the faster vehicle join the queue;

x_s the time when the slower vehicle join the queue;

x_s^i the position of the stop-line of Intersection i;

$y(\tau)$ the remaining yellow time when the phase is yellow at time τ;

γ_a a constant acceleration rate;

γ_d a constant deceleration rate;

δ_c a constant occupancy critical value to identify traffic flow pattern from detector;

τ the time instant;

Δt a constant tracing time step;

State Variables of the Virtual Probe (with P at the right upper corner)

$L^P(\tau)$ the distance between the virtual probe and the "*barrier*" at time τ;

$L_q^P(\tau)$ the distance between the back of the last queued vehicle ahead of the virtual probe and the stop-line at time τ;

$L_s^P(\tau)$ the safe space headway of the virtual probe at time τ;

$L_y^P(\tau)$ the yellow time travel distance of the virtual probe at time τ;

$n_q^P(\tau)$ the number of queued vehicles accumulated between the virtual probe and the stop-line from time T_r to time τ;

$u^P(\tau)$ the speed of the virtual probe at time τ;

$u_q^P(\tau)$ the speed of the last queued vehicle ahead of the virtual probe at time τ;

$x^P(\tau)$ the position (x-coordinate) of the virtual probe at time τ;

$x_q^P(\tau)$ the position of the rear of the last queued vehicle ahead of the virtual probe at time τ;

$y^P(\tau)$ the time required for the virtual probe accelerating to the desired speed at time τ;

$\gamma_d^P(\tau)$ the recalculated deceleration rate that guarantee the virtual probe can safely decelerated at time τ;

Appendix B

LIST OF ACRONYMS

ACS	the Adaptive Control Software;
ADT	average daily traffic;
APeMS	the Arterial Performance Measurement Systems;
CID	the Controller Interface Device;
FHWA	the Federal Highway Administration;
GLS	generalized least-squared;
HCM	the Highway Capacity Manual;
HILS	hardware-in-the-loop simulation;
IQA	incremental queue accumulation;
ITS	intelligent transportation systems;
LOS	level of service;
LS	least-squares;
ME	maximum entropy;
NCHRP	the National Cooperative Highway Research Program;
PeMS	the freeway Performance Measurement Systems;
PMRG	the Performance Measure Report Generator;
RMSP	the Root Mean Squared Percent Error;
SCATS	the Sydney Coordinated Adaptive Traffic System;
SCOOT	the Split Cycle Offset Optimization Technique;
SMART-SIGNAL	Systematic Monitoring of Arterial Road Traffic and Signals;
TMP	turning movement proportion;
TSER	the Traffic Signal Event Recorder;
TSPMS	the Traffic Signal Performance Measurement System;
TTI	the Texas Transportation Institute;